ISTANBUL TECHNICAL UNIVERSITY ★ GRADUATE SCHOOL OF SCIENCE
ENGINEERING AND TECHNOLOGY

ELECTRIC AND MAGNETO-TRANSPORT PROPERTIES OF MAGNETIC AND SUPERCONDUCTIVE IRON PNICTIDE AND SKUTTERUDITE COMPOUNDS

Ph.D. THESIS

Murat SERTKOL

Department of Physics Engineering

Physics Engineering Programme

OCTOBER 2016

ISTANBUL TECHNICAL UNIVERSITY ★ GRADUATE SCHOOL OF SCIENCE
ENGINEERING AND TECHNOLOGY

ELECTRIC AND MAGNETO-TRANSPORT PROPERTIES OF MAGNETIC AND SUPERCONDUCTIVE IRON PNICTIDE AND SKUTTERUDITE COMPOUNDS

Ph.D. THESIS

Murat SERTKOL
(509102121)

Department of Physics Engineering

Physics Engineering Programme

Thesis Advisor: Prof. Dr. Yıldırhan ÖNER

OCTOBER 2016

İSTANBUL TEKNİK ÜNİVERSİTESİ ★ FEN BİLİMLERİ ENSTİTÜSÜ

MAGNETİK VE SÜPERİLETKEN DEMİR PNİKTİD VE SKUTTERUDİT BİLEŞİKLERİNİN ELEKTRİK VE MAGNETO-TRANSPORT ÖZELLİKLERİ

DOKTORA TEZİ

Murat SERTKOL
(509102121)

Fizik Mühendisliği Anabilim Dalı

Fizik Mühendisliği Programı

Tez Danışmanı: Prof. Dr. Yıldırhan ÖNER

EKİM 2016

Murat SERTKOL, a Ph.D. student of ITU Graduate School of Science Engineering and Technology 509102121 successfully defended the thesis entitled "ELECTRIC AND MAGNETO-TRANSPORT PROPERTIES OF MAGNETIC AND SUPERCONDUCTIVE IRON PNICTIDE AND SKUTTERUDITE COMPOUNDS", which he/she prepared after fulfilling the requirements specified in the associated legislations, before the jury whose signatures are below.

Thesis Advisor :	**Prof. Dr. Yıldırhan ÖNER** Istanbul Technical University	....
Jury Members :	**Prof. Dr. Gönül ERYÜREK** Istanbul Technical University	....
	Assoc. Prof. Dr. Burak ÖZKAL Istanbul Technical University	....
	Assoc. Prof. Dr. Sedat BALLIKAYA Istanbul University	....
	Prof. Dr. Faik MİKAİLZADE Gebze Technical University	....

Date of Submission : 29 September 2016
Date of Defense : 19 October 2016

Aileme...

FOREWORD

During my PhD, I would like to express my gratitude and thanks to my supervisor Prof. Yıldırhan ÖNER, for his infinite teaching energy, encouragement, leadership, struggles to provide funding for me, giving me opportunities to work with valuable devices in his lab., sharing his experiences in liquid helium with me, moral help and the motivation.

I would like to thank to Prof. Bekir AKTAŞ for giving me opportunity to work at PPMS at Gebze Technical University, leadership, encouragement and helps.

I would like to thank to Prof. Joseph H. ROSS JR. for helping me in analysis of the datas, for helping me in some measurements, moral help and motivation. I would like to thank to Laziz SARIBAEV for helping me in some measurements.

I would like to thank to Ünal ATEŞ and Fatih AYDOĞDU for their helps in sample preparation, Labview software, sharing experiences with me.

I would like to thank to Assoc. Necmettin KILINÇ for his valuable helps in Labview software.

I would like to thank to Assoc. Prof. Sedat BALLIKAYA and Prof. Ctirad UHER for preparing and measuring skutterudite compounds, moral help and motivation.

I would like to thank to Assoc. Prof. Numan AKDOĞAN for giving me opportunity to work at resistivity measurement system, I would like to thank to Assist Prof. Mustafa ÖZTÜRK for his helps in Labview software, Assist Prof. Ramazan TOPKAYA and Assist Prof. Ali Cemil BAŞARAN for sample preparation and measurements at PPMS.

I would like to thank to Assoc. Prof. Mustafa ÖZDEMİR for leading me during resistivity measurement system.

I would like to thank to Assist. Prof. Adil GÜLER for; giving me opportunity to work together, sharing me his experiences and helping me during the preparation of samples, helping me to work with liquid helium.

I would like to thank to Assoc Prof. Seda Aksoy ESİNOĞLU for helping me to learn FULLPROF software.

I would like to thank to Prof. Orhan KAMER and İsmail BORAZAN for helping me with the thin film preparing system in diffusion pump.

I would like to thank to Prof. Fatma TEPEHAN and Dr. İbrahim TÜRHAN for thin film characterization.

I would like to thank to specialist Tansu ERSOY for XRD measurements.

I would like to thank to Assoc Prof. Burak ÖZKAL for his valuable moral help and motivation, consumables.

I would like to thank to PhD student Didem OVALI, for XRD analysis, helping me for diamond cutter. I would like to thank to PhD student Deniz KAVRAR for valuable helps and discussions.

I would like to thank and express my gratitude to Turkey Higher Education Council (TÜBİTAK) for funding me in 111T779 project, for funding me in 2211-C Öncelikli Alanlar program.

I would like to thank to İTÜ Bilimsel Araştırma Projeleri Birimi for funding me in TFD32 Congress, held in Bodrum, TURKEY.

I would like to thank to my beloved wife, Sümeyye Bahçeci SERTKOL, for her valuable supports, moral help, motivation, giving me permission to work at lab at late hours of nights, encouraging me, and for her unlimited love.

I would like to thank to my father Sinan SERTKOL; for letting me survive during my cancer treatment when I was three, for providing me motivation and moral help during my whole life. His love is unique.

I would also thank to my mom and brother Seyhan and Serhat SERTKOL for their moral help and motivation.

October 2016 Murat SERTKOL
(Physicist)

TABLE OF CONTENTS

ABBREVIATIONS

AC	: Alternating Current
BG	: Bloch-Grüneisen
FC	: Field Cooling
HTS	: High Temperature Superconductivity
JR	: Japan Railways
MAGLEV	: Magnetic Levitation
MBE	: Molecular Beam Epitaxy
SC	: Superconductivity
SDW	: Spin Density Wave
SMT	: Shanghai Maglev Train (China)
TGV	: Fast Train (Train à grande vitesse, France)
VSM	: Vibrating Sample Magnetometer
XRD	: X-Ray Diffraction
YBCO	: Yttrium Barium Copper Oxide
ZFC	: Zero Field Cooling

SYMBOLS

a	:	Lattice Parameter
α	:	Alpha
β	:	Beta
γ	:	Gamma
Å	:	Angström
K	:	Kelvin
$^{\circ}C$	:	Celcius degree
$\vec{B}$	:	Magnetic Field Density
$\vec{H}$	:	Magnetic Field Strength
H_c	:	Critical Field
δ	:	Energy gap
e^{-}	:	Electron
eV	:	Electron volt
ε	:	Energy
G	:	Gibbs Free Energy
$\hbar$	:	Planck's Constant
J_c	:	Critical Current
k_B	:	Boltzmann Constant
λ	:	London Penetration Depth
M	:	Magnetization
μ	:	Micrometer
μ_0	:	Magnetic Permeability
nm	:	Nanometer
Oe	:	Oersted
Ω	:	Ohm
P	:	Pressure
$\vec{q}$	:	Wave Vector
ρ	:	Resistivity
θ	:	Bragg Diffraction Angle
T	:	Tesla
T_c	:	Critical Temperature
T_{sf}	:	Spin Fluctuation Temperature
V	:	Potential Energy; Volume
ω	:	Frequency
ζ	:	Coherence Length
χ	:	Magnetic Susceptibility; the goodness of an XRD fit

LIST OF TABLES

LIST OF FIGURES

Page

ELECTRIC AND MAGNETO-TRANSPORT PROPERTIES OF MAGNETIC AND SUPERCONDUCTIVE IRON PNICTIDE AND SKUTTERUDITE COMPOUNDS

SUMMARY

Superconductivity has gained its popularity after the high T_c materials have been explored. Cuprates (copper-oxide systems) and Hg based 1223 systems still have research interest allowing to examine new chemical compounds for high T_c superconductors (HTS). Unconventional materials such as Fe-based pnictides (group V-B elements in 122 systems) are frontier compounds in which magnetism and superconductivity can be observed together in these materials, presenting them as an option for high T_c superconductors.

Iron-arsenide (Fe-As) and copper-oxide (Cu-O) layers in the structure of a crystal are responsible for the superconductivity phenomenon observed in these systems. Fe-As system has similar properties with Cu-O like having d electrons, layered structures and antiferromagnetic (AFM) spin ordering and they are still earning interest. In addition to this, iron has a magnetic moment which plays a key role in superconductivity-magnetism colleration. Up to now, two physical problem in our study are the superconducting phase transition temperature T_c and magnetic behavior of superconducting materials. Lattice changes, symmetry breaking in the unit cell, applying pressure are some of reasons that shift T_c up or down. For the magnetic behavior of superconductive samples, establishment of a new magnetic ordering is key parameter under the T_c. Magnetic changes are said to be affect superconductivity. The exclusion of magnetic field lines by Meissner effect is a clear evidence for superconductive mechanism. Our study here is focused on iron pnictide compounds on the basis of these two physical problem.

The most popular iron pnictide systems are Fe-As based ones. The material $BaFe_2As_2$ has a tetragonal structure and it goes a structural phase transition from tetragonal $I4/mmm$ to orthorhombic Fmmm lattice. Same behaviors are found in AFe_2As_2 (A:Ba, Sr, Ca, etc.) systems at low temperatures like in cuprates. This kind of phase transition is named as spin density wave (SDW) transition and it is valid for both cuprates and iron-pnictides. A chemical change in composition with a dopant or applying pressure results magnetic transition in Fe-As compounds and thereby superconductivity emerges. By doping electron or hole to a AFe_2As_2 system like $BaFe_{2-x}Pt_xAs_2$, superconductivity can be observed. Since the change in chemical composition may effect the T_c, Lanthanum is doped to the $BaFe_{2-x}Pt_xAs_2$ system. And a new serie of $Ba_{1-x}La_xFe_{1.9}Pt_{0.1}As_2$ polycrystalline samples are successfully synthesized by a solid-state reaction method. The synthesis of Pt and La doped compounds was physically remarkable since some of them are synthesized for the first time. Data obtained from those samples are investigated in detail by Rietveld refinement. Our target to produce "single phase" polycrystalline samples is achieved successfully. Unit cell parameters and symmetry group of samples are determined in agreement with the literature.

Structural analyses of samples are made by X-Ray diffraction after the chemical synthesis part. Results are analyzed by FullProf software. Profile matching are done for whole samples and structural parameters are determined. Some samples are found single phase in which we published in the articles during our study.

Resistivity measurements are performed with the liquid nitrogen followed by liquid helium by the help of a hand made glass cryostat. It is seen that the temperature dependence of the resistivity for the parent sample, $BaFe_2As_2$ exhibits the same behavior including a very close match to reported values given in the literature. The structural phase transitions from tetragonal $I4/mmm$ to orthorhombic Fmmm lattice in $BaFe_2As_2$ and $BaFe_{1.9}Pt_{0.1}As_2$ samples are observed. Temperature dependent transition is compatible with the corresponding phase changes observed at XRD measurement, which is known to be tetragonal at room temperature.

Superconductive phase transition temperature, T_c for the samples in different Pt doping levels is investigated in the literature. It is found that Pt doping is effective on the change of T_c at lower doping rates like $x = 0.2$. x=0 sample is the parent sample ($BaFe_2As_2$) in which it is not superconductive but the $BaFe_{1.9}Pt_{0.1}As_2$ sample has the highest value in Pt doped group for phase transition temperature, T_c. In addition to the literature, we revealed that superconductivity can be observed even in x=0.3 doping rates in such materials.

Lanthanum doped samples are successfully synthesized in addition to the Pt doped ones. And resistivity measurements are showed that superconductivity still can be observed in such tetragonal I4/mmm systems. Resistivity of these samples are showed a clear evidence for superconductivity that our results approve.

The magnetic measurements of materials are done by measuring zero field cooling (ZFC) and field cooling (FC) curves. Critical temperature, critical current density, coherence length (also known as Ginzburg-Landau parameter), volume magnetization and magnetic susceptibility values are obtained from the analysis. Magnetization behavior of samples are observed as a function of temperature and phase transition temperatures are determined. The critical current density, which is remarkable sign for how much charge a superconductor can carry, is estimated by models given in the literature. Coherence length is calculated from the M-H curves (from the Meissner effect observed in these samples). Results show that samples based on a tetragonal structure are convenient to be a host material for the superconductive behavior. This means the doping of rare-earth ions to those samples provide materials that have characteristic properties like showing zero resistivity and the exclusion of magnetic field lines. In our study, platinum and lanthanum are doped to our host material, $BaFe_2As_2$; and new sample sets are prepared.

It is seen that ZFC-FC curves are separated in the phase transition temperature, T_c, showing superconductive behavior compatible with the resistivity measurements. Meissner effect is observed in both platinum and lanthanum doped samples. Critical current densities are calculated from the magnetic measurements and phase transition temperatures are determined. The samples are in superconducting regime where their temperatures are lower than the T_c. M versus H curves are measured in several temperatures in this regime below the phase transition temperature. Analysis of the results helped us to calculate coherence length ζ for the samples by obtaining H_c readings at different measurement temperatures. From the M-H curves of samples measured below the T_c, lines are extrapolated to T=0 K and coherence lengths are found in nm range.

By transforming magnetization from emu/g to volume magnetization, susceptibility for the samples are obtained in terms of magnetization data. The termination of ZFC and FC curves in to close values to -1 in y axis, shows that samples are mostly diamagnetic with a high volume fraction. Samples are mostly presented superconductivity in general. Phase transition temperatures found from ZFC-FC curves are compatible with the resistivity data. La doped samples are showed a clear evidence for superconductivity that both resistivity and magnetic results approve.

Thin films of $BaFe_2As_2$ sample is prepared and the amorphous structure is proved by the XRD measurement. Resistivity of sample is measured between 4.2-300K at liquid He. A phase transition at $T_c = 6.7K$ is seen clearly with reproducible experiments which is very similar to a superconductive phase transition. We observe superconductivity for the first time in an amorphous thin film. This result is interesting because current macroscopic theory of superconductivity is based on Cooper pairing mechanism. The drop of resistivity down to zero obeys filamentary superconductivity that is seen in literature in principle.

The difference in our study is that we create a disorder in material and it is amorphous. This process is realized in a simple flash evaporation system under vacuum. This is important because same kind of samples are produced in molecular beam epitaxy (MBE) or similar systems that we are not able to. Some studies are reported that both in bulk and thin film samples, showing that it is possible to apply pressure to the system and create disorder. This method is a way in order to trigger the superconductivity in such systems. For the first time, we observe the superconductivity in an amorphous thin film above the liquid He temperature, at ambient conditions. Magnetic characterization of this sample still continues and results will be presented in an appropriate publisher.

In case of any failure in preparing superconducting samples, antimony doped compounds are prepared. $BaFe_4Sb_{12}$ sample is prepared first. This sample is known as skutterudite compound in literature and it is thermoelectrically efficient. Since the synthesis was successful, the thermoelectric and magnetic properties of Pt substituted $BaFe_{4-x}Pt_xSb_{12}$ (x = 0, 0.1, 0.2) compounds were investigated in this part of study.

Thermoelectric (TE) materials are available to capture a part of wasted energy that is rejected to atmosphere and convert it into the useful electrical power. The efficiency of a TE generator is strongly depending on the dimensionless figure of merit *ZT*, defined as $ZT = S^2\sigma T/\kappa$ where S, σ and κ are the Seebeck coefficient, electrical conductivity, total thermal conductivity ($\kappa = \kappa_e + \kappa_L$ where κ_e is the electronic contribution and κ_L the lattice contribution) and T stands for the absolute temperature. Efficient thermoelectric materials are required to have high electrical conductivity, high Seebeck coefficient and lower thermal conductivity. Filled skutterudites fulfill these requirements. In the past decade years, experimental and theoretical tremendous effort have been conducted on skutterudites compounds in order to optimize their TE and magnetic properties for enhancing *ZT* value further and characterize low temperature behavior. The filled skutterudites with chemical formula RT_4M_{12} where R = alkaline earth and rare earth metal, T = Fe, Ru, and Os and M = P, As, and Sb have been studied extensively due to their both high TE performance and exotic magnetic properties. Even though, there are many reports in literature on thermoelectric and magnetic properties of RT_4M_{12} family skutterudite compounds. There is still lack of understanding about correlation between magnetic and thermoelectric phenomena for these compounds.

In this work, we aim for contribute to understanding of relation between two phenomenon by characterization low temperature magnetic and thermoelectric properties $BaFe_{4-x}Pt_xSb_{12}$ (x = 0, 0.1, 0.2) compounds.

X-Ray diffraction, resistivity, magnetic measurements, Seebeck coefficient and thermal conductivity of samples are measured. Temperature depending resistivity shows that all samples show semi metallic behavior in the temperature range of 4.2 K to 300 K.

Increases in resistivity with Pt content is interpreted as existing of different scattering mechanisms such as spin fluctuation and Kondo impurity in these compounds or decreasing hole concentration. Kondo minimum are confirmed by temperature dependence of logarithmic resistivity analysis at 2-50 K which might be due to local deformation in crystal structure as a result of spin fluctuation mechanism. Local minimum and maximum in Seebeck coefficient observed might be due to paramagnon drag or spin fluctuation effect in materials. Magnetic susceptibility for the compounds x = 0.1 and x = 0.2 show that there are two successive transition, paramagnetic to magnetic state at T_c = 48 K and short range magnetic to long range magnetic ordering at lower temperatures, however there is only one transition from paramagnetic to long range ordering transition in Pt free compound.

The lattice part of thermal conductivity versus temperature plot shows that the major part of total thermal conductivity is dominated by lattice contribution.

Local maximum & minimum in Seebeck coefficient versus temperature plot, Kondo minimum observed in logarithmic resistivity show that there is a close relation between magnetic and thermoelectric properties due to spin fluctuation effect in Pt substituted $BaFe_{4-x}Pt_xSb_{12}$ (x = 0, 0.1, 0.2) compounds.

MAGNETİK VE SÜPERİLETKEN DEMİR PNİKTİD VE SKUTTERUDİT BİLEŞİKLERİNİN ELEKTRİK VE MAGNETO-TRANSPORT ÖZELLİKLERİ

ÖZET

Süperiletkenlik çalışmaları yüksek sıcaklık malzemelerin keşfinden sonra popülarite kazandı. Kupritler (bakır-oksit sistemler), cıva tabanlı 1223 örnekleri gibi yeni kimyasal bileşiklerin sentezi, yüksek sıcaklık süperiletkenlik araştırmalarında halen ilgi çekmektedirler. Demir tabanlı pniktidler (122 sistemindeki grup V-B elementleri) olarak bilinen malzemeler, yüksek süperiletken faz geçiş sıcaklığına (T_c) sahiptirler ve süperiletkenlik ve manyetizmanın bir arada gözlendiği öncü malzemelerdir.

Demir-arsenik (Fe-As) ve bakır-oksit (Cu-O) tabakaları, bir kristal yapıda süperiletkenlik fenomeninin gözlenmesinden sorumlu tabakalar olarak bilinirler. Fe-As örnekleri tabakalı yapıda olmaları, d elektronlarına sahip olmaları ve anti ferromanyetik spin düzenine (AFM) sahip olmaları açısından Cu-O örnekleri ile benzer özelliklere sahiptir. Buna ek olarak demir bir manyetik momente sahiptir ve bu özellik süperiletkenlik-manyetizma ilişkisinde önemli rol oynamaktadır. Şimdiye kadar yapılan çalışmalardaki iki fiziksel problem süperiletkenlik faz geçiş sıcaklığı T_c ve süperiletken örneklerin manyetik davranışıdır. Faz geç sıcaklığının yukarı çekilmesi, yüksek sıcaklık süperiletken örneklerin sentezlenmesi için motivasyon sağlamıştır. Manyetik özelliklerin süperiletken örneklerde gözlenmesi, faz geçiş sıcaklığının ayırt edilmesi gibi bazı fiziksel parametrelerinin belirlenmesinde önemli rol oynamaktadır. Sonuç olarak süperiletken örneklerde yeni manyetik düzenlerin oluşturulması, kristal yapıdaki birim hücre değişiklikleri, simetri değişimi ve basınç uygulanması yoluyla süperiletkenlik faz geçiş sıcaklığının yukarı yönde değişmesi olarak karşımıza çıkmaktadır. Manyetik değişikliklerin süperiletkenliği etkilediği bilinmektedir. Manyetik alan çizgilerinin örnekten dışlanması süperiletkenlik mekanizması için çok açık bir kanıttır. Burada bizim odaklandığımız iki fiziksel problem faz geçiş sıcaklığının değişimi ve manyetik özelliklerin etkisidir.

Demir pniktid sistemleri üzerinde bir çok çalışma bulunmaktadır. Bunların arasında en bilinen örneklerden olan $BaFe_2As_2$ örneği, tetragonal bir yapıya sahiptir ve belli sıcaklıkta tetragonal I4/mmm simetriden ortorombik Fmmm simetriye yapısal faz geçişi göstermektedir. Aynı davranış düşük sıcaklıklarda, kuprit örneklerinde olduğu gibi AFe_2As_2 (A:Ba, Sr, Ca, vs.) sistemlerinde de gözlenmektedir. Bu tür faz geçişlerine spin yoğunluk dalgası (SDW) geçişi denir ve hem Kuprit lerde hem de demir pniktidlerde gözlenmektedir. Kimyasal bileşimde bir değişimle (elektron ya da deşik katkılanması) ya da basınç uygulayarak demir arsenik bileşiklerinde süperiletkenlik gözlenebilmektedir. Bu çalışmada AFe_2As_2 sistemine elektron ya da deşik katkılanarak $BaFe_{2-x}Pt_xAs_2$ örnekleri hazırlanlanmıştır ve süperiletkenlik gözlenmiştir. Kimyasal bileşimideki değişim T_c'yi etkileyeceği için $BaFe_{2-x}Pt_xAs_2$ sistemine lantanyum katkılanmıştır. Ve $BaFe_{2-x}Pt_xAs_2$ serisine ek olarak polikristal $Ba_{1-x}La_xFe_{1.9}Pt_{0.1}As_2$ örnekleri, katı hal kimyasal reaksiyon metoduyla başarılı bir şekilde sentezlenmiştir. Platin ve lantanyum katkılı örnekler ilk defa grubumuzca tek

faz olarak sentezlenmiştir. Bu örneklerden elde edilen numuneler Rietveld analizi ile detaylı olarak incelenmiştir. Hedefimiz olan tek faz polikristal örneklerin sentezi başarıyla yapılabilmiştir. Örneklerin yapılan analizinde, birim hücre parametreleri ve simetri grubu literatür ile uyumlu olarak belirlenmiştir.

Kimyasal sentez kısmının ardından örneklerin yapısal analizi, X-ışını kırınımı ile yapılmıştır. Sonuçlar FullProf yazılımı ile analiz edilmiştir. Örnekler için X-ışını profili analizi yapılmış ve birim hücre parametreleri belirlenmiştir. Tek faz elde edilen örnekler yayına dönüştürülmüştür.

Direnç ölçümleri önce sıvı azot ta, ardından da sıvı helyumda el yapımı bir cam kriyostat yardımıyla yapılmıştır. $BaFe_2As_2$ örneğin sıcaklık bağımlılığının literatürde verilen değerlerle uyumlu olduğu görülmüştür. Tetragonal I4/mmm yapıdan ortorombik Fmmm yapıya yapısal faz geçişi hem $BaFe_2As_2$ örneğinde hem de örneğinde $BaFe_{1.9}Pt_{0.1}As_2$ görülmüştür.

Farklı platin katkılama düzeyleri için süperiletkenlik faz geçiş sıcaklığı (T_c) davranışı, literatürde araştırılmıştır. Platin katkılamanın faz geçiş sıcaklığında $x = 0.2$ gibi katkılama oranlarına kadar etkili olduğu görülmüştür. x=0 örneği ana materyaldir ($BaFe_2As_2$) ve süperiletken değildir. Ama platin katkılı $BaFe_{1.9}Pt_{0.1}As_2$ örneği, platin katkılı diğer örnekler içerisinde en yüksek faz geçiş sıcaklığına sahip örnektir. Bizim çalışmamızda bu örneklerde x=0.3 katkılama düzeyinde bile süperiletkenlik gözlenebilmiştir.

Platin katkılı örnekler gibi lantanyum katkılı örnekler de başarılı bir şekilde sentezlenmiştir. Direnç ölçümleri örneklerin tetragonal I4/mmm simetriye sahip birim hücrede katkılama ile süperiletkenlik gözlenebileceğini ortaya koymuştur. Bu örneklerdeki direnç ölçüm sonuçlarımız, açık bir şekilde süperiletkenlik fenomeninin varlığını göstermektedir.

Örneklerin manyetik ölçümleri, manyetik alan uygulayarak (FC) ve alansız soğutma (ZFC) deneyleri ile yapılmıştır. Analiz sonuçlarından kritik sıcaklık, kritik akım yoğunluğu, ilinti uzunluğu, (Ginzburg-Landau parametresi olarak ta bilinir), hacim manyetizasyonu ve manyetik duygunluk değerleri elde edilmiştir. Örneklerin manyetik davranışı sıcaklığın bir fonksiyonu olarak gözlenmiştir ve faz geçiş sıcaklıkları belirlenmiştir. Kritik akım yoğunluğu bir süperiletkenin ne kadar yük taşıyabileceği ile ilgili önemli bir özelliktir. Bu parametre literatürde verilen modeller ile yaklaşık olarak hesaplanmıştır. Meissner etkisi görülen M-H ölçümlerinden ilinti uzunluğu ζ hesaplanmıştır. Sonuçlar, tetragonal yapıya sahip örneklerin katkılanan elementler için birim hücrede kolaylıkla yer alabilmesine olanak tanıdığını, ve süperiletkenlik özelliği gösterdiğini doğrulamıştır. Bu sayede nadir toprak grubu elementlerin tetragonal yapıya katkılanması, bu materyallerin sıfır direnç gösterme ve manyetik alan çizgilerini dışlama gibi özelliklere sahip olabileceklerini göstermişlerdir. Bizim çalışmamızda, platin ve lantanyum ana materyal olan $BaFe_2As_2$ örneğine katkılanmıştır ve örnek setlerimiz bu şekilde hazırlanmıştır. Direnç ölçümleri ile uyumlu olarak faz geçiş sıcaklığında ZFC-FC eğrilerinin ayrıldığı görülmüştür. Meissner Etkisi hem platin hem lantanyum katkılı örneklerde görülmüştür. Tüm örneklerde kritik akım yoğunlukları hesaplanmış ve manyetik ölçümlerden elde edilen faz geçiş sıcaklıkları bulunmuştur. Örnekler faz geçiş sıcaklığı olan T_c'nin altında süperiletken bölgededirler. Manyetik alanın fonksiyonu olarak mıknatıslanma (M-H), faz geçiş sıcaklığının altında bu bölgeler için bazı sıcaklıklarda ölçülmüştür. Analiz sonuçları ilinti uzunluklarının hesaplanmasında ve kritik akım yoğunluğu hesaplanmasında kullanılmıştır. M-H eğrilerinden elde edilen veri noktaları kullanılarak interpolasyonla ilinti uzunlukları kabaca hesaplanmış ve nm mertebesinde bulunmuştur.

Mıknatıslanma verisi birimi emu/g ’dan, birimsiz manyetik duygunluk verisine dönüştürülmüş ve manyetik duygunluk değerleri elde edilmiştir. ZFC ve FC eğrilerinin y ekseninde -1’e yakın yerlerde sonlanması örneklerin büyük oranda diamagnetik olduğunu göstermektedir. Örnekler genel olarak süperiletkenlik özellik sergilemişlerdir. ZFC-FC ölçümlerinden elde edilen faz geçiş sıcaklıkları, direnç verileri ile uyumludur. Lantanyum katkılı örnekler direnç ölçümleri ve manyetik sonuçların gösterdiği gibi açıkça süperiletkenlik özellik göstermişlerdir.

İnce film $BaFe_2As_2$ örnekleri hazırlandı ve X-ray kırınımı ölçümleri ile amorf yapı doğrulandı. 4.2-300K arasında sıvı helyumda direnç ölçümü yapıldı. Açık bir şekilde $T_c = 6.7K$’de süperiletkenlik faz geçişi görüldü. Direncin aniden sıfıra gittiği süperiletkenlik faz geçişi, ilk defa grubumuz tarafından görülmüştür. Bu sonuç oldukça ilginçtir çünkü süperiletkenliğin makroskopik teorisi (BCS), Cooper çiftlenme mekanizması üzerine kuruludur. Bu mekanizma kristal yapılarda görülmektedir. Biz burada süperiletkenlik fenomenini ince film örneklerde görmekteyiz. Bu şekilde dirençte gözlenen ani düşme filamenter süperiletkenlik olarak literatürde prensipte görülmüştür.

Bizim bu çalışmadaki farkımız ince filmlerde düzensizlik üretmemiz ve bu ince filmi amorf olarak elde etmemizdir. Bu işlem basit bir flaş buharlaştırma sisteminde vakum altında gerçekleştirilmektedir. Bu sonuç yöntem itibariyle önemlidir çünkü benzer örnekler sadece moleküler ışın büyütme yöntemi (MBE) ile elde edilebilmektedir. Laboratuvarımızda bu tür imkanlar bulunmadığından bu filmleri hazırlayabilmemiz, ölçüm yapmamıza imkan tanımıştır. Bazı çalışmalar, hem ince filmlerde hem toz örneklerde basınç altında süperiletkenlik gözlenebildiğini göstermiştir. Biz, çalışmamızda basınç olmadan normal koşullarda ince filmlerde süperiletkenlik gözleyebilmekteyiz. Bu sayede amorf yapıda elde edilen düzensizlik süperiletkenliği tetiklemek için kullanılan yöntemlerden biri olabilir. Örneklerin manyetik karakterizasyonu halen devam etmektedir ve uygun bir dergide yayınlanacaktır.

Süperiletken örnekleri hazırlamada herhangi bir başarısızlığa önlem olarak antimon katkılı örnekler hazırlandı. İlk önce $BaFe_4Sb_{12}$ örneği hazırlandı ve karakterize edildi. Bu örnek literatürde skutterudite örneği olarak bilinir ve termoelektrik olarak verimli bir malzemedir. Çalışmanın bu kısmında kimyasal sentezi başarılı olan örneklerde, termoelektrik ve manyetik özellikler incelenmek üzere platin katkılı $BaFe_{4-x}Pt_xSb_{12}$ (x = 0, 0.1, 0.2) örnekleri hazırlandı.

Termoelektrik (TE) malzemeler, genellikle çoğu atmosfere yayılan ısı enerjisinin bir kısmını elektrik enerjisi olarak geri kazanmada kullanışlı malzemelerdir. Bir termoelektrik üretecin verimliliği, doğrudan $ZT = S^2\sigma T/\kappa$ şeklinde tanımlanan ZT değerine bağlıdır. Burada S Seebeck katsayısı, σ elektriksel iletkenlik ve κ toplam termal iletkenlik ($\kappa = \kappa_e + \kappa_L$ olup, burada κ_e:elektronik katkı ve κ_L:örgü katkısı) ve T mutlak sıcaklığı ifade etmektedir. Verimli termoelektrik malzemeler, yüksek elektriksel iletkenliğe, yüksek Seebeck katsayısına ve düşük termal iletkenliğe sahiptir. Katkılı skutterudit bileşikler, bu özellikleri karşılamaktadır. Bu bileşiklerin termoelektrik ve magnetik özelliklerini iyileştirmek (özellikle *ZT* değeri) ve düşük sıcaklıklarda davranışlarını karakterize etmek amacıyla deneysel ve teorik bir çok çalışma yapılmıştır. RT_4M_{12} formülüne sahip katkılı skutterudite bileşikler (burada R = alkali toprak ve nadir toprak elementlerini, T = Fe, Ru, ve Os , M = P, As, ve

Sb ’u temsil etmektedir), hem termoelektrik özellikleri için hem de ilginç manyetik özelliklerinden dolayı ayrıntılı olarak çalışılmıştır. RT_4M_{12} örnek ailesine ait bir çok çalışma olmasına rağmen, manyetik ve termoelektrik özellikleri arasındaki ilişkiyi anlamaya yönelik çalışmalar halen yetersizdir.

Bu çalışmada skutterudite bileşiklerine platin katkılanarak $BaFe_{4-x}Pt_xSb_{12}$ (x = 0, 0.1, 0.2) örneklerinin sentezlenmesi amaçlanmış, düşük sıcaklık manyetik özelliklerin ve termoelektrik özelliklerin karakterize edilmesi üzerinde durulmuştur. X-ray kırınımı, direnç, manyetik ölçümler, Seebeck katsayısı ve termal iletkenlik ölçümleri yapılmıştır.

Sıcaklığa bağlı direnç tüm örneklerin 4.2 - 300 K aralığında yarı metalik davranış gösterdiğini sergilemektedir. Platin katkısına bağlı olarak dirençdeki artış, çeşitli saçılma mekanizmalarının (spin dalgalanmaları, Kondo safsızlıkları ya da azalan deşik konsantrasyonu) varlığı olarak öngörülmüştür. Spin dalgalanma mekanizmasının bir sonucu olarak kristal yapıda deformasyondan kaynaklanan 2-50 K arası logaritmik dirençte sıcaklığa bağlı kondo minimum gözlenmiştir. Seebeck katsayısındaki yerel minimum ve maksimum, bu materyallerde spin dalgalanma efekti veya paramagnon sürüklenme etkisine bağlı olarak gözlenmiştir.

x = 0.1 ve x = 0.2 örnekleri için para manyetik durumdan manyetik duruma iki geçiş gözlenmiştir. T_c = 48 K’de gerçekleşen bu geçiş, kısa erimli manyetik düzenden uzun erimli manyetik düzene doğru gözlenmiştir. Platin katkılı olmayan örnekte para manyetik bölgeden uzun erimli bölgeye sadece bir geçiş görülmektedir.

Termal iletkenliğin sıcaklığa bağlı analizinde, toplam termal iletkenliğin büyük kısmının örgü tarafından baskılandığı görülmüştür. Sıcaklığa bağlı Seebeck katsayısında, dirençte yerel maksimum ve minimumlar, Kondo minimumu şeklinde gözlenmiştir. Manyetik ve termoelektrik özelliklerin platin katkılı $BaFe_{4-x}Pt_xSb_{12}$ (x = 0, 0.1, 0.2) örneklerde spin dalgalanmasına bağlı olarak gerçekleştiği düşünülmektedir.

1. INTRODUCTION

Superconductivity is a phenomenon observed in some materials when they lose their electrical resistance at a critical temperature. Electrical resistance is zero below the critical temperature and the material conducts the electricity perfectly. A superconducting material have the ability to carry an electric charge along an infinite wire without corresponding any resistance. Also it blocks out magnetic field lines by providing surface currents because of the Meissner Effect. If we could control the mechanism at room temperature, it would be possible to transport electricity from Earth to a point in space without any losses, or to create fast computer circuits with no resistance, or to produce fast trains which have ability to travel without no friction.

Superconductivity takes place at extremely low temperatures, which makes it difficult to apply at ordinary temperatures. The temperature in which superconductive behavior is observed, T_c, namely superconductive phase transition temperature, is generally low on pure elements. In order to increase T_c to higher values, much works are done to synthesize new compounds and still going on. After the invention of new materials, physical relation between structural properties and reasons will facilitate to produce industrial products. Benefits mostly in medicine, engineering, defense industry are inevitable. The use of such materials yields to improve machinery and equipment production. Magnetic levitating trains with high costs are produced according to this technology. (MAGLEV: JR Tokai-Japan, Transrapid SMT: China (built in Germany), TGV: France etc.).

Since superconductor wire can carry much larger electric current than a copper wire, it has several advantages in conduction of current: The heat occurring during the operation of energy generating systems can be prevented. When the cause of fire is thought to arise from a single spark (or from a shortcut arising in a basic circuit) this is a dangerous problem for the companies having such systems in large areas around cities by bringing economical responsibilities. The usage of such cables having zero resistivity have significant importance because the decrease in heat by maximizing the efficiency at the core of a colossal coil is remarkable. After the discovery of giant magnetoresistance by Albert Fert and Peter Grünberg in 2007, scientific research projects and groups are grown up in the improvement and design of magnetic sensors. The progress resulted the production of commercial Superconducting Quantum Interference Devices (SQUID) , for scientific research purposes at physics, biology and some engineering areas which are sold by many companies all around the world. Superconducting materials also provide us to create high magnetic fields ($\sim$ 20T). Magnetic imaging devices in hospitals, Nuclear Magnetic Resonance (NMR) machines and particle accelerators & spectrometers are manufactured on the basis of this probe.

1.1 Purpose of Thesis

Cuprates (copper-oxide systems) and unconventional materials such as Fe-based 122 (Fe-As systems) pnictides (group V-B elements) have gained much popularity after the discovery of high T_c compounds. Iron-arsenide and copper-oxide layers are responsible from the superconductivity in the structure. Since Fe-As system has similar properties with Cu-O like having d electrons, layered structures and antiferromagnetic (AFM) spin ordering they are still earning interest. In addition to this, iron has a magnetic moment which plays a key role in superconductivity-magnetism relation. Up to now, two physical problems in our study are the superconducting phase transition temperature T_c and magnetic behavior of superconducting materials. Lattice changes, symmetry breaking, applying pressure are some of reasons that shift T_c up or down. For the magnetic behavior of superconductive samples, establishment of a new magnetic ordering is key parameter under the T_c. Magnetic changes are said to be affect superconductivity. The exclusion of magnetic field lines by Meissner effect is a clear evidence for superconductive mechanism. Our study is then focused on iron pnictide compounds on the basis of these two physical problem.

The most popular iron pnictide systems are Fe-As based ones. Our starting material $BaFe_2As_2$ has a tetragonal structure and it goes a structural phase transition from tetragonal I4/mmm to orthorhombic Fmmm lattice. Same behaviors are found in AFe_2As_2 (A:Ba, Sr, Ca, etc.) systems at low temperatures like in cuprates. It is named as spin density wave (SDW) transition and valid for both cuprates and iron-pnictides. A chemical change in composition with a dopant or applying pressure results magnetic transition in Fe-As compounds and thereby superconductivity emerges. By doping electron or hole to a AFe_2As_2 system like $BaFe_{2-x}Pt_xAs_2$, superconductivity can be observed. Since the change in chemical composition may effect the T_c, Lanthanum is doped to the $BaFe_{2-x}Pt_xAs_2$ system. And a new serie $Ba_{1-x}La_xFe_{1.9}Pt_{0.1}As_2$ samples are studied.

In case of any failure in preparing Fe-As layered samples, antimony doped compounds are prepared. $BaFe_4Sb_{12}$ sample is prepared first. This sample is known as skutterudite compound in literature and it is thermoelectrically efficient.

In this part of study, the understanding of relation between two phenomenon by characterization of low temperature magnetic and thermoelectric properties $BaFe_{4-x}Pt_xSb_{12}$ (x = 0, 0.1, 0.2) compounds are aimed.

1.2 Literature Review

Superconductivity is first discovered in mercury metal by cooling it with the help of helium liquefier system. Experimental set up is invented by Heike Kamerlingh Onnes in 1908. Onnes showed that the metal exhibited zero resistance to electric current at 4.2 K and called as "superconducting" in 1911 [1]. The discovery became the starting point for many further studies on several elements. Since such temperatures are close to liquid helium temperature, materials are not preferred for feasibility. The impact of the physics of a superconducting material can only be useful at high temperature applications. The tendency of researchers to find a high temperature superconductor then became compulsory. In 1960's, Niobium-Titanium (Ni-Ti) alloy [2] is found, that is a good candidate for superconductivity , showing a resistivity drop at 9.2K. Niobium-Tin intermetallic material was an alternative for higher magnetic fields. In 1986, J. G. Bednorz and K. A. Müller showed that Ba-La-Cu-O based ceramic materials have superconducting properties in 30K range [3]. In March 1987 , a revolutionary announcement is done by Paul C. W. Chu that a Yttrium barium copper oxide system (often abbreviated YBCO) is a superconducting at 93 K [4]. The contribution of this work paid much attention to temperature which is close to liquid nitrogen boiling point. In 1995, Dai showed that Thallium doping to the Hg based

1223 system has a superconductive phase transition at 138 K [5]. The H_2S compound synthesized by Drozdov has the highest T_c , 203 K at 155 GPa pressure [6].

Iron-based pnictide compounds have attracted great attention since the superconducting $La[O_{1-x}F_x]FeAs$ compound was discovered in 2008. Hideo Hosono and collaborates carried superconductivity in a new research area by iron-arsenide. Study received much attention that the superconductivity is triggered due to some deformations in crystal lattice. It is seen that layered iron-based compound, LaOFeAs [7] which undergoes superconducting transition under doping with F^- ions at the O^{2-} site; showed superconductivity at 26K at ambient pressure. The Fe-based superconductor system is very similar to the high-T_c cuprates, however the superconducting pairing mechanism in the iron-based superconductors remains elusive. LaOFeAs systems consist Fe-As layers this is because why they are named as "layered structure". This study directs the ongoing research from ordinary CuO_2 conduction units to iron-based oxypnictides, which mainly differs from the works that done up to 2008. $BaFe_2As_2$ sample is prepared by Rotter et. al. [8] in same year. The correspondence of same resistivity value with the LaOFeAs at room temperature in magnitude was remarkable. They then studied the K doped $BaFe_2As_2$ system [9] and showed that it is superconductive at 38 K. They proved that $Ba_{0.6}K_{0.4}Fe_2As_2$ sample is nearly a perfect diamagnet ($\sim$ %94). Following their study, Saha [10] (in single crystals-T_c= 23 K) and Guo et. al. (polycrystalline sample-T_c= 24.2 K) [11] are succeed to prepare Pt doped $BaFe_2As_2$ sample and hence the superconductivity is observed. Guo also said that electron-phonon coupling is meaningless in the $BaPt_xFe_{2-x}As_2$ samples at superconducting state. Boeri et. al. [12] made density functional theory calculations and they showed that electron-phonon coupling is too weak in the pnictides to account for the high-T_c's. C.W. Wu and B.Lorenz made review of high pressure studies on Fe-pnictide superconductors [13] and discussed different classes of doped and undoped FeAs-compounds: ROFeAs (R = rare-earth), AFe_2As_2 (A = Ca, Sr, Ba), and AFeAs (A = Li, Na). Their idea was to examine the if the electronic states are modified under pressure and search how can this effect the T_c in rare-earth doped materials. LaOFeAs structure differs from tetragonal $BaFe_2As_2$ unit cell and has P4/nmm symmetry. This unit cell consists Fe-As and LaO layers. Here Fe-As are responsible from charge carriers and LaO layers are said to be reservoirs for the blocking the charge. Both layers are sandwiched together and the integrity of the mechanism is supplied by this way it is reported.

Current research in literature is focused on high T_c superconductivity (HTS). But the reason for change in phase transition temperature, the physical problem that arises superconductivity mechanism is examined in more detail. It is widely believed that superconductivity is mediated by magnetic fluctuations rather than by electron-phonon coupling as in conventional superconductors. But the relation between superconductivity and magnetism are still under debate [14–17]. Studies are mostly focused to show if there is a host mechanism or not as mentioned by explaining layered structure above. Since the magnetic order and change in lattice should be responsible for superconductive behavior, the existence of structural and magnetic properties are examined.

In addition to superconductive samples, Sb doped sample series have common role in energy efficient systems. Similar to zero resistivity behavior in superconductors, Ba-Fe compounds have thermoelectric properties as well. Since an important part of energy used in all world is rejected to atmosphere as industrial wasted heat, it is a smart way to use thermoelectric (TE) materials to capture a part of this wasted energy and convert it into the useful electrical power [18, 19]. The efficiency of a TE generator is strongly depending on the dimensionless figure of merit ZT, defined as $ZT = S^2\sigma T/\kappa$ where S, σ and κ are the Seebeck coefficient, electrical conductivity, total thermal conductivity ($\kappa = \kappa_e + \kappa_L$ where κ_e is the electronic contribution and κ_L the lattice contribution) and T stands for the absolute temperature. Efficient thermoelectric materials are required to have high electrical conductivity, high Seebeck coefficient and lower thermal conductivity. Filled skutterudites fulfill these requirements [20, 21]. The term "filled" here is used to emphasize the interplay between filler ions and host structure constructed by transition metals in the lattice. The chemical formula usually given by RT_4M_{12} where R = alkaline earth and rare earth metal, T = Fe, Ru, and Os and M = P, As, and Sb have been studied extensively due to their both high TE performance and exotic magnetic properties [22–24]. In the past decade years, experimental and theoretical tremendous effort have been conducted on skutterudites compounds in order to optimize their TE and magnetic properties for enhancing ZT value further and characterize low temperature behavior [24–32]. There is still lack of understanding about correlation between magnetic and thermoelectric phenomena for these compounds.

1.3 Hypothesis

The superconductivity behavior is the key parameter according to the some physical properties observed from several measurements. These are phase transition temperature, T_c; the changes in unit cell according to the doping ion, critical current J_c, coherence length ζ and the comparison of phase transition temperatures obtained from both resistivity and magnetization experiments.

In this study, polycrystalline $BaFe_2As_2$ sample, platinum doped samples of $BaFe_{2-x}Pt_xAs_2$, lanthanum doped $BaFe_{2-x}Pt_xAs_2$ samples and thin films are synthesized. The measurements to be performed on samples are focused on the observation of superconductivity phenomena according to resistivity and magnetic measurements.

Up to now most of work is done on superconductor materials was about crystals. Symmetry break due to temperature and phase change are observed. And many theories are constructed on the behavior of a superconductor; suggesting the coupling of electron pairs over hundreds of nanometers. Since it is the manner of two electron system, it is bosonic and called as Cooper Pair mechanism. It is still an interest for researchers that how can an a material having crystal structure produce pairs. A material having long range order should behave superconductive according to theoretical description. In contrast to ordered crystal structure, this behavior is not understand when an amorphous material with short range order behaves superconductive.

Objectives in this study are to examine the expectation about the transition temperature, T_c, its relation with doping ions, possibility to have higher values in iron pnictide systems. The changes in critical current J_c, coherence length ζ are also basic questions that we struggle to answer. For a thin film samples our targets are to prepare $BaFe_2As_2$ thin film under vacuum and investigate if the material is amorphous or crystal. If it behaves superconductive, what are the causes: like substrate, thickness, availability to take control on T_c if it shifts towards higher values. Experiments will be tested on ceramic substrate, and will be repeated on several annealing temperature at different temperatures. To discover if there is any relation between crystal structure parameters and thin films created from these samples like lattice constant, symmetry, volume etc. The observations showed that:

I. Magnetism and superconductivity are closely related to each other.

II. Special attention should be paid to the pressure conditions to extract meaningful data.

III. The intriguing temperature-pressure phase diagram needs further study to extract possible important information concerning not just superconductivity but also the physico-chemical formation of the Fe-pnictides that may lead to higher T_c .

If some clues are found, the origin of our research in high T_c superconductivity will be presented in iron-based superconductors, oxide systems (La-O), their magnetic structure and the role with the superconductivity.

Second part of the study is constructed on the thermoelectric properties of Ba-Fe based bulk samples. Besides having superconductive property, these materials are energetically efficient for recovering wasted heat energy to transform electricity. Sample family $BaFe_{4-x}Pt_xSb_{12}$ has a relatively high figure of merit, ZT; higher than 1 providing this property. Skutterudite samples have a filler ion (like a rare earth element in RT_4M_{12}) and they have low thermal conductivity. In addition to high electrical conductivity and high Seebeck coefficient; this property increases ZT value in skutterudite compounds. In this part of study, the effects of platinum doping in to $BaFe_4Sb_{12}$ material will be discussed. The main physical problems are:

I. to synthesize $BaFe_4Sb_{12}$ material by doping platinum with the same unit cell,

II. to reveal the relation between resistivity behavior and magnetic ordering,

III. to search if thermoelectric materials have magnetic property.

If they have such properties, a change in thermal conductivity or Seebeck coefficient should be observed in magnetic behavior simultaneously. Since relation is not known extensively in the correlation between magnetic and thermoelectric phenomena for these compounds, expectations given above should help understanding the nature of these kind of materials.

2. BASIC CONCEPTS OF SUPERCONDUCTIVITY

Some remarkable properties are evident with superconductivity.

I. When a current flows through a superconductor (SC), it behaves like it does not encounter a resistance inside.

II. A superconductive material has a perfect diamagnetic behavior. A superconductor in thermodynamic equilibrium, produces surface currents at a few T magnetic fields. Such surface currents create additional magnetic field and compensate the external magnetic field.

III. The energy gap of 2Δ is produced in a superconductor in allowed fermi energy level. e^{-}'s having an energy of ε will play an important role in superconductivity process.

2.1 Critical Temperature

Metals have normal behavior above critical temperature, $T > T_c$. But at$T < T_c$, they show superconductive behavior.T_c normally changes between mK ($10^{-7} eV$) to 20K (10eV) temperature (E=k_bT) interval.

2.2 Non-Damping Current

Resistivity in a normal metal and superconductor is shown in Fig 2.1. ρ_0 is responsible from remedial resistance and e^{-} scattering from impurities; BT^5 is responsible from the scattering of phonons. But for $T < T_c$, this mechanism is dominated by the non-damping currents. Superconducting currents are exist together with the non-damping current but superconductivity is destroyed if;

I. high magnetic fields are applied,

II. the current is higher than the critical current,

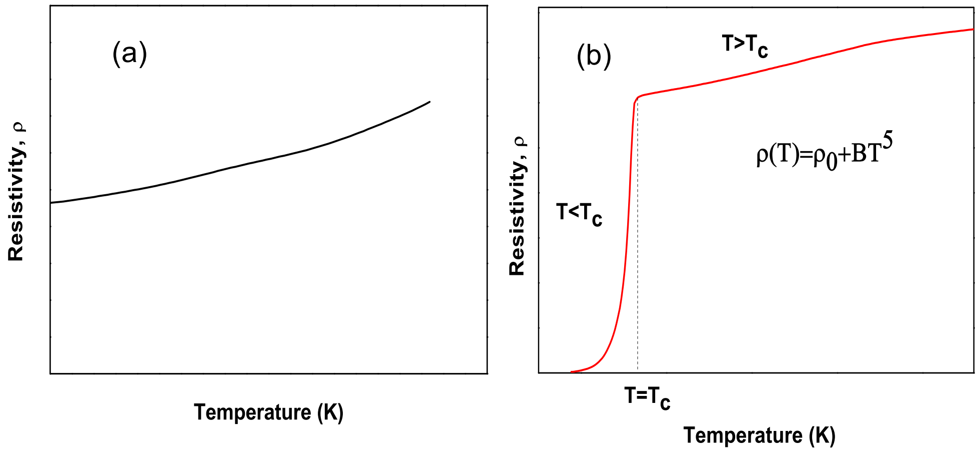

Figure 2.1 : Resistivity of (a) metal, (b) superconductor.

III. critical current is on the order of 100A passing through $1mm^2$ crossectional area of a wire.

Critical current has a dependence on critical magnetic field occurred on the surface of the material as well. Surface is degenerated above the critical magnetic field. If $T <<< T_c$, then non-damping currents survive at low frequency electromagnetic field. The limit for current between normal state and non-damping state has a frequency dependence as follows:

$$\omega \sim \frac{\Delta}{\hbar} \tag{2.1}$$

2.3 Thermoelectric Properties

Conduction of heat is usually takes place by the molecular vibration in a material in a wide range temperature interval. In the independent electron approximation good elecrtical conductors are also good conductors of heat because the conduction electrons transport entropy as well as electric charge. Superconductors, contrary to this are poor thermal conductors [33]. In this manner they exhibit no Peltier effect. Electrons in which participate non-damping currents carry no entropy. Only a fraction of conduction electrons are responsible from the transport of the entropy in superconductors. The absence of Peltier effect indicates that the non-damping currents do not contribute the heat transfer. Such poor heat conductance observed in superconductors is because only small amount of e^- play a part. Non-damping currents at $T < T_c$ regime never contribute to the heat transfer.

2.4 Magnetic Properties:Perfect Diamagnetism and Critical Field

Magnetic field cannot penetrate to the superconductor volume unless it is too high. An example for this behavior is observed in Meissner-Ochsenfeld effect. If the temperature of a metal is decreased below T_c, magnetic flux is excluded from the sample. Transition about T_c takes place in the volume of superconductor material where surface currents produce their own magnetic fields. According to the Faraday's law of induction, vortex currents occur in a perfect conductor and make magnetic field zero inside the conductor volume. If $\vec{H}$ exists in a conductor's volume (for non-diamagnetic materials), surface currents responsible from this field prevents magnetic field lines to enter the conductor volume. So perfect conductivity realizes time-independent magnetic field inside conductor. But in a superconductor $\vec{B} = 0$ inside the material [34, 35]. Hence the magnetic susceptibility is then equal to:

$$\begin{aligned} \vec{B} = 0 = \vec{H} + 4\pi\vec{M} \quad (CGS) \\ \chi = M/H = -1/4\pi \end{aligned} \tag{2.2}$$

in a superconductor which shows perfect diamagnetism. Consider a superconducting material is placed in a magnetic field. Then a significant amount of energy is spent for shielding currents at $T < T_c$. Shielding currents cause magnetic field to be zero in superconductor volume. If the applied external field is big enough, sample turns back to its metallic state. Since it is energetically favorable, magnetic field is able to penetrate into the volume of a metallic sample. Energy of a normal state is bigger than the superconductor state. The difference between these two regime is balanced by the shielding currents originated from the decrease in the energy of magnetic field. Superconductors are classified in two types according to their responses in magnetic field: type I and type II.

2.4.1 Type-I superconductors

Magnetic field below the critical temperature T_c is increased. Lower part of the curve in fig. 2.2(a) denotes superconductor phase where the upper part shows metallic state. Magnetic flux do not enter the sample unless $H > H_c$. Above the critical field,

field lines are allowed to diffuse the sample in which the sample is in metallic state. Magnetization as a function of external field is shown in fig. 2.2(b). Magnetic field is about 100 G in type I superconductors which is the limit between the metallic and superconductive phase. Normal metals like mercury, aluminum, lead etc. are type-I superconductors.

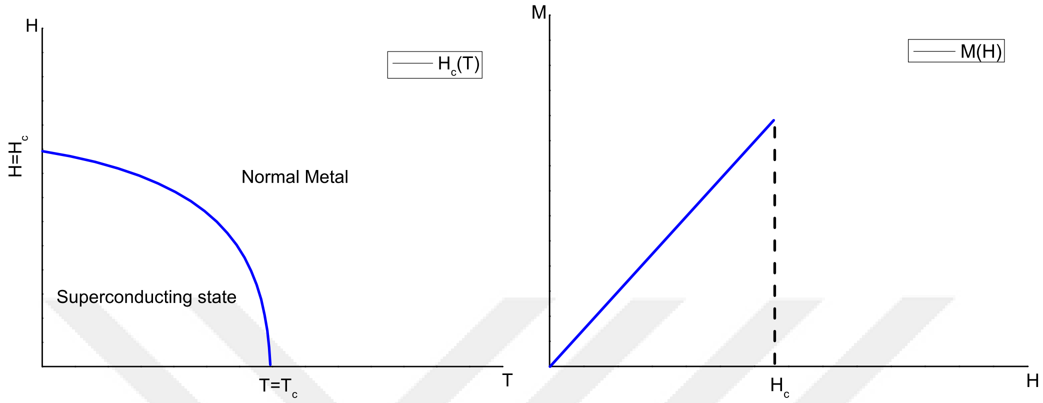

(a) (b)

Figure 2.2 : (a) Magnetic field as a function of temperature, (b) Magnetization as a function of applied magnetic field in type I superconductors.

2.4.2 Type-II superconductors

Type II superconductors have two critical field, H_{c1} and H_{c2}. Magnetic field behavior changes according to the strength of these fields. If $H < H_{c1}$ then magnetic field cannot enter the sample (left part-lower limit of the fig.2.3a). If $H > H_{c2} > H_{c1}$, magnetic flux Φ_H is fully penetrated inside the material (right part upper limit of fig. 2.3(a)). For $H_{c2} > H > H_{c1}$ (mid-regime), sample is exposed to partial diffusion of magnetic flux which is a bit complicated in type-II superconductors. Normal and superconductive regions now construct mixed microstructures inside the material. Magnetic field is now exist inside in the form of vortices. This hypothesis proposed by Alexei Abrikosov in 1957 is proved by experimentally.

Vortices are demonstrated in ellipsoidal shape in fig. 2.3(b). Superconductive regions are now created and vortices are separated with the green line. Magnetic field can "partially penetrate" in this mixed state but definitely zero at the middle point of a vortice. Material behaves superconductive in red shaded region and it behaves metallic inside (grey color region). Current loops creating this separation occur on the green lines, which are the main reason that prevents magnetic field lines to penetrate

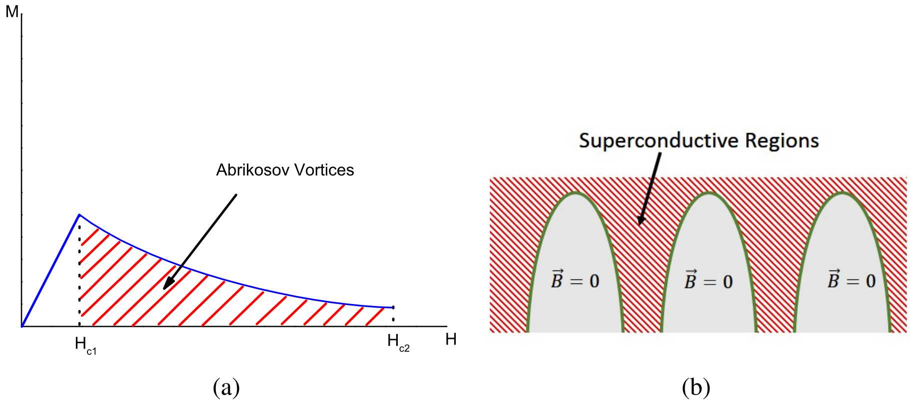

Figure 2.3 : (a) Magnetic field as a function of applied field and Abrikosov Vortices limit (b) Superconductive regions surrounding vortices in type-II superconductors.

inside the material. The order of magnetic field to create these vortices in type-II superconductors is about 10^5 G.

2.5 Thermodynamics of Superconductivity

The exclusion of magnetic field lines as explained above results a change in energy since the magnetic state is diamagnetic inside and paramagnetic in the outside of the sample. So the increase in energy due to exclusion of magnetic field is compensated by Gibbs Free Energy described below:

$$G = F + PV = E - TS \quad dG = dF + PdV$$
$$dG = dE - TdS - SdT \tag{2.3}$$

Gibbs free energy is a potential energy. If sample is tought as cylindrical,

$$G(B,T) = G_s(0,T) - \int_0^B MdB \qquad \vec{B} = \mu_0 \vec{H}$$
$$G(B,T) = G_s(0,T) - \int_0^B \frac{BdB}{\mu_0} = G_s(0,T) + \frac{B^2}{2\mu_0} \tag{2.4}$$

The term $B^2/2\mu_0$ here represents the amount of additional magnetic energy to exclude field lines from the sample. If weak magnetization is ignored, Gibbs Free Energy for the normal condition is $G_N(B,T) \sim G_S(0,T)$ so,

$$G_N(B,T) - G_S(0,T) = \frac{B^2}{2\mu_0} \tag{2.5}$$

This energy is the condensation energy of the superconducting state at the phase transition.

$$S = -(\frac{\partial G}{\partial T})$$
$$\delta S = S_S - S_N = \frac{1}{2\mu_0} 2B_c \frac{dB_c}{dT} = \frac{B_c}{\mu_0}\frac{dB_c}{dT} \tag{2.6}$$
$$C = T\frac{\partial S}{\partial T}$$

per unit volume at zero magnetic field

$$\triangle C = C_S - C_N = \frac{T}{2\mu_0}\frac{d^2}{dT^2}(B_c^2)$$
$$\triangle C = \frac{T}{\mu_0}[B_s \frac{d^2 B_c}{dT^2} + (\frac{dB_c}{dT})^2] \tag{2.7}$$

$dB_c/dT > 0$ at the phase transition point.

I. Entropy difference is zero since $dB_c = 0$ at the T_c.

II. $\triangle S = 0$ if T=0 from the first law of thermodynamics. So $\triangle C = 0$ (Nernst Theorem).

III. $dB/dT < 0$ for a temperature providing $0 < T < T_c$. And $\triangle S < 0$, which shows that the superconducting phase is more stable than the normal phase.

IV. $\triangle S$ is finite at $T < T_c$. Transforming heat of a superconducting phase transition inside a finite magnetic field is presented as T$\triangle S$.

2.6 London-London Equation and Penetration Depth

Londons (Fritz and Heinz London) qualitatively showed that $\vec{H}$ can not penetrate inside the superconductor volume for the first time. They revealed this relation by taking basis of Gorter and Kazimir's two fluid model.

When we assume that some part of e^-'s are in superconducting current, $n_s(T)/n$ at $T < T_c$. $n_s(T)$ converges to n if $T <<< T_c$. $n_s(T)$ goes to zero if T is close to T_c. Electrons probably construct a fluid behavior $n - n_s$. Normal metal conducts the current with heat dissipation. Here $n - n_s$ stands for dissipative and n_s stands for non-dissipative number of e^-'s in two fluid model. Superconducting current does not encounter resistivity and conducts current even at small perturbations of magnetic field. Normal e^-'s are more mobile than the superconducting e^-'s. Lets assume that an electrical field $\vec{E}$ is applied, superconducting e^-'s accelerate and their average speed is then defined by:

$$\frac{mdv_s}{dt} = -eE$$
$$\vec{J} = -e\vec{V}_s n_s \quad \vec{V}_s = -\frac{\vec{J}}{n_s e} \tag{2.8}$$
$$\frac{d\vec{v}_s}{dt} = \frac{n_s e^2}{m}\vec{E}$$

Frequency dependent conductivity in the Drude model for the electron gas having n_s was:

$$\vec{J}(\omega) = \sigma(\omega)\vec{E}(\omega) \quad \sigma(\omega) = \frac{in_s e^2}{m\omega} \tag{2.9}$$

If we substitute eqn. (2.8) into Faraday's Law of induction, we get:

$$\vec{\nabla} x\vec{E} = -\frac{1}{c}\frac{\partial \vec{B}}{\partial t} \quad \frac{\partial}{\partial t}[\vec{\nabla} x\vec{J} + \frac{n_s e^2 \vec{B}}{mc}] \tag{2.10}$$

$\vec{B}$ and current $\vec{J}$ is defined as follows for a perfect metal:

$$\vec{\nabla} x\vec{B} = \frac{4\pi\vec{J}}{c} \tag{2.11}$$

Static current defined in e static magnetic field can not be seen in superconductors. The idea of Londons' equation is explaining the characteristic behavior of superconductors. Eqn 2.10 figures out that the rotational of current $\vec{J}$ and additional term have no change in time, this means it is time independent and must be zero. So,

$$\vec{\nabla} x\vec{j} = -\frac{n_s e^2 \vec{B}}{mc} \tag{2.12}$$

Equation 2.12 explains the current without dissipation in a superconductor and is known as London-London equation. Meissner effect is also derived from the Londons' equation. By taking the rotational of both sides in eqn. 2.12:

$$\vec{\nabla} x\vec{\nabla} x\vec{j} = \vec{\nabla} x[-\frac{n_s e^2 \vec{B}}{mc}] = \vec{\nabla} x\vec{B}[-\frac{n_s e^2}{mc}]$$
$$\vec{\nabla}^2 \vec{J} = -\frac{4\pi n_s e^2}{mc^2}\vec{J}$$
$$if \quad \frac{1}{\Lambda^2} = \frac{4\pi n_s e^2}{mc^2} \tag{2.13}$$
$$\Lambda = [\frac{mc^2}{4\pi n_s e^2}]^{1/2}$$

Here Λ is defined as London penetration depth which means that current and magnetic field can only survive at a layer in a thickness of Λ. Usually penetration depth is in the order of $10^2 - 10^3$Å at the temperatures far below T_c.

2.7 Microscopic Theory of Superconductivity: BCS Theory

This theory is based on the existence of an effective attraction between e^-'s near Fermi surface. As a result of their responses against ion vibration, phonons' behavior can be categorized as small amounts of heat. But phonons cannot response to e-vibration where as ions can perform. Ion movements is the key parameter in this theory that occurs in superconductors. The dependence of critical temperature T_c with mass is related by ${m_{ion}}^{-1/2}$ in superconductors and such relation proves that ions have dynamical role. Since ion movement is depend on e^- movement, an attractive potential will be created between e^-'s having wave vectors of $\vec{k}$ and $\vec{k}'$. Attractive potential is then given by:

$$V_{eff.} = \frac{4\pi e^2}{q^2 + K_0} \frac{\omega^2}{\omega^2 - \omega_{\vec{q}}^2} \tag{2.14}$$

where ω show frequency, K_0 is Thomas-Fermi wave vector, $\vec{q}$ is the difference between e^-'s wave vectors, $\omega_{\vec{q}}$ is phonon frequency with $\vec{q}$ wave vector. As a result of this relation, e^- having same energy results an attraction on each other implementing the basic idea of superconductor theory. Energy difference of e^-'s are higher than the $\hbar\omega_p$ energy. Effective attraction is then provided by that of $\hbar\omega_p$ energy difference and thereby e^- couples are formed. Cooper attributed this attraction due to two electron's interaction and based the idea to the existence of the Fermi sphere. Because Fermi sphere can be exist only as a result of Pauli principle. Main aspect for the BCS theory is that the ground state is formed by the bound e^- couples in which it is more generalized form compared with the Cooper model. As a result, two assumptions are made for superconductors for the microscopic theory:

1. Free e^-'s are used for the conductance and the existence of the band structure is considered.

2. Equation 2.14 basically describes an effective V potential near the Fermi surface where the e^-'s are attractive.

2.8 Critical Current and Coherence Length

Critical current of samples is calculated from the M-H measurements of samples below the critical temperature, T_c. Kim model and Bean model are available for the critical current calculations in type II superconductors. Kim model which is predicted for magnetization of type II superconductors [36]. Schematics given below in Fig. 2.4 , shows how magnetic field encounters with sample geometry. The formula used for the

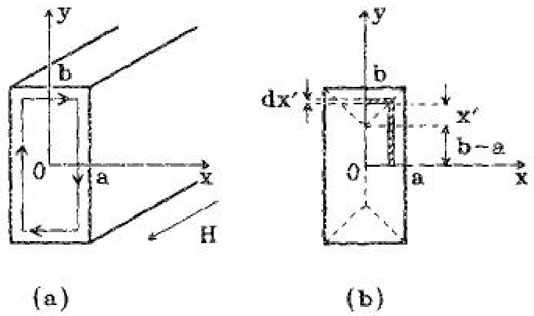

Figure 2.4 : (a) Sample configuration (b) supercurrent path. [36].

calculation for orthorhombic samples is:

$$J_c(H) = 20\frac{\Delta M(H)}{a(1-\frac{a}{3b})} \tag{2.15}$$

Since our samples have cylindrical geometry, we calculated critical current J_c by using the Bean model assuming to have a cylindrical shape with radius r=2 mm [37].

$$J_c(H) = 30\frac{\Delta M(H)}{d} \tag{2.16}$$

C. Bean also reports several assumptions starting from the constant field, time independent penetration of the external applied field etc. Below formula is obtained from the field independent magnetization values upon Bean's suggestion. The study emphasizes that this can be an "estimation" and actual values may change according to the current flow that passes through the material and its shape as well.

Coherence length ζ is also calculated for the samples as reported in the literature [38, 39].

$$\zeta = \sqrt{\frac{\Phi_0}{2\pi H_c}} \tag{2.17}$$

Actually H_c shows $H_c(0)$ namely the upper critical field obtained at T=0 K. Since such measurement can not be possible, H_c readings are obtained from different measurement temperatures from the M-H curves of samples measured below the T_c and extrapolated to T=0 K. Φ_0 is the magnetic flux quantum and equal to $2.0679 \times 10^{-15} Gm^2$.

3. EXPERIMENTAL

3.1 Bulk Samples

Polycrystalline samples of $BaFe_2As_2$ and platinum doped $BaFe_{2-x}Pt_xAs_2$ sample group, $Ba_{1-x}La_xFe_{1.9}Pt_{0.1}As_2$ sample group were prepared by a solid-state reaction method. High purity ($\geqslant 99.95$ %) elements bought from Sigma Aldrich were weighted and then mixed according to the desired stoichiometry. All samples were then pressed into pellets. The press equipment (15000 kg) is shown in Fig. 3.1 (a).

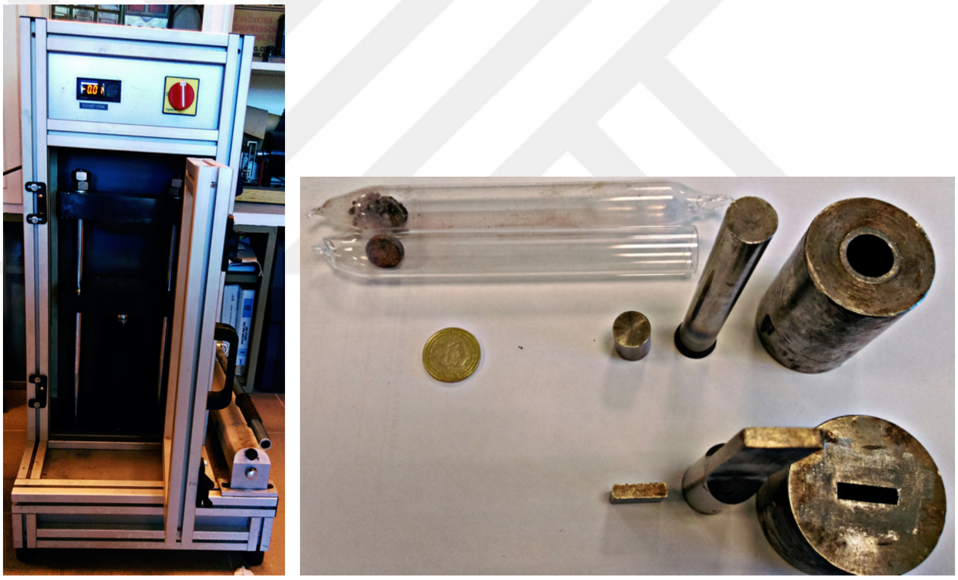

(a) (b)

Figure 3.1 : (a) Press, (b) Quartz tubes, pellets and cylindrical shapers for sample sealing.

Obtained pellets were loaded in a quartz tube and sealed under 1/3 atm of Ar gas. Pellets ready for sintering in quartz tubes before heat treatment are shown in Fig.3.1(b). The samples were held first at 873 K for 24 hours, then the temperature was increased to 1273 K and held for 72 hours. The compacted pellets were sealed in every heat process by quartz tubes under rough vacuum. After that samples were loaded into the furnace for second heat treatment and the temperature of furnace arranged to 1273

K for 24 for a further annealing process. The resulted samples were cut in different diameters for resistivity and magnetism measurements.

Pt doped skutterudite compounds, $BaFe_{4-x}Pt_xSb_{12}$ (with $x = 0, 0.1, 0.2$) were prepared by a solid-state reaction method as well. High purity Ba (99.95%), Pt (99.99%), Sb (99.95%) and Fe (99.99%) were mixed in ratio of their stoichiometry. Then samples were ground and pressed into a pellet. The pellet was then loaded quartz tube and sealed under the vacuum of 1/3 atm of Ar gas pressure. The quartz tubes were placed in furnace then heated to 873 K in rate of 40 K/hour and then hold there for 40 hours to complete the reaction. The furnace was finally turned off and cooled to room temperature. The ingots were ground into a fine powder and loaded into a cylindrical graphite die for spark plasma sintering under a dynamic vacuum. The powders were first cold pressed under a pressure of 50 MPa then the pressure was reduced to 10 MPa. The samples were heated under this reduced load at a rate of 50 K/min to a final temperature of 913 K at which point the uniaxial pressure was increased to 50 MPa, with a subsequent isothermal/isobaric hold for 10 min. The power was shut off and the pressure removed and the sample was allowed to cool to room temperature over the course of 2 hours.

(a) (b)

Figure 3.2 : Owens used for solid state reaction synthesis; (a) programmable, (b) manual controlled.

3.2 Thin Films

A flash evaporation system is given in Fig. 3.3(a). System is designed to make films as a result of evaporation of powders directly to films held by the grids, shown in Fig. 3.3(b). Vacuum part consists of a rough pump, a diffusion pump and vacuum chamber made by glass. Rough pump gauge and ion gauge are used to observe vacuum inside. Exhaust is carried outside of the laboratory by the help of a silicon pipe.

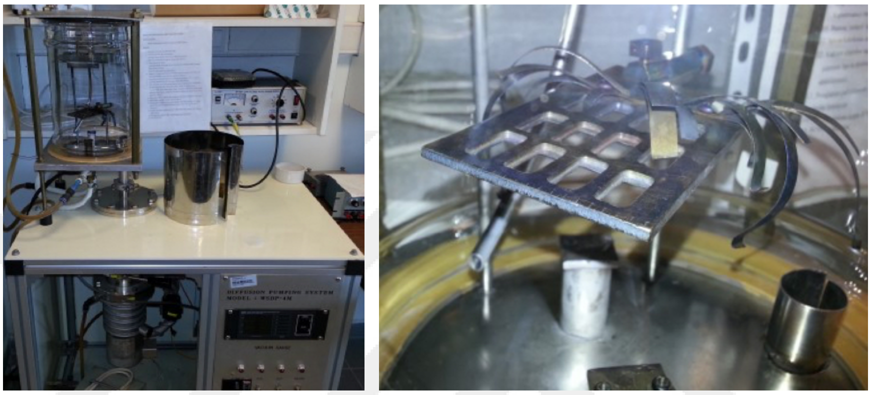

(a) (b)

Figure 3.3 : (a) Flash evaporation system, (b) Grids for films.

Rough pump is able to decrease vacuum inside the chamber down to 10^{-3} Torr. Water cooled diffusion pump starts to work at this stage. When main valve is open, it reduces vacuum down to 10^{-6} Torr ($\sim 10^{-7}$ if sealed well). Quartz plates are used as substrates. A sample film and a mask are shown in Fig. 3.4(a). Electrically motorized

(a) (b)

Figure 3.4 : (a) Sample mask and a film on quartz,(b) electrically motorized part.

part has holes at the bottom. These tiny containers are made to be hold for powder. The system made from cylindrical metal stands at the top and is shown in Fig. 3.4(b).

It consists a powder container depicted in Fig. 3.5(a), and a switch for hand control. It is designed to release powder on to filament by minimum loss. This handmade technic provides us to control powder amount when empty hole overlaps with powder filled containers. Particles flowing on to incandescent filament move towards to the gravitation (Figure 3.5(b)). Because of its high temperature, powder evaporates before it reaches to the tungsten filament. Finally quartz substrates are coated by evaporation and thin films are obtained.

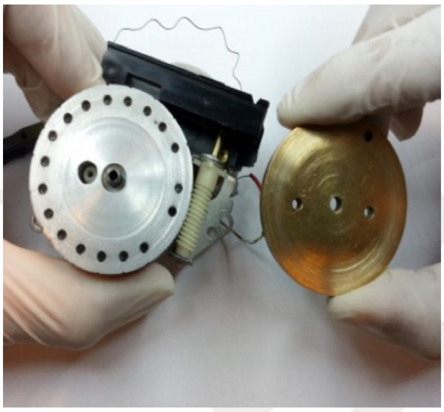

(a)

(b)

Figure 3.5 : (a) Bottom view of electric motorized part and its holes, (b) metal pipe targeted to release powder directly on the tungsten filament.

XRD (X-Ray diffraction), resistivity, magnetic and thermoelectric properties of obtained samples were measured. Commercial Rigaku diffractometer for XRD measurement and Quantum Design PPMS (Physical Property Measurement System) were used for structural and magnetic characterization respectively. Resistivity and thermoelectric properties of samples were measured in handmade experiment set ups.

Four-probe resistivity measurements are done between 77- 300K temperature interval. Experiment set up and data acquisition scheme is shown in Fig. 3.6. Two types of handmade sample holders, used for measurements are shown in fig. 3.7(a) (for liquid nitrogen) and in fig. 3.7(b) (for liquid He) respectively. Their dimensions are designed to fit for liquid nitrogen and liquid He dewars. Every sample holder has eight wires; two of them drives current (plus and minus) and two of them reads. A Keithley 6221 source meter was used to drive current and HP Agilent 3458A multimeter was used to read potential difference. Lakeshore A340 temperature controller was used for temperature control, which has a sensor giving different resistance readings at different

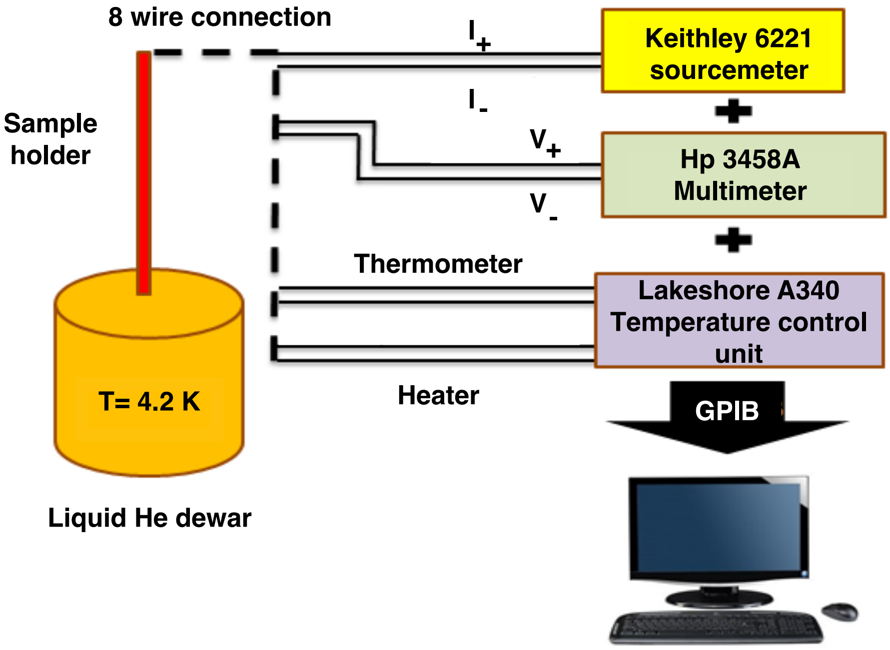

Figure 3.6 : Data acquisition scheme.

temperatures. It has current – voltage terminals as well. Last two cables are connected to the heater. Total of eight cables work on the system. A lab view script controls inputs like; current, data read interval, ramp (when heater is connected), PID values, data file name and location. All data obtained during measurement were registered realtime. Data were processed via computer. Samples were connected into holders

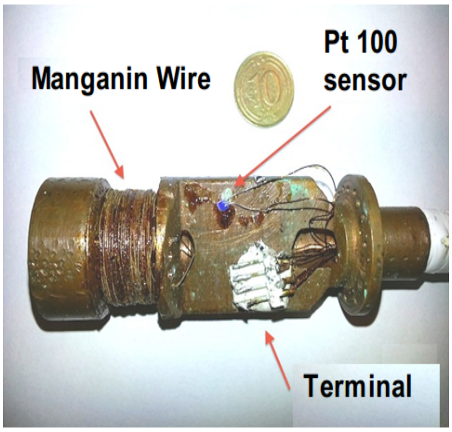

(a)

(b)

Figure 3.7 : Sample holders used in resistivity measurements designed for (a) liquid nitrogen, (b) liquid helium.

by the help of cold epoxy. The bottom of metal stick consists a copper made sample holder. Since it is designed to measure four-wire method to measure resistivity, eight wires used in the experiment can be seen on the holder. Connection cables are fixed to terminal which is located on heat conductive part. A platinum sensor (Pt100) is used for temperature control for the sample holder used in fig. 3.7 (a). Platinum itself has a resistance about 107 Ω at room temperature. They are used over a wide temperature range (from -200 to +850°C). Pt100 sensors are stable down to 55K temperature. Last two wires are connected to the manganite wire, which has a temperature independent resistivity (95Ω). This part is used as heater. A carbon-glass sensors is used for sample holder shown in fig. 3.7(b) in order to sense temperature during experiments in liquid He. Fig 3.8(a) shows glass cryostat with vacuum jacket for resistivity measurements

(a)

(b)

Figure 3.8 : (a) Hand made glass cryostat with vacuum jacket for liquid He sample holder, (b) cryostat fixed on helium dewar.

in liquid He. Such design is required to control temperature changes. Cooling is done spontaneously and heating is done by heater. When system is under rough vacuum ($\sim 10^{-3}$ Torr), temperature decreases smoothly and system starts to measure. Compact view of system when cryostat is fixed to liquid He dewar is given in Fig 3.8(b). Measurements for resistivity are done under rough vacuum using this system.

Low temperature electrical conductivity (σ), Seebeck constant (S) and thermal conductivity measurements were performed realtime by using longitudinal four-point steady state technic [40]. The diagram is shown in fig. 3.9. A temperature controlled cryostat was used during the experiment made in liquid helium. Samples were fixed into the holder in rod shape with $2\times3\times10$ mm dimensions.

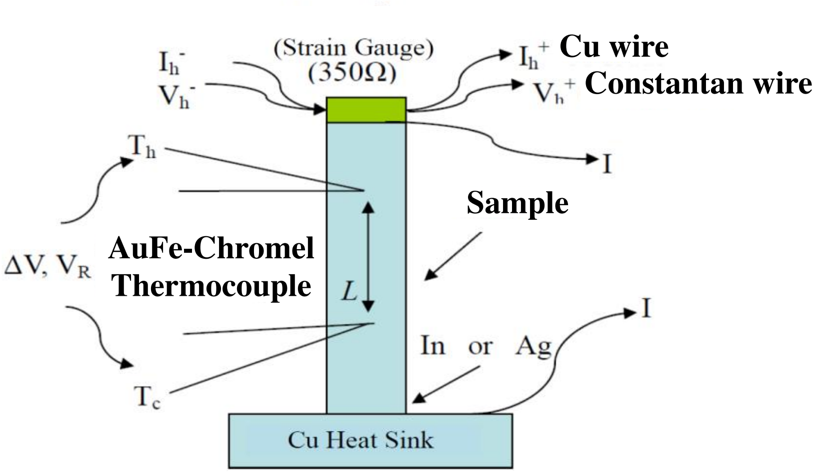

(a)

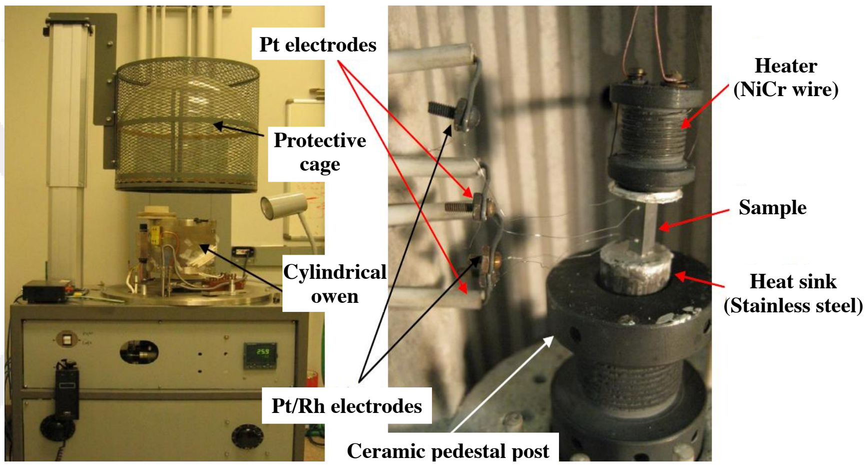

(b)

Figure 3.9 : (a) Low temperature electrical conductivity, thermal conductivity measurement system, (b) High temperature Seebeck and electrical conductivity measurement system [40].

In order to minimize heat loss by radiation, two cylindrical and concentric copper rods are used during the experiment made under 10^{-7} Torr vacuum. Rod shape sample is fixed by an adhesive having high thermal conductivity. The heater is connected above the sample (strain gauge in the fig. 3.9(a)) which has a 350 Ω resistance. The power as a result of driven current through the sample and potential reading will be P=IV. The temperature difference of material between hot and cold edges was measured by the help of AuFe-Chromel thermocouple. Since it has low resistivity and low Seebeck constant, thin copper wires (fig. 3.9(b)) were used to measure Seebeck potential and resistivity. The total thermal conductivity when the temperature difference is very low (assuming $\Delta T \leq 0.05$ and $\Delta T = (T_h + T_c)/2$) is given by,

$$\kappa = \frac{P_h}{\Delta T}\frac{L}{A} \tag{3.1}$$

Here $P_h, \Delta T, L$ and A are the power of heater, average temperature of sample, distance between the thermocouples and vertical cross section area of the sample respectively. The Seebeck constant of sample was calculated as given in eq. 3.2. The difference in potentials between cold and hot edges of sample was divided by the change in temperature and added with the Seebeck constant of wire.

$$S_{sample} = \frac{V_c - V_h}{\Delta T} + S_{wire} \tag{3.2}$$

Materials having very low Seebeck constants like Cu, Ag, Au and Pt are commonly used in order to make contacts during the experiment. And they are mostly ignored since they have very low Seebeck constants.

4. STRUCTURAL CHARACTERIZATION

X-Ray powder diffraction and thickness measurements are done for bulk and thin film samples respectively. Structural parameters are used to compare the crystal parameters of powder samples with the literature. Thin films are measured whether they have amorphous or crystal. Thickness is used for the resistivity measurements in order to calculate crosssection in which current passes through.

4.1 Bragg's Law and X-Ray Diffraction

Substances are investigated in two groups: amorphous materials and crystals. Crystals have unit cells and they are repetitive structures throughout the material. A translation vector $\vec{T}$, can repeat the coordinate of i_{th} atom by the translation vectors $\vec{a}_1$, $\vec{a}_2$ and $\vec{a}_3$.

$$\vec{T}_i = x_i\vec{a}_1 + y_i\vec{a}_2 + z_i\vec{a}_3 \tag{4.1}$$

Amorphous materials usually have short range order and arrangement of atoms are irregular. Since crystals have an order, they are grouped by mathematical groups which are called as basis and these set of points attached to the basis is called lattice [34].

Table 4.1 : The 14 lattice types in three dimensions [34].

System	Number of lattices	Cell Parameters	Angles
Triclinic	1	$a_1 \neq a_2 \neq a_3$	$\alpha \neq \beta \neq \gamma$
Monoclinic	2	$a_1 \neq a_2 \neq a_3$	$\alpha = \gamma = 90^\circ \neq \beta$
Orthorhombic	4	$a_1 \neq a_2 \neq a_3$	$\alpha = \beta = \gamma = 90^\circ$
Tetragonal	2	a_1=$a_2 \neq a_3$	$\alpha = \beta = \gamma = 90^\circ$
Cubic	3	a_1=$a_2 = a_3$	$\alpha = \beta = \gamma = 90^\circ$
Trigonal	1	a_1=$a_2 = a_3$	$\alpha = \beta = \gamma =< 120^\circ, \neq 90^\circ$
Hexagonal	1	a_1=$a_2 \neq a_3$	$\alpha = \beta = 90^\circ, \gamma = 120^\circ$

Every crystal structure has its specific symmetry group. There are 230 types of symmetry declared in International Tables of Crystallography.

The most used symmetry type in our samples is tetragonal I4/mmm (No:139) [41], given in Fig. 4.1. Big square shows unit cell with the translation operators at the intersection points. Starting from one of them, operators are generally used to generate

Crystal Type	Bravais Lattice	Point Group
Triclinic	P	1, $\bar{1}$
Monoclinic	P, C	2, m, 2/m
Ortorhombic	P, C, F, I	222, 2mm, 2/m 2/m 2/m
Trigonal	P, R	3, $\bar{3}$, 32, 3m,$\bar{3}$2/m
Hexagonal	P	6, $\bar{6}$, 6/m, 622, 6mm, $\bar{6}$m2, 6/m 2/m 2/m
Tetragonal	P, I	4, $\bar{4}$, 4/m, 422, 4mm, $\bar{4}$2m, 4/m 2/m 2/m
Cubic	P, F, I	23, 2/m$\bar{3}$, 432, $\bar{4}$3m, 4/m $\bar{3}$ 2/m

Figure 4.1 : Point group and Herrmann-Mauguin notation.

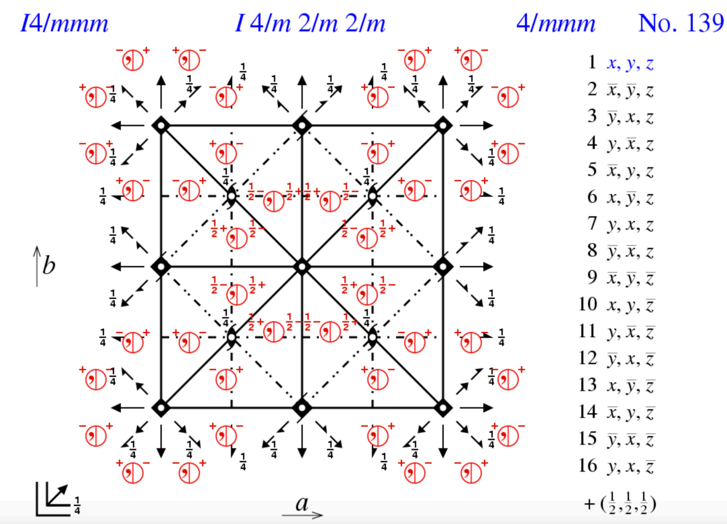

Figure 4.2 : Space group sample: Designation of tetragonal I4/mmm symmetry group [41].

atomic coordinates. Red circles show where an atom can be placed e.g. "corner" or "face center". Arrows guide operator how to determine the position of next atom, for instance 1/4 means that next atom will be located at a/4 distance down or up through the allowed rotation. Symmetry operators work according to the rules [42] , and hence atomic positions are determined by the help of this method.

5. RESULTS

Powder XRD patterns of samples between 10-90° 2θ degrees are studied in a Rigaku diffractometer for both bulk samples and thin films. A dektak profilometer is used to measure the thickness of thin films. Standard four-probe transport measurements are done in the temperature range of 4.2-300 K. The superconducting state with magnetization measurements in the temperature range of 5-300 K, up to a field of 9 T is investigated The magnetization as a function of temperature, ZFC (Zero Field Cooling) and FC (Field Cooling) are measured. Results are discussed.

5.1 X−Ray Powder Diffraction Measurements

5.1.1 $BaFe_2As_2$: parent material

Parent material $BaFe_2As_2$ given in Fig. 5.1 is successfully synthesized by a solid state reaction method. Powder X-ray diffraction (XRD) was used at room temperature. FullProf program is used in order to find lattice parameters by employing profile matching with constant scale factor.

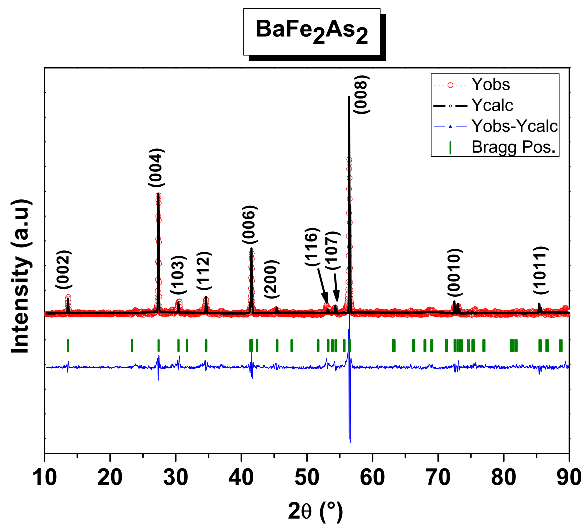

Figure 5.1 : Powder XRD profile fit of $BaFe_2As_2$ sample.

Red circles show the data collected from the diffractometer. This describes experimental data and named as "$Y_{obs.}$" in fig. 5.1. The black line following the experimental data shows the fitting made by the program. The trace is determined by theoretical calculation and program requires some input parameters. They are lattice parameters (a,b and c), angles, α, β and γ and symmetry group of compound. Such parameters are accumulated in a single file and stored in XRD databases. They are called "cif" files. Once these numerical values are given to the FullProf in order to the calculate real values, program can be run for several times and work to match "exact" profile. Hence the calculation is done. Theoretical data is shown as a result of fitting given by "$Y_{calc.}$". The difference between these two data are subtracted and plotted on the screen by naming as "$Y_{obs.} - Y_{calc.}$". The symmetry group of our sample provides us to determine where (in which 2θ) reflection will occur. This describes the position of the Bragg intensity collated by the diffractometer. Green bars located below the graph is named as "Bragg Pos.".

The results showed that the $ThSi_2Cr_2$-type crystal structure with space group I4/mmm is obtained as reported in the literature. Sample is single phase, and lattice parameters are a=b=3.992077 Å, c=13.031074 Å respectively. Main peaks corresponding to the tetragonal structure are fitted to the experimental data. After having prepared parent material, we then tried to dope platinum to the structure. Our target is:

I. to search if platinum has resolution in $BaFe_2As_2$ sample,

II. to find a stable stoichiometry of system.

In order to do this, platinum is doped at the ratios of x=0.1, and x=1.0 in $BaFe_{2-x}Pt_xAs_2$ sample group.

5.1.2 Platinum doped samples: $BaFe_{1.9}Pt_{0.1}As_2$

x=0.1 compound synthesized via expected stoichiometry, $BaFe_{1.9}Pt_{0.1}As_2$. By applying same symmetry, X-ray diffraction pattern is fitted in Fig 5.2.

Profile matching is satisfied and lattice parameters are found as follows: a=b=3.982941 Å and c=13.001225 Å. It is seen that lattice parameters decreased when compared with parent material $BaFe_2As_2$, resulting % 1 volume loss. platinum has contributed

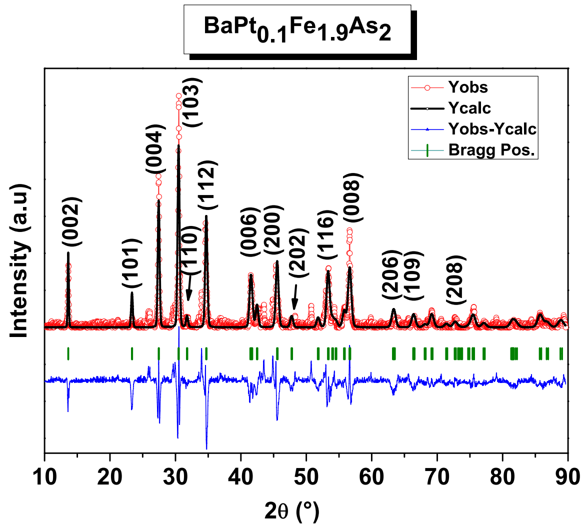

Figure 5.2 : Powder XRD profile fit of $BaFe_{1.9}Pt_{0.1}As_2$ sample.

to the structure at x=0.1 mole fraction, and resulted the same symmetry without any impurities.

5.1.3 $BaFePtAs_2$ sample

Platinum doping level is investigated by adding %50 percent Pt, aiming to have same crystal structure. Same synthesis is applied to obtain a clear sample. Resulting X-ray profile was unsatisfactory. Many impurities are observed. A secondary sintering process is applied to obtain single phase. Fig 5.3 shows the results for $BaFePtAs_2$

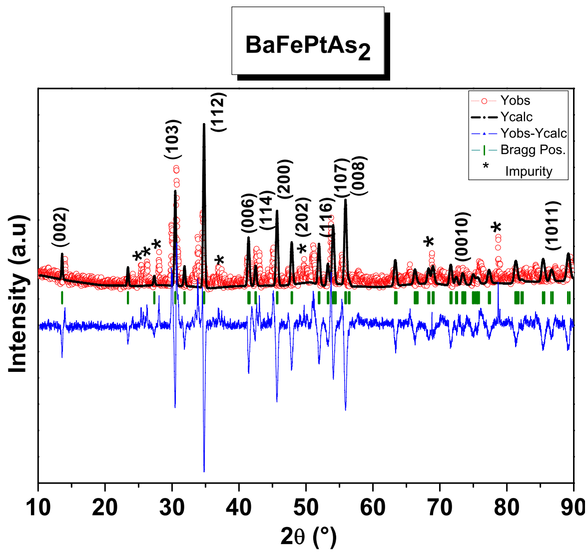

Figure 5.3 : Powder XRD profile fit of $BaFePtAs_2$ sample.

sample after secondary sintering. Our attempt to prepare 1:1 ratio in Fe/Pt system failed. It is thought that platinum required more heat for melting. So we increased the temperature to 1273K to melt the elements in pellet. Following a heat treatment of 1273K, temperature of furnace decreased slowly (100K/hour) down to 973K. And then decreased to 873K slowly (15K/hour). Profile fit results showed a low amount of I4/mmm type crystal structure was obtained. Remaining percentage has mostly impurity phases, in which it is difficult to recognize (denoted by *). Lattice parameters are calculated as a=b= 3.973073Å, c= 13.040128Å. When the sample is left to room temperature for cooling, bright particles are observed. Optical microscope images are shown in fig 5.4. Despite having a crystallite view, sample is not pure and therefore it is clear that platinum resolution can not join to the I4/mmm structure at 1:1 Fe/Pt ratio. Saha et al. [10] reported a study with $BaFe_{2-x}Pt_xAs_2$ for x=0 and x=0.1. Since platinum has higher molecular weight (195g/mol), lower doping ratio of platinum doping (about %5-%10) is easier to obtain. Briefly, insisting on $BaFePtAs_2$ sample, excess amount of iron or arsenide will bring intermediate phases like Fe_2As , FeAs or Pt_2As impurities mixed with the main $ThSi_2Cr_2$ type structure.

5.1.4 $BaFe_{1.8}Pt_{0.2}As_2$ sample

Platinum resolution is investigated by raising doping level to %10 to obtain higher stoichiometry samples. $BaFe_{1.8}Pt_{0.2}As_2$ sample is prepared and XRD result is given in Fig. 5.5. Lattice parameters are calculated as a=b= 3.977873Å and c= 12.944031Å. A remarkable decrease in unit cell parameters is observed.

5.1.5 $BaFe_{1.7}Pt_{0.3}As_2$ sample

Platinum resolution is investigated by raising doping level to %15. $BaFe_{1.7}Pt_{0.3}As_2$ sample is prepared and XRD result is given in Fig. 5.6. Lattice parameters are calculated as a=b= 3.978521Å and c= 12.926636Å. It is seen that all samples are prepared successfully and crystal structure parameters are found consistent with the literature. Refined parameters are reported in table 5.1. Lattice parameters, unit cell volume, c/a ratio, χ^2 and R_{Bragg} values are given in same order. Tetragonal unit cell is fitted to I4/mmm symmetry (space group no. 139) by employing constant scaling factor.

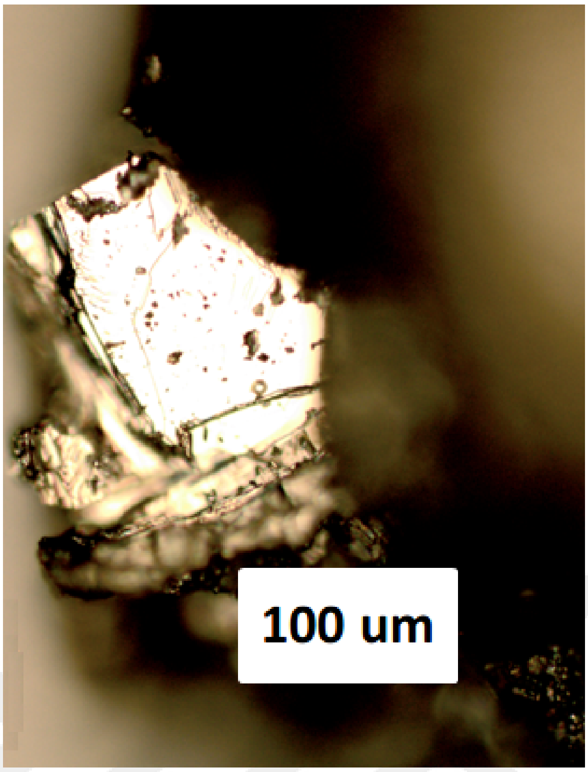

(a)

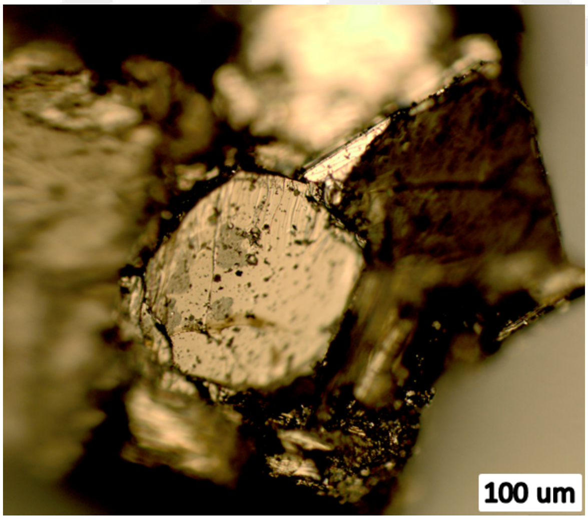

(b)

Figure 5.4 : Optical microscope photograph of $BaFePtAs_2$ sample, (a) 70μm x 120μm dimension,(b) different view of a hexagonal shape sample which is 250 μm in size.

Lattice parameters a and c, volume of unit cell, c/a ratio and structural parameters χ^2 and R_{Bragg} for the whole La doped series is given in table 5.1. Unit cell dimensions did not show remarkable change in volume. A small decrease in c is observed which may

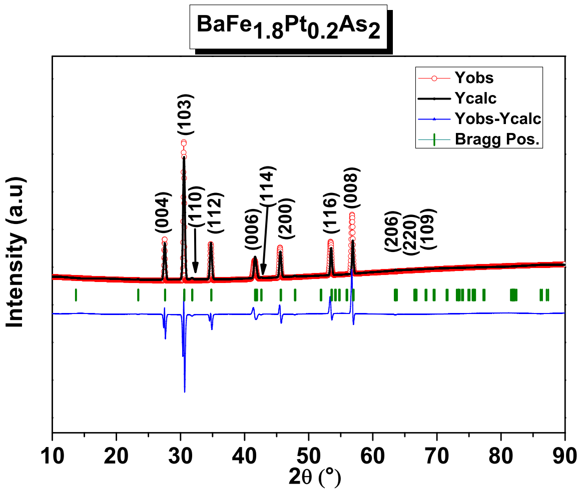

Figure 5.5 : Powder XRD profile fit of $BaFe_{1.8}Pt_{0.2}As_2$ sample.

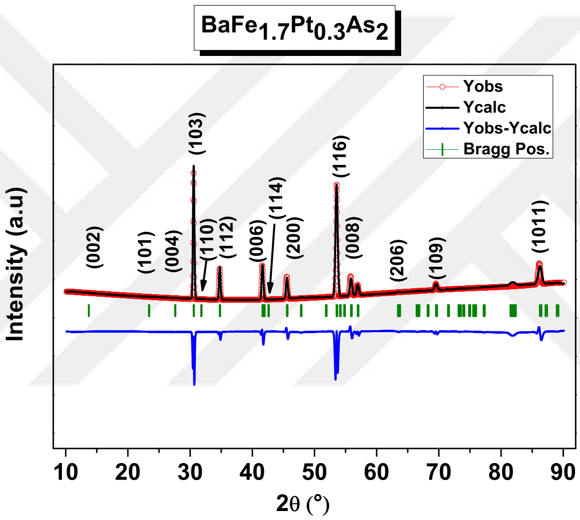

Figure 5.6 : Powder XRD profile fit of $BaFe_{1.7}Pt_{0.3}As_2$ sample.

be a result of changing Fe hosts with platinum. The goodness of fits χ^2, is acceptable for all compounds since it is lower than 10.

Table 5.1 : Structural parameters of samples obtained from XRD analysis.

x	$a = b$(Å)	c(Å)	V(Å)^3	c/a	χ^2	R_{Bragg}
0	3.9922	13.0319	207.69	3.2644	5.56	37.03
0.1	3.9922	13.0100	207.35	3.2589	8.60	7.73
0.2	3.9779	12.9440	207.82	3.2540	13.39	68.14
0.3	3.9785	12.9266	207.61	3.2491	4.13	18.51

5.1.6 La doped samples $Ba_{1-x}La_xFe_{1.9}Pt_{0.1}As_2$: x=0.03

La doping is studied in $Ba_{1-x}La_xFe_{1.9}Pt_{0.1}As_2$ sample sets. For x=0, $BaFe_{1.9}Pt_{0.1}As_2$ sample was already given in fig. 5.2. La doped first sample, x=0.03 is given in

Fig. 5.7 is successfully prepared by solid state reaction method. Powder X-ray diffraction (XRD) was used at room temperature. The results are consistent with the $ThSi_2Cr_2$-type crystal structure with space group I4/mmm is obtained as reported in the literature. FullProf program is used in order to find lattice parameters by employing profile matching with constant scale factor. Lattice parameters are a=b=3.9874(8) Å,

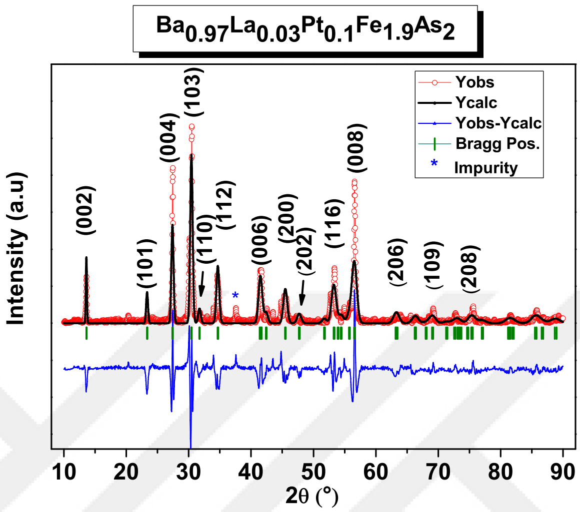

Figure 5.7 : Powder XRD profile fit of $Ba_{0.97}La_{0.03}Fe_{1.9}Pt_{0.1}As_2$ sample.

c=13.019(6) Å respectively. Main peaks corresponding to the tetragonal structure are fitted to the experimental data. Impurity is observed in this sample. Observed and calculated patterns are nearly matched.

5.1.7 La doped samples: x=0.05

La doped sample $Ba_{0.95}La_{0.05}Fe_{1.9}Pt_{0.1}As_2$ (x=0.05) is given in Fig. 5.8. Powder X-ray diffraction (XRD) result at room temperature is presented. The results are compared with the $ThSi_2Cr_2$-type crystal structure with space group I4/mmm.

Sample is mainly single phase and lattice parameters are determined as a=b=3.9838(7) Å, c=13.004(0) Å respectively. Most of peaks corresponding to the tetragonal structure are fitted to the experimental data.

5.1.8 La doped samples: x=0.1

La doped sample $Ba_{0.9}La_{0.1}Fe_{1.9}Pt_{0.1}As_2$ (x=0.10) given in Fig. 5.9 is prepared. Powder X-ray diffraction (XRD) result at room temperature is presented. The results are compared with the $ThSi_2Cr_2$-type crystal structure with space group I4/mmm.

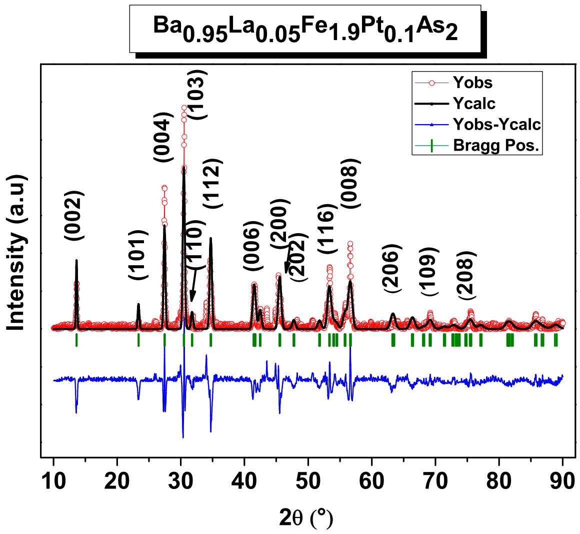

Figure 5.8 : Powder XRD profile fit of $Ba_{0.95}La_{0.05}Fe_{1.9}Pt_{0.1}As_2$ sample.

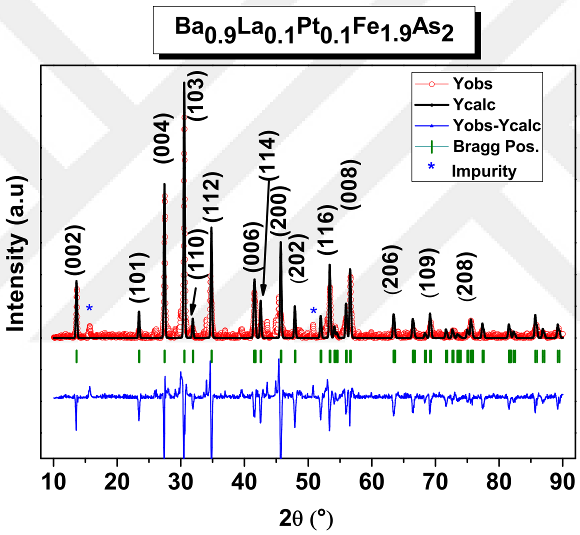

Figure 5.9 : Powder XRD profile fit of $Ba_{0.9}La_{0.1}Fe_{1.9}Pt_{0.1}As_2$ sample.

Sample consists impurity phases when compared with the previous one. Impurity peaks are denoted by blue star.

Lattice parameters are determined as a=b=3.968(4) Å, c=13.000(6) Å respectively. Most of peaks corresponding to the tetragonal structure are fitted to the experimental data. Since the amount of Lanthanum is increased, further doping levels will make more contribution to the structure. Expected extra phase can be superconductive LaFeAsO unit cell, which is proposed by Hosono et al. in 2008 [7]. Since the weight of second phase is low, it is not shown exactly in the profile.

5.1.9 La doped samples: x=0.3

La doped sample $Ba_{0.7}La_{0.3}Fe_{1.9}Pt_{0.1}As_2$ (x=0.30) given in Fig. 5.10 is prepared. Powder X-ray diffraction (XRD) result at room temperature is presented. The results are compared with the $ThSi_2Cr_2$-type crystal structure with space group I4/mmm. Sample consists impurity which is denoted by blue star. Lattice parameters

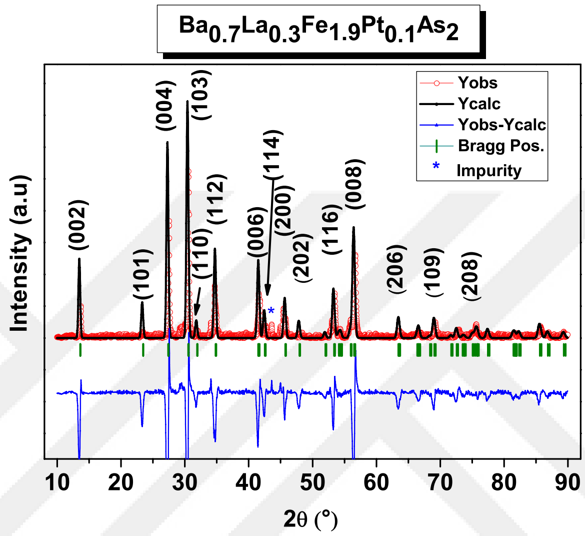

Figure 5.10 : Powder XRD profile fit of $Ba_{0.7}La_{0.3}Fe_{1.9}Pt_{0.1}As_2$ sample.

are determined as a=b=3.964(0)Å, c=13.012(4) Å respectively. Most of peaks corresponding to the tetragonal structure are fitted to the experimental data. Since the amount of Lanthanum is increased, further doping levels will make more contribution to the structure. Expected extra phase can be superconductive LaFeAsO unit cell, which is proposed by Hosono et al. in 2008 [7].

5.1.10 La doped samples: x=0.4

La doped sample $Ba_{0.6}La_{0.4}Fe_{1.9}Pt_{0.1}As_2$ (x=0.40) given in Fig. 5.11 is prepared. Powder X-ray diffraction (XRD) result at room temperature is presented. A second phase survives with space group symmetry I4/mmm. Both of them are observed at relatively high La doping level (% 40). Sample consists impurity.

Lattice parameters are determined as a=b=3.967(9)Å, c=13.001(4) Å respectively. This sample consists LaFeAsO phase with the space group P4/nmm. Lattice parameters belonging second phase is determined as a=b=4.033(6)Å, c=8.746(9)Å.

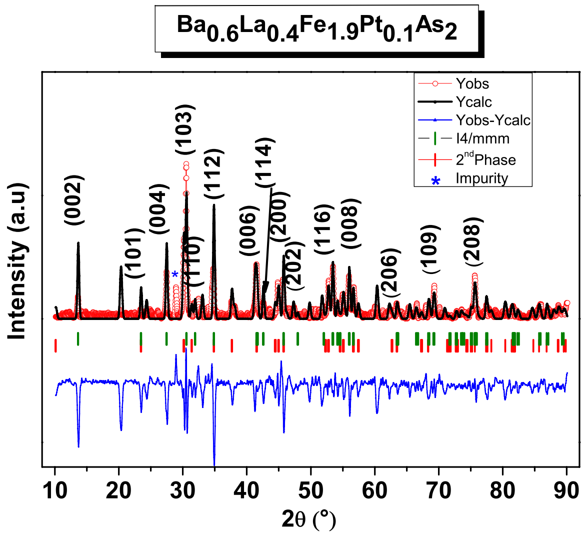

Figure 5.11 : Powder XRD profile fit of $Ba_{0.6}La_{0.4}Fe_{1.9}Pt_{0.1}As_2$ sample.

Most of peaks corresponding to that of space groups are fitted to the experimental data.

Table 5.2 : Structural parameters of La doped samples obtained from XRD analysis.

x	$a=b$(Å)	c(Å)	V(Å)^3	c/a	χ^2	R_{Bragg}
0	3.992(2)	13.03(2)	207.69	3.2644	5.56	37.03
0.03	3.987(5)	13.019(6)	207.35	3.2589	8.60	7.73
0.05	3.983(8)	13.004(0)	207.82	3.2540	13.39	68.14
0.10	3.968(4)	13.000(6)	207.61	3.2491	4.13	18.51
0.30	3.964(0)	13.012(4)	207.61	3.2491	4.13	18.51
0.40	3.967(9)	13.001(4)	207.61	3.2491	4.13	18.51

Lattice parameters a and c, volume of unit cell, c/a ratio and structural parameters χ^2 and R_{Bragg} for the whole La doped series is given in table 5.2.

5.1.11 Thermoelectric samples: $BaFe_{4-x}Pt_xSb_{12}$

PXRD patterns of Pt doped skutterudite samples, $BaFe_{4-x}Pt_xSb_{12}$ show that all samples crystallize in the body-centered cubic structure of skutterudite with space group Im$\bar{3}$. Rietveld analyses for $BaFe_{4-x}Pt_xSb_{12}$ samples is shown in Fig. 5.12. The calculated lattice parameters are found as 9.202(5), 9.199(5), 9.202(1) Å for $x = 0$, 0.1 and 0.2 respectively consistent with the literature [23]. The reason not observing any shrinkage or expansion in lattice volume might be because Pt (135 pm) and Fe (140 pm) have identical atomic radius.

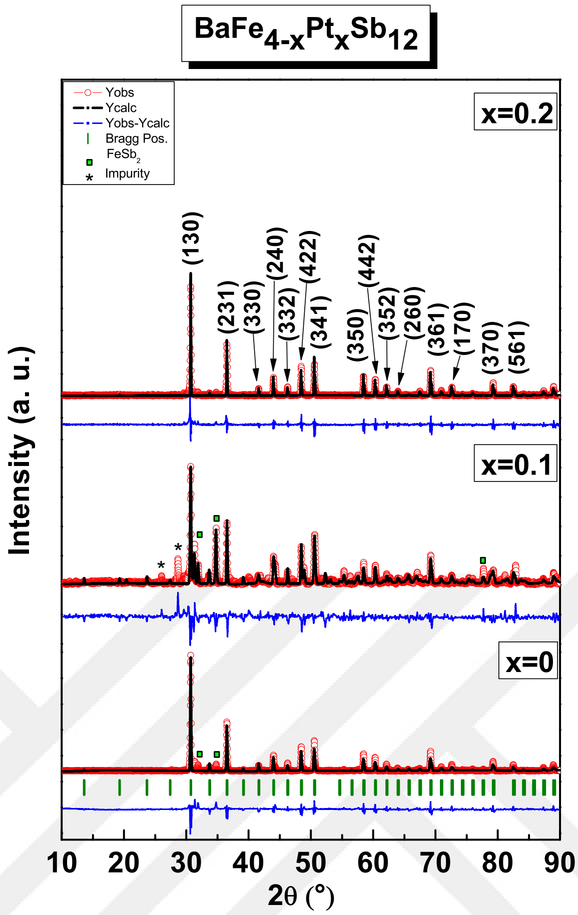

Figure 5.12 : PXRD pattern of $BaFe_{4-x}Pt_xSb_{12}$ (x=0, 0.1, 0.2) samples at room temperature [43].

5.1.12 XRD of thin film samples: $BaFe_2As_2$, and $BaFe_{1.8}Pt_{0.2}As_2$

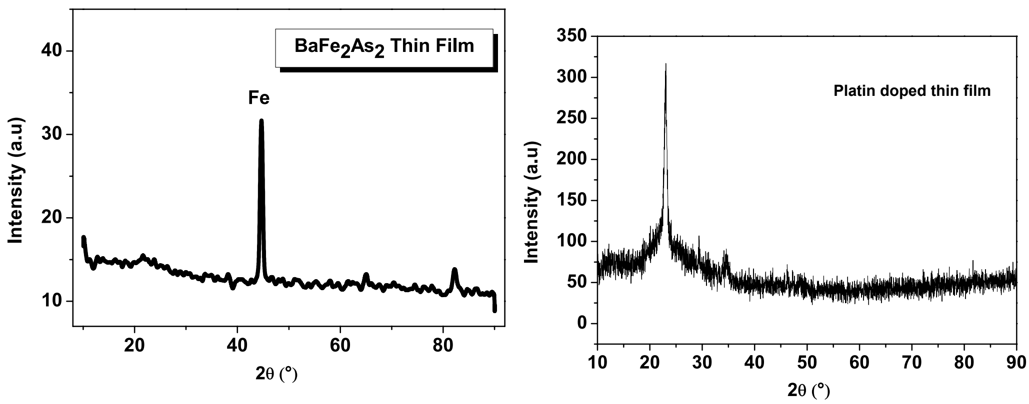

(a) (b)

Figure 5.13 : Thin film XRD patterns of (a) $BaFe_2As_2$, and (b) Pt 0.2 doped $BaFe_{1.8}Pt_{0.2}As_2$.

Thin film of parent material is successfully prepared at 8.3×10^{-6} Torr vacuum in accordance with the works in literature [44]. It is seen that $BaFe_2As_2$ thin film has an amorphous structure.This result is expected because our primary system was only able to prepare samples down to 10^{-7} Torr vacuum. Note that there is a significant intensity difference when compered with Pt 0.2 doped sample. Platinum doped sample has higher intensity in the peak profile (fig. 5.13).

As a result, highly equipped systems such as MBE have opportunity to prepare atomic level thick films in Å(angström) level resolution. Our achievement here is to prepare "almost thin" films in our laboratory.

Thickness is given in Fig. 5.14. A dektak profilometer is used to measure the thickness of thin films. Obtained values for h, are employed in s/L calculation. Thickness of $BaFe_2As_2$ is found as 1.392μm. Since the system is manually controlled, it is hard to estimate the amount of coating on the quartz substrate. Temperature is about 2000°C. A rough surface is obtained by flashing for several times. A 531nm thin film is achieved at 7.5×10^{-6} Torr vacuum in $BaFe_{1.9}Pt_{0.1}As_2$ sample. By lowering the evaporation time, it is seen that thickness can be half compared with the previous experiments. Thickness of film starts from a positive value and terminates at around -600 nm. The reason for the negativity comes from the measurement starting point since the reference is taken on the thin film. 0-125μm distance is thin film and 150-200 μm distance is quartz substrate. Pt 0.2 doped sample $BaFe_{1.8}Pt_{0.2}As_2$ has a thickness of 248nm. Several measurements show different values in dektak profilometer. Coatings over first layer creates roughness and burns the material. Vacuum was 9.4×10^{-6} Torr during the experiment. Pt 0.3 doped $BaFe_{1.7}Pt_{0.3}As_2$ thin film is produced at 8.3×10^{-6} Torr. The film was flashed one time in order to have a homogenous layer. Thickness is shown as 559 nm (Fig. 5.15).

5.2 Resistivity Measurements

5.2.1 Parent sample: $BaFe_2As_2$

The resistivity measurements were carried out using a four-probe technique on the pressed pellets in the temperature range of 4.2-300 K. The temperature dependence of the resistivity for the parent sample, $BaFe_2As_2$ (Fig. 5.16), exhibits the same behavior (including a very close match to reported amplitudes) as those given in the literature. A sharp kink at T = 144 K, where a structural phase transition upon cooling is known

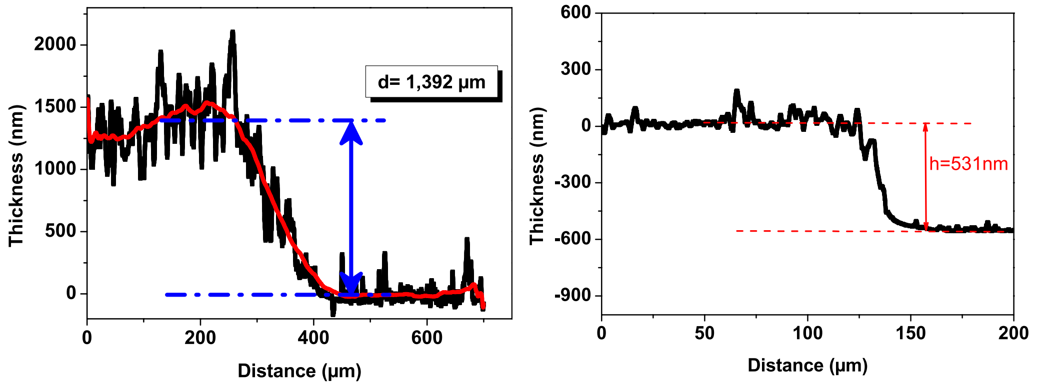

(a) (b)

Figure 5.14 : Thickness of (a) $BaFe_2As_2$ thin film, and (b) $BaFe_{1.9}Pt_{0.1}As_2$ thin film.

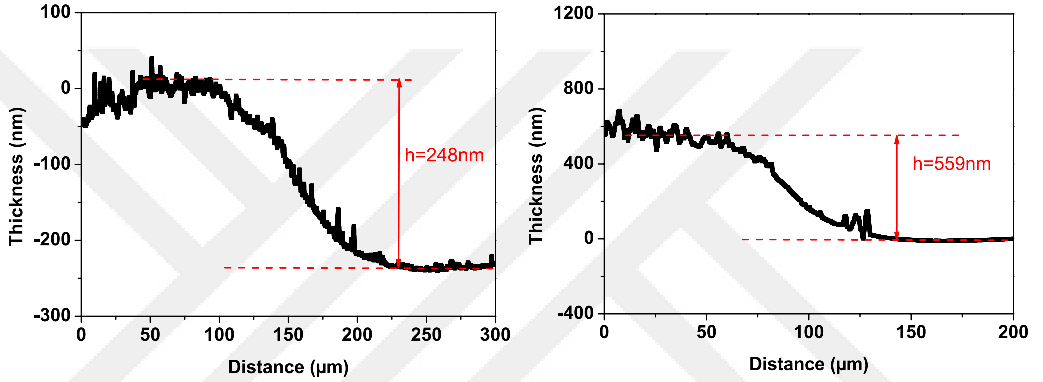

(a) (b)

Figure 5.15 : Thickness of (a) $BaFe_{1.8}Pt_{0.2}As_2$ thin film, and (b) $BaFe_{1.7}Pt_{0.3}As_2$ thin film.

to coincide with the onset of antiferromagnetic (AFM) order. Rotter et. al. argued that crystal symmetry of unit cell is changed from tetragonal to orthorhombic unit cell. Crystal symmetry here transforms from I4/mmm to Fmmm [8, 9, 45]. This behavior is attributed to spin density wave (SDW) transition at this temperature.

5.2.2 $BaFe_{1.9}Pt_{0.1}As_2$ sample

Pt doped sample is superconducting at about $T_c = 24K$. Saha et. al. [10] made same experiment on single crystal $BaFe_{1.9}Pt_{0.1}As_2$ sample and observed same behavior at $T_c = 21.5K$. The difference in our bulk sample is that; in addition to superconductivity, we observe SDW anomaly in this sample at T=138 K (fig. 5.17). Results are published [46].

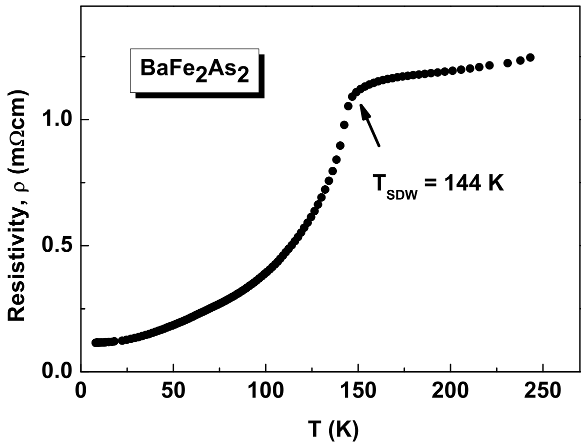

Figure 5.16 : Resistivity of parent material: $BaFe_2As_2$ sample [46].

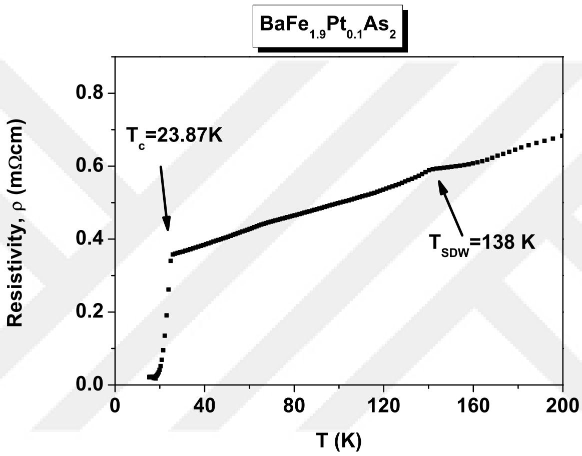

Figure 5.17 : Resistivity of platinum doped $BaFe_{1.9}Pt_{0.1}As_2$ sample.

5.2.3 $BaFe_{1.8}Pt_{0.2}As_2$ sample

Resistivity of Pt 0.2 doped sample is given in Fig. 5.18. Material is superconducting at about $T_c = 21K$. A remarkable change in resistivity is not seen at around $T = 140K$. Y. Guo et. al. prepared the polycrystalline samples of Pt doped $BaPt_xFe_{2-x}As_2$. Resistivity and susceptibility measurements proved that the largest fractions of superconductivity is observed in $0.08 < x < 0.14$ interval. Our value $T_c = 21K$ is close to the readings reported in that study [11].

All platinum doped samples are shown in fig. 5.19(a). $BaPt_xFe_{2-x}As_2$ samples with $0 < x < 0.5$ are measured between room temperature and $T = 4.2K$. Results showed superconducting transitions at different T_c's. Phase diagram is obtained as a function of T_c. Critical temperature decreases with increasing Pt substitution (Fig. 5.19(b)). SDW

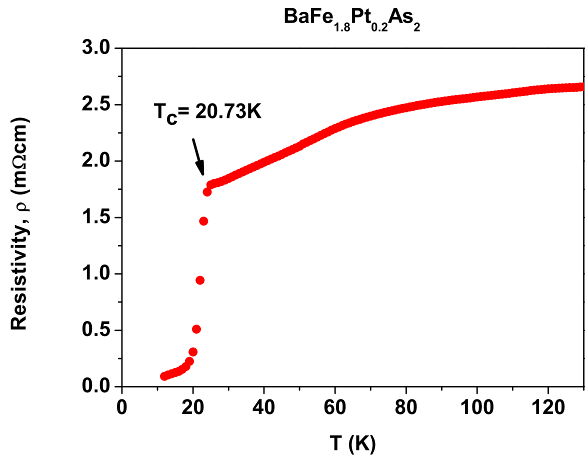

Figure 5.18 : Resistivity of platinum doped $BaFe_{1.8}Pt_{0.2}As_2$ sample.

anomaly is observed only in x=0 and x=0.1 samples. Resistivity values are found in the range of 0.2-1 mΩ cm except x=0.3. Higher value of resistivity in x=0.3 should be due to oxidation problem during measurement. Platinum resolution was reported up to x=0.2 by Y. Guo. Our samples showed superconducting behavior even at high platinum doping levels.

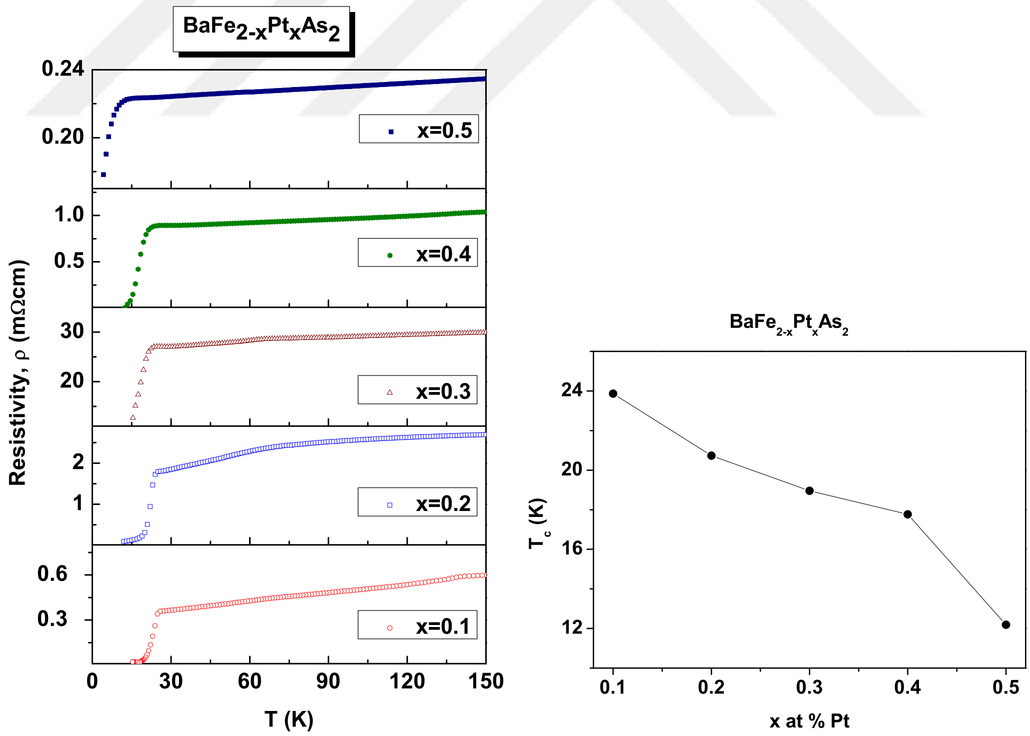

(a) (b)

Figure 5.19 : (a) Resistivity of all samples, (b) Phase diagram of samples as a function of Pt doping.

Measurements showed that Pt triggered Fe-As layers and resulted superconductivity at around $T_c = 20K$. Further measurements are focused on Ba-La exchange and test if critical temperature T_c will shift up or down. Our aim here is to enhance phase transition temperature by exchanging La with Ba. Starting from %3 amount, La is doped in to $Ba_{1-x}La_xFe_{1.9}Pt_{0.1}As_2$ sample serie and resistivities are measured. Results are discussed. Superconducting phase transition temperatures are observed and reported.

5.2.4 Resistivity of La doped samples $Ba_{1-x}La_xFe_{1.9}Pt_{0.1}As_2$: x=0.03

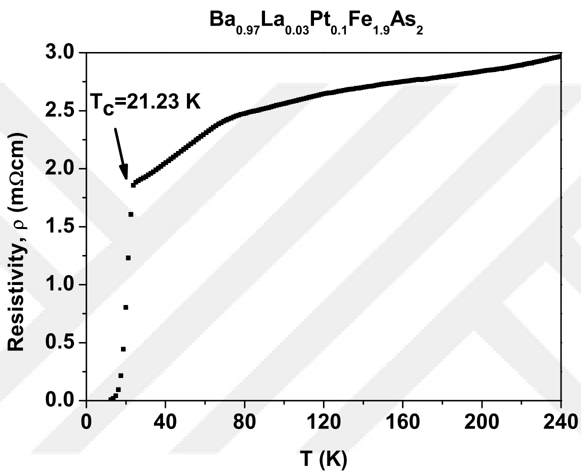

Figure 5.20 : Resistivity of La doped $Ba_{0.97}La_{0.03}Fe_{1.9}Pt_{0.1}As_2$ sample.

Synthesis of La doped bulk samples and their XRD patterns were analyzed at the beginning of this chapter. Here resistivity measurements between 4.2-300 K temperature interval are discussed. It is noted that La doped samples have more impurity peaks compared with the Pt doped serie. Single phases of powder materials and their results are discussed. Fig. 5.20 shows that the superconducting temperature of $Ba_{0.97}La_{0.03}Fe_{1.9}Pt_{0.1}As_2$ sample is $T_c = 21.2K$. The change in slope around 75 K is remarkable. Non-linear behavior should be caused by magnetic origin.

5.2.5 Resistivity of La doped samples: x=0.05

Fig. 5.21 shows resistivity behavior of $Ba_{0.95}La_{0.05}Fe_{1.9}Pt_{0.1}As_2$ sample with $T_c = 16.6K$. Inset shows the derivative of resistivity with respect to temperature. Anomaly is observed at T=63 K. Please note that this sample has a clean XRD pattern without any impurity peak.

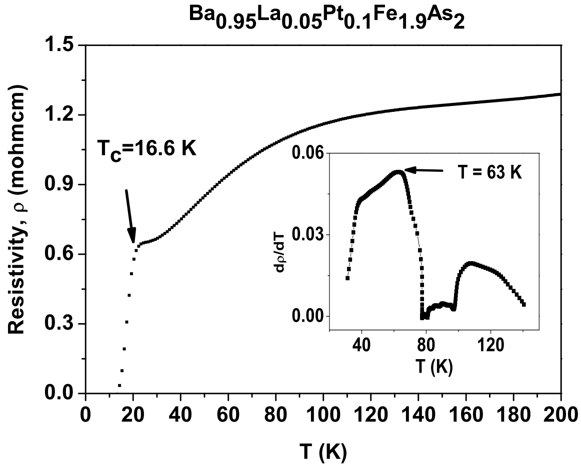

Figure 5.21 : Resistivity of $Ba_{0.95}La_{0.05}Fe_{1.9}Pt_{0.1}As_2$ sample (derivative with respect to temperature in the inset).

5.2.6 Resistivity of La doped samples: x=0.1

Resistivity of La doped sample with x=0.1 is shown in Fig. 5.22. Sample is superconducting at $T_c = 20K$. Same anomaly is found around T=60 K by taking the derivative of the sample with respect to temperature.

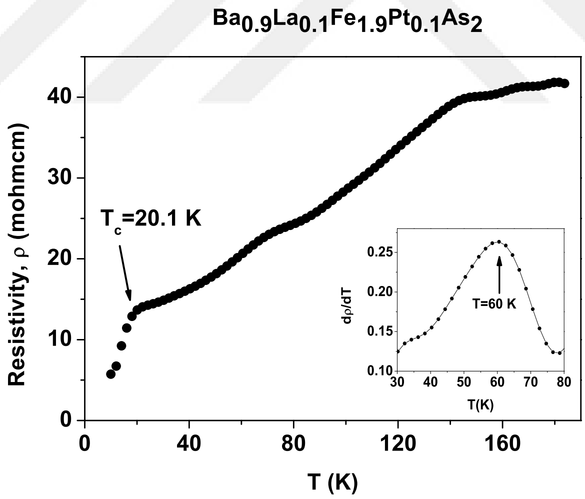

Figure 5.22 : Resistivity of $Ba_{0.9}La_{0.1}Fe_{1.9}Pt_{0.1}As_2$ sample (derivative with respect to temperature in the inset).

5.2.7 Resistivity of La doped samples: x=0.4

$\rho(T)$ for sample with x=0.4, increases slightly with decreasing temperature (Fig. 5.23). Sample is superconducting at $T_c = 24.2K$. Same anomaly still maintains at T=60 K.

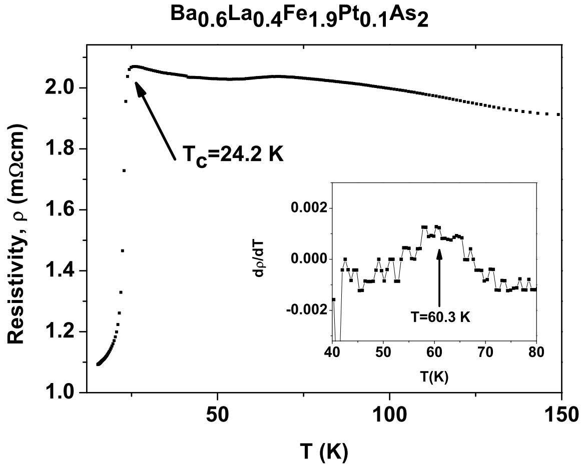

Figure 5.23 : Resistivity of $Ba_{0.6}La_{0.4}Fe_{1.9}Pt_{0.1}As_2$ sample (derivative with respect to temperature in the inset).

5.2.8 Resistivity of thermoelectric samples

The temperature dependence resistivity for three compounds is shown in Fig. 5.24(a). It is seen that all compounds show semi metallic behavior [47, 48]. The resistivity value of reference material, $BaFe_4Sb_{12}$ is consistent with literature [23]. It is seen that resistivity increases with increasing content of Pt. This might be due to different scattering mechanism in these compounds such as Kondo impurities or spin fluctuation scattering [22, 47, 49, 50]. The spin fluctuation temperatures T_{sf} are obtained from the dρ/dT vs T graphs of samples. We assume that Matthiessen,s rule is valid. According to this model, the contribution of the scattering processes to the resistance are independent ; thus for an alloy at temperature T, the resistivity predicted by the rule is $\rho_m(T) = \rho_0 + \rho_h(T)$ where ρ_0 is the residual resistivity of the alloy due to scattering on lattice defects, impurities including spin-orbit interaction, and spin disordering etc. , and $\rho_h(T)$ is the resistivity of the pure host-metal at temperature T . (This temperature dependent term includes all the different scattering terms for the host-metal). The scattering of electrons by chemical disorder, lattice imperfections, as well known, Pt impurities (assuming distributed randomly in the films) induce a large spin-orbit interaction. Even though the contribution of all the scattering mechanisms mentioned above is significant (estimated to be a few 0.10 $\mu\Omega$m), it is not enough to explain such a big residual resistivity. In our previous work, it was pointed out that the sum of coherent and incoherent electron-magnon scattering mechanisms (since they cancel each other quantitatively when summed) might have a profound influence on temperature-independent part of the resistivity at low temperatures [51, 52]. At low temperature we use $\rho = \rho_0 + AT^2$ expression to fit resistivity data given in Fig. 5.24(b). The term A here shows the T^2 dependence of resistivity at low temperature. We assume the electron-phonon scattering mechanism is dominant at high temperatures and thereby we use Bloch-Grüneisen equation. High temperature resistivity data for the samples is used to fit where n=5 is taken into account for the scattering of electrons by phonons. θ_D indicates the Debye Temperature for samples in equation shown below. All fitting parameters are presented in Table 5.3.

$$\rho(T) = \rho_0 + \alpha \left(\frac{T}{\theta_D}\right)^n \int_0^{\frac{\theta_D}{T}} \frac{x^n}{(e^x - 1)(1 - e^{-x})} dx \tag{5.1}$$

Table 5.3 : ρ-T^2 and Bloch-Grüneisen Fitting Parameters For $BaFe_4Sb_{12}$ Compounds.

x	$\rho_0(\mu\Omega$m)	A($\mu\Omega mK^{-2}$)$\times 10^4$	$\Theta_D(K)$
0	3.03	2.96	326
0.1	4.02	2.60	298
0.2	4.09	3.28	285

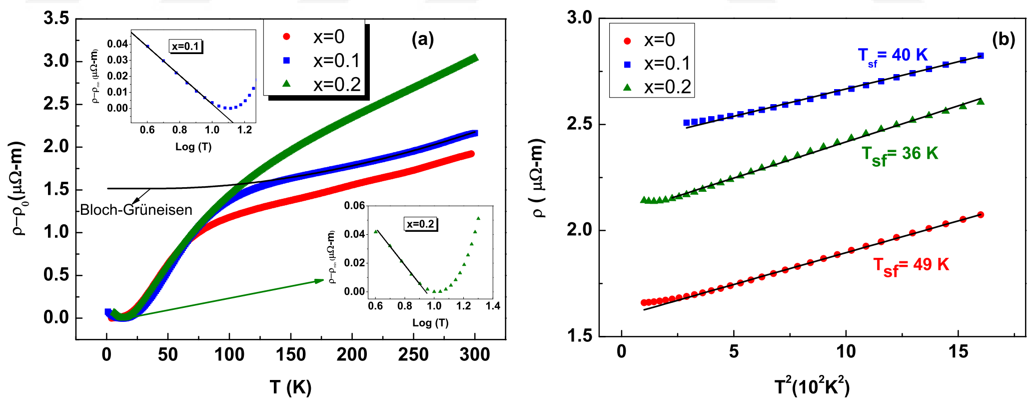

(a) (b)

Figure 5.24 : (a) Temperature dependence of resistivity and observed Kondo minima, (b) linear temperature dependence of resistivity, ρ-T^2 graph for all compounds [43].

Typical behavior of resistivity fit is shown for x = 0.1 with continuous line. The decrease in θ_D from 326 K for x = 0 to 285 K for x = 0.2 is expected since Pt atoms have larger atomic mass (195.1 g/mol) compared with Fe (55.85 g/mol) atoms. Low temperature dependence of the resistivity has been attributed to Kondo effect. This behavior was observed by linear fitting of $\Delta\rho(\rho$-$\rho_{min}) = -\Delta\rho_0 \log(T/T_K)$ for $x = 0.1$ and

x = 0.2 samples, Kondo minima temperatures were then found T_{K1} = 10.7 K and T_{K2} = 8.8 K respectively (see Fig. 5.24(a)). Kondo minimum temperature increases with increasing content of Pt. Even this situation has not fully understood yet we believe that Pt substitution on Fe side makes deformation on lattice due to large difference of atomic mass between Pt and Fe atoms, this might induce to Kondo minimum. As far as we know, there is only one study reported to show Kondo minimum for skutterudite compounds [48].

5.2.9 Resistivity of thin film samples

Resistivity of $BaFe_2As_2$ thin film at liquid He is measured between 4.2-300K. A phase transition at $T_c = 6.7K$ is seen clearly with reproducible experiments which is very similar to a superconductive phase transition. This result is interesting because current macroscopic theory of superconductivity is based on Cooper pairing mechanism. Since our thin film sample is amorphous, the causes for the resistivity at 500 mΩcm value must be discussed in detail. In 2013, Engelmann et. al. [53] studied that strain induced superconductivity in epitaxial $BaFe_2As_2$ thin films on Fe-buffered $MgAl_2O_4$ single crystalline substrates can be possible. Even if the thickness of our thin film is not comparable with this study, the drop of resistivity down to zero seen in Fig. 5.25 obeys filamentary superconductivity that Engelmann argues in Fig. 5.25 (b) in principle.

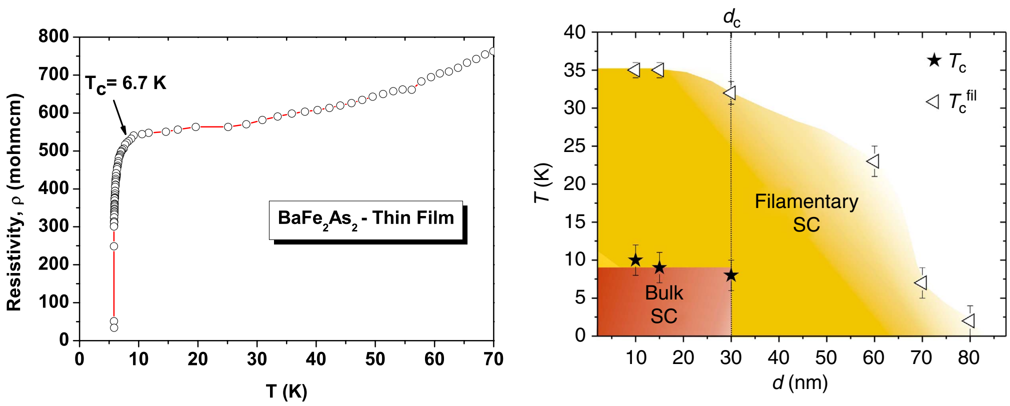

(a) (b)

Figure 5.25 : (a) Resistivity of $BaFe_2As_2$ Thin Film at liquid He, (b) T_c vs thickness diagram for $BaFe_2As_2$ thin films [53].

The difference in our study is that we create a disorder in material and it is amorphous. This process is realized in a simple flash evaporation system under vacuum. This is important because same kind of samples are produced in molecular beam epitaxy

(MBE) or similar systems that we are not able to. Some studies are reported that both in bulk [6] and thin film samples [53], showing that it is possible to apply pressure to the system and create disorder. This method is a way in order to trigger the superconductivity in such systems. For the first time, we observe the superconductivity in an amorphous thin film above the liquid He temperature, $T_c = 6.7K$ at ambient conditions (without applying any pressure). Magnetic characterization of this sample still continues and results will be presented in an appropriate publisher.

5.3 Magnetic Measurements

5.3.1 Magnetic behavior of $BaFe_2As_2$ sample

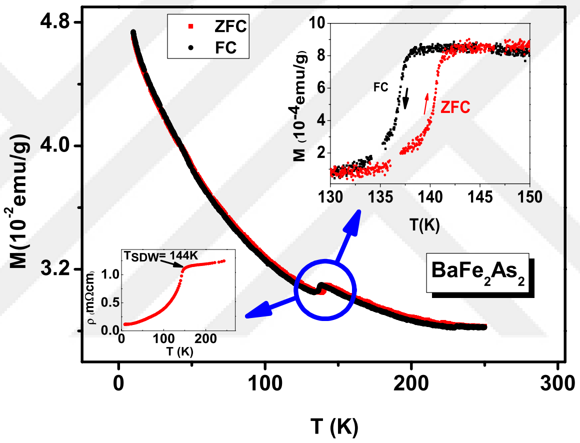

Figure 5.26 : ZFC-FC measurement in bulk $BaFe_2As_2$: upper inset shows a larger view focused on SDW transition; lower inset shows resistivity with the T_c corresponding same temperature [46].

Magnetization measurements were carried out using a commercial physical property measurement system (PPMS, Quantum Design Model 6500) including a vibrating sample magnetometer (VSM) attachment. The measurement was first done for bulk $BaFe_2As_2$. Magnetization as a function of temperature, T at H = 5 kOe for the parent material is depicted exclusively in Fig. 5.26. Upper inset shows the data in the expanded scale, describing a typical first order phase transition at T =144 K, associated with a tetragonal to orthorhombic structural/AFM phase transition [46].

5.3.2 Magnetic behavior of $BaFe_{1.9}Pt_{0.1}As_2$ sample

Fig. 5.27 shows the ZFC versus FC magnetization curves for the $BaFe_{1.9}Pt_{0.1}As_2$. Sample was first cooled to low temperature in the background field (zero field). H=20 Oe was subsequently applied and the moment measured as a function of slowly increasing temperature, yielding curves labeled ZFC (zero-field cooled). The temperature was then slowly reduced through the superconducting transition, T_c, yielding the curves labeled FC (field cooled) in the figures. Meissner effect measurements in fields up to $\pm$ 9T are given in the insets. Note that the ZFC data decrease rapidly for temperatures below Tc and quickly saturate to negative values. We have calculated roughly the effective magnetic susceptibility, $4\pi\chi_{eff}$, after demagnetization field correction (experimental samples had long cylindrical shapes). The values for samples are approximately -1, indicating that the system is indeed fully shielded. The measured field-cooled moment, MFC, below T_c (cooling in field leads to flux trapping and a significantly reduced negative magnetization) decreases significantly with Pt and La doping. The increasing difference between the experimental ZFC and FC data with La doping can be explained by the possible coexistence of regions of superconductivity within a strongly ferromagnetic host, resulting in a highly suppressed diamagnetic transition in the FC situation [46].

Since $T_c = 21.7K$ in ZFC-FC measurement, M-H curves taken at 5, 10, 15 and 20 K in Fig. 5.28 (a). Coherence length is calculated by using these data in Fig. 5.28 (b). It is found that ζ is equal to 15.79 nm for this sample.

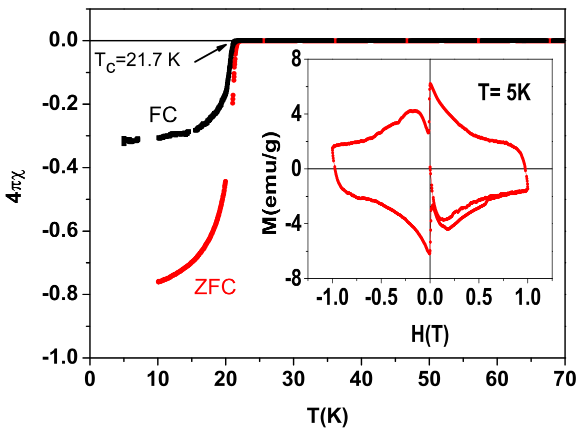

Figure 5.27 : ZFC-FC measurement in bulk $BaFe_{1.9}Pt_{0.1}As_2$ sample. Inset shows Meissner effect observed at T=5 K.

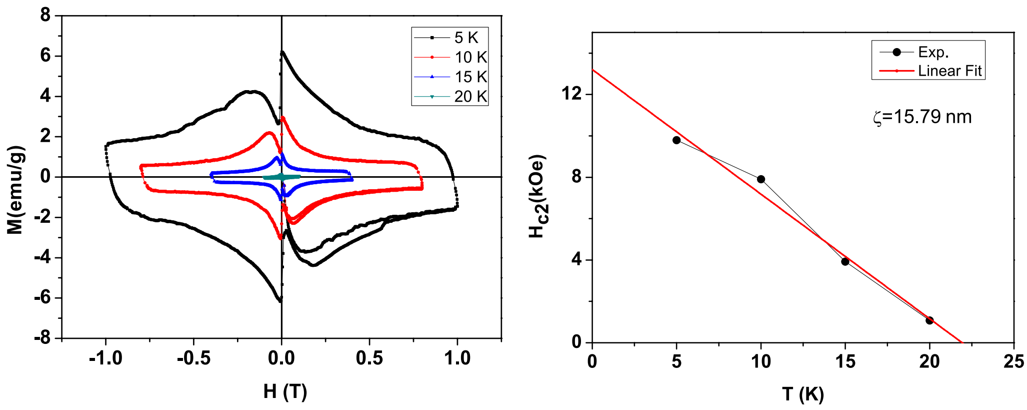

(a) (b)

Figure 5.28 : (a) M-H measurements of $BaFe_{1.9}Pt_{0.1}As_2$ sample at 5, 10, 15 and 20 K at $\pm$ 10 kOe applied field, (b) coherence length.

5.3.3 Magnetic behavior of $BaFe_{1.7}Pt_{0.3}As_2$ sample

Fig. 5.29 shows the ZFC versus FC magnetization curves for the $BaFe_{1.7}Pt_{0.3}As_2$. Sample was first cooled to low temperature in the background field (zero field). H=20 Oe was subsequently applied and the moment measured as a function of slowly increasing temperature, yielding curves labeled ZFC (zero-field cooled). The temperature was then slowly reduced through the superconducting transition, Tc, yielding the curves labeled FC (field cooled) in the figures. Meissner effect measurements in fields up to $\pm$ 0.05 T are given in the inset. Note that the ZFC data decrease rapidly for temperatures below T_c and quickly saturate to negative values. We have calculated roughly the effective magnetic susceptibility, $4\pi\chi_{eff}$, after demagnetization field correction (experimental samples had long cylindrical shapes). The value for $BaFe_{1.7}Pt_{0.3}As_2$ sample is approximately -0.98. T_c is found as 20.2 K from the graph. M-H curve taken at 5 K is given in the inset.

Table 5.4 : Pt content and superconducting phase transition temperatures of $BaFe_{2-x}Pt_xAs_2$ samples.

Pt Content, x	$T_c(K)(VSM)$	$T_c(K)(\rho)$	$T_c(K)(SDW)$
0	-	-	144
0.1	21.7	23.87	138
0.2	-	20.73	-
0.3	20.2	18.96	-
0.4	-	17.77	-

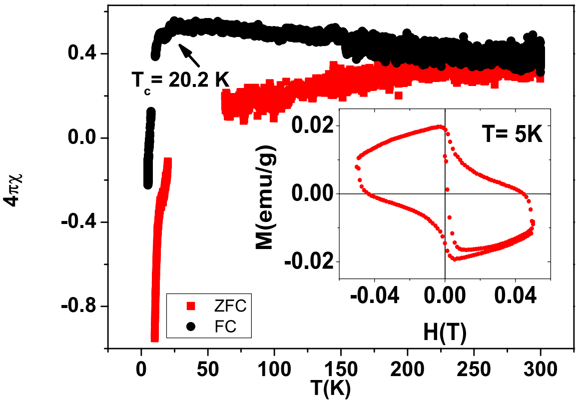

Figure 5.29 : ZFC-FC measurement in bulk $BaFe_{1.7}Pt_{0.3}As_2$ sample. Inset shows Meissner effect observed at T=5 K.

Pt content and superconducting phase transition temperatures of $BaFe_{2-x}Pt_xAs_2$ samples are given in table 5.4. x=0 sample is the parent sample ($BaFe_2As_2$) in which it is not superconductive. The resistivity of sample group has the highest value for phase transition temperature, T_c. Samples with x=0 and x=0.1 show an additional spin density wave (SDW) transition about 140 K. This is the value where an antiferromagnetic order sets in and it still persists in a lower amplitude for Pt doped sample [8].

5.3.4 Magnetic behavior of $Ba_{0.97}La_{0.03}Fe_{1.9}Pt_{0.1}As_2$ sample

The ZFC versus FC magnetization curves for the $Ba_{0.97}La_{0.03}Fe_{1.9}Pt_{0.1}As_2$ sample are given in Fig. 5.30. It was first cooled to low temperature in the background field, H=20 Oe. The temperature was then slowly reduced through the superconducting transition, $T_c = 19.9K$, yielding the curves labeled FC (field cooled) in the figures. Meissner effect measurement in fields up to ± 10 T applied field is given in the inset. Effective magnetic susceptibility, $4\pi\chi_{eff}$, after demagnetization field correction, is found as -0.79, indicating that the system is partially shielded.

M-H curves are taken at ± 0.1 T for the temperatures of 16.5, 17, 17.5, 18 and 18.5 K are shown in Fig. 5.31 (a). Note that Meissner effect is more visible at lower temperatures where sample is in superconducting state. Coherence length is calculated by using these data in Fig. 5.31 (b). It is found that ζ is equal to 24.48 nm for this sample.

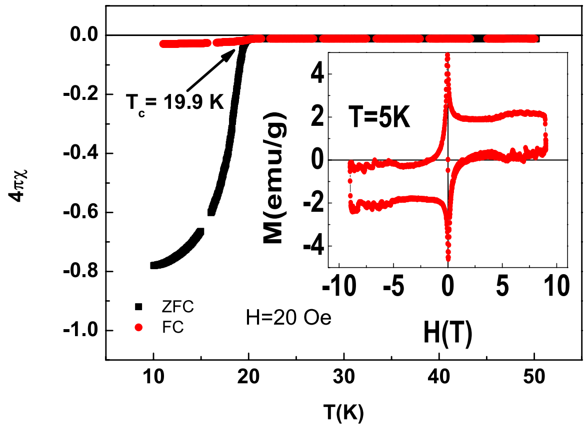

Figure 5.30 : ZFC-FC measurement in bulk $Ba_{0.97}La_{0.03}Fe_{1.9}Pt_{0.1}As_2$ sample. Inset shows Meissner effect observed at T=5 K.

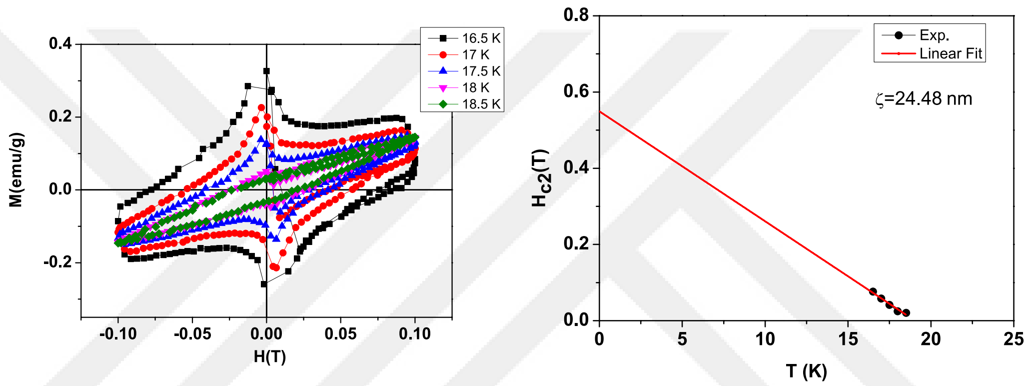

(a) (b)

Figure 5.31 : (a) M-H measurements of $Ba_{0.97}La_{0.03}Fe_{1.9}Pt_{0.1}As_2$ sample at 16.5, 17, 17.5, 18 and 18.5 K at ± 0.1 T applied field, (b) coherence length.

5.3.5 Magnetic behavior of $Ba_{0.95}La_{0.05}Fe_{1.9}Pt_{0.1}As_2$ sample

ZFC versus FC magnetization curves for the $Ba_{0.95}La_{0.05}Fe_{1.9}Pt_{0.1}As_2$ are shown in Fig. 5.32. Sample was first cooled to low temperature in the background field, H=20 Oe. The temperature was then slowly reduced through the superconducting transition, $T_c = 22.1K$, yielding the curves labeled FC (field cooled) in the figures. Meissner effect measurement at T=5 K in fields up to ± 10 T is given in the inset. Effective magnetic susceptibility, $4\pi\chi_{eff}$, after demagnetization field correction, is found as -0.78.

M-H curves are taken at ± 10 T applied field for the temperatures of 5, 10, 15,20 and 25 K are shown in Fig. 5.33 (a). Coherence length is calculated by using these data in Fig. 5.33 (b). It is found that ζ is equal to 5.21 nm for this sample.

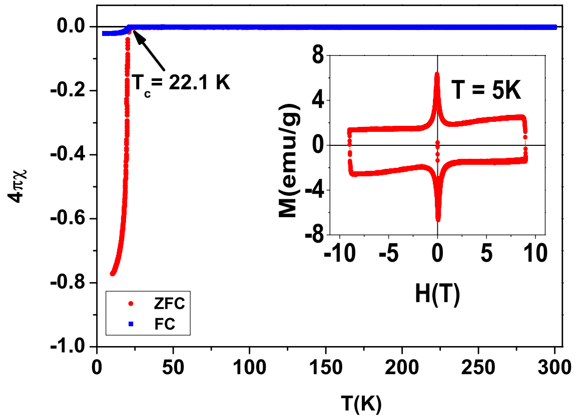

Figure 5.32 : ZFC-FC measurement in bulk $Ba_{0.95}La_{0.05}Fe_{1.9}Pt_{0.1}As_2$ sample. Inset shows Meissner effect observed at T=5 K.

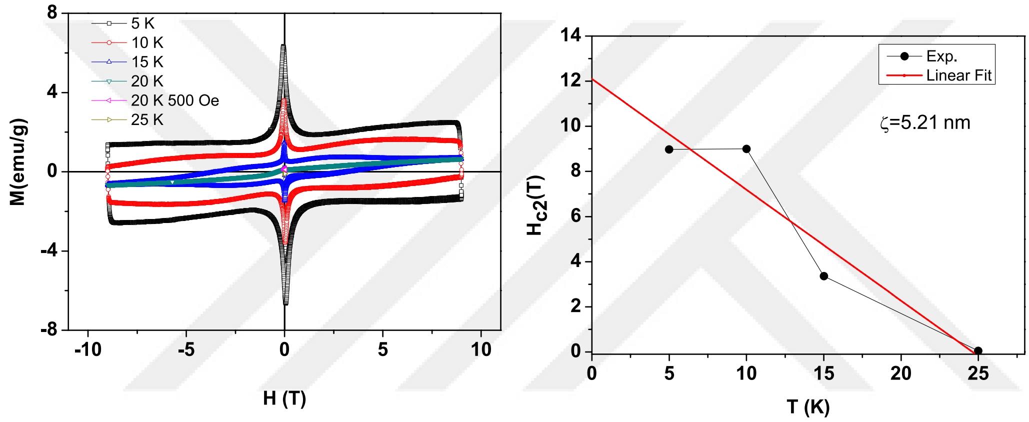

(a) (b)

Figure 5.33 : (a) M-H measurements of $Ba_{0.95}La_{0.05}Fe_{1.9}Pt_{0.1}As_2$ sample at 5, 10, 15, 20, 25 K at ± 10 T and 20K at 500Oe applied field, (b) coherence length.

5.3.6 Magnetic behavior of $Ba_{0.9}La_{0.1}Fe_{1.9}Pt_{0.1}As_2$ sample

ZFC versus FC magnetization curves for the $Ba_{0.9}La_{0.1}Fe_{1.9}Pt_{0.1}As_2$ are shown in Fİg. 5.34. Sample was first cooled to low temperature in the H=20 Oe background field. The temperature was then slowly reduced through the superconducting transition, $T_c = 21.3K$, yielding the curves labeled FC in the figures. Meissner effect measurement at T=5 K in fields up to ± 6 T is given in the inset. Effective magnetic susceptibility, $4\pi\chi_{eff}$, after demagnetization field correction, is found as -0.63 which means that sample is partially shielded against applied magnetic field.

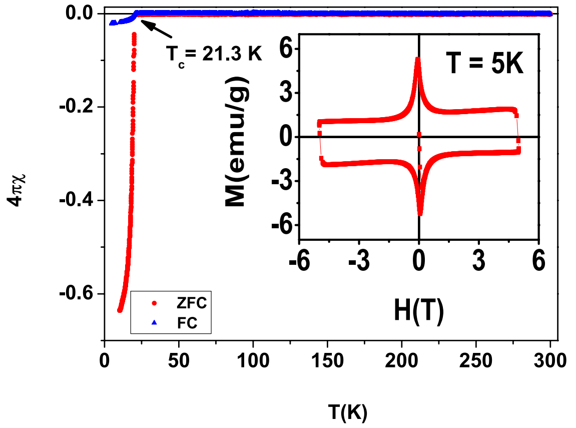

Figure 5.34 : ZFC-FC measurement in bulk $Ba_{0.9}La_{0.1}Fe_{1.9}Pt_{0.1}As_2$ sample. Inset shows Meissner effect observed at T=5 K.

5.3.7 Magnetic behavior of $Ba_{0.6}La_{0.4}Fe_{1.9}Pt_{0.1}As_2$ sample

Fig. 5.35 shows the ZFC versus FC magnetization curves for the $Ba_{0.6}La_{0.4}Fe_{1.9}Pt_{0.1}As_2$ compound. Sample was first cooled to low temperature in the background field, H=20 Oe. The temperature was then slowly reduced through the superconducting transition, $T_c = 23.3K$, yielding the curves labeled FC in the figures. Meissner effect measurement in fields up to ± 10 T applied field is given in the inset. Effective magnetic susceptibility, $4\pi\chi_{eff}$, after demagnetization field correction, is found as -0.70, indicating that the system is partially shielded.

M-H curves are taken at ± 10 T for the temperatures of 5,10 and 15 K are shown in Fig. 5.36 (a). Meissner effect is seen clearly at T=5 K. Coherence length is calculated by using these data in Fig. 5.36 (b). It is found that ζ is equal to 5.47 nm for this sample.

The superconductive behavior is observed for the La doped $BaFe_{1.9}Pt_{0.1}As_2$ samples. ZFC versus FC magnetization curves are measured at H=20 Oe. Superconducting temperatures , T_c, are determined from the measurements and it is seen that superconducting transition occurs in the $T_c = 19-24K$ interval. Meissner effect measurements in fields up to ± 10T are a clear evidence that samples exclude magnetic field lines. Roughly calculated the effective magnetic susceptibility, $4\pi\chi_{eff}$, are approximately equal to -1, indicating that the system is almost shielded where diamagnetic behavior is seen for the samples.

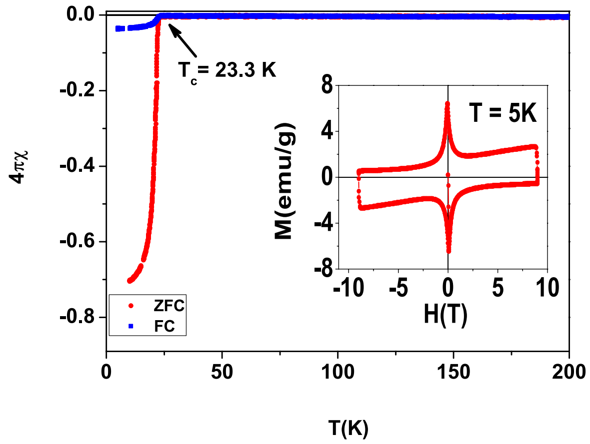

Figure 5.35 : ZFC-FC measurement in bulk $Ba_{0.6}La_{0.4}Fe_{1.9}Pt_{0.1}As_2$ sample. Inset shows Meissner effect observed at T=5 K.

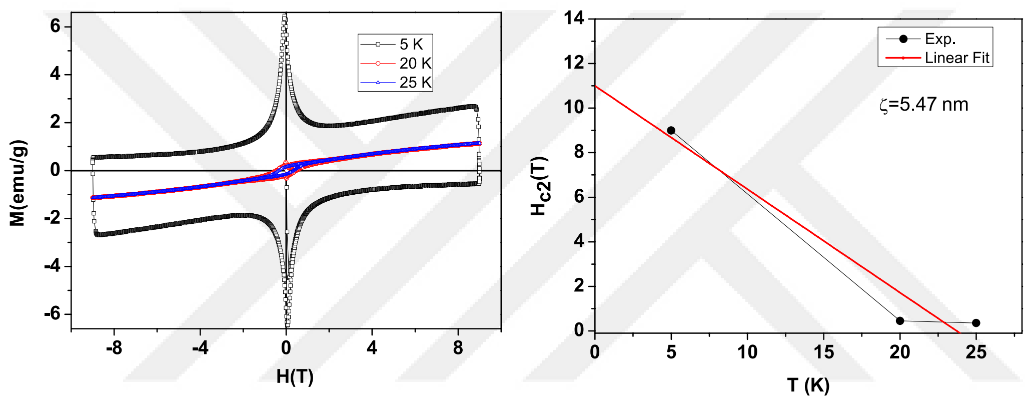

(a) (b)

Figure 5.36 : (a) M-H measurements of $Ba_{0.6}La_{0.4}Fe_{1.9}Pt_{0.1}As_2$ sample at 5, 20, and 25 K at ± 1 kOe, (b) coherence length.

Table 5.5 : La content, critical current, coherence length and superconducting phase transition temperatures of $Ba_{1-x}La_xFe_{1.9}Pt_{0.1}As_2$ samples.

La Content, x	$J_c(A/cm^2)x10^4$	Coherence Length $\zeta(nm)$	$T_c(K)(VSM)$	$T_c(K)(\rho)$
0	1.10	15.79	21.7	23.9
0.03	1.78	24.48	19.9	21.2
0.05	2.64	5.21	22.1	16.6
0.1	2.15	-	21.3	20.1
0.4	2.61	5.47	23.3	24.2

La content, critical current, coherence length and superconducting phase transition temperatures of $Ba_{1-x}La_xFe_{1.9}Pt_{0.1}As_2$ samples are given in table 5.5. The highest value for the critical current, $2.64 \times 10^4 A/cm^2$ is observed in $Ba_{0.95}La_{0.05}Fe_{1.9}Pt_{0.1}As_2$ sample in which it has the lowest values for the coherence length ζ and the phase transition temperature, T_c obtained from the resistivity measurement. La doped samples are showed a clear evidence for superconductivity that our results approve.

5.3.8 Magnetic behavior of Pt doped thermoelectric $BaFe_{4-x}Pt_xSb_{12}$ samples

Magnetization in the fields between H = ± 9T and its function of temperature are shown in Fig. 5.37 (a). It is seen that all samples obey Curie Weiss law above the Curie temperatures, but slightly deviates from linear behavior in paramagnetic regime. Below the T_c , there exist two successive magnetic transitions in Pt substituted compounds however, it is only one (transition from paramagnetic state to long range magnetic ordering) in Pt free compound . In Pt substituted compounds we observe that the first transition appears at T_c = 48 K. In addition, the second transition is observed at T_{irr} = 30 K. What we expect is a magnetic cluster state before the magnetic ordering transforms from paramagnetic to an irreversible ferromagnetic state. The magnetic moment calculation by fitting the inverse susceptibility to the Curie-Weiss equation for all samples in 80-180 K interval is given in Fig. 5.37 (b) and the magnetic moments per formula unit (f.u.) are shown in Table 5.6.

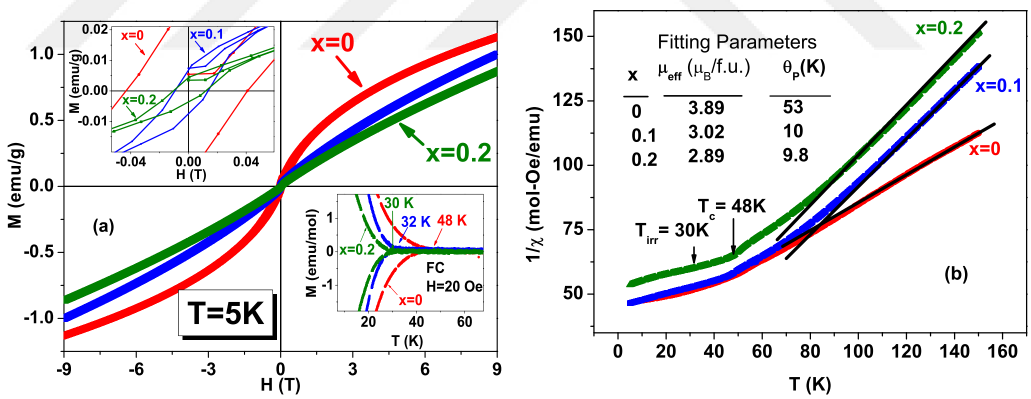

(a) (b)

Figure 5.37 : (a) Magnetization vs. temperature graphs at H = 20 Oe, (b) Reciprocal of magnetic susceptibility versus temperature plots for $BaFe_{4-x}Pt_xSb_{12}$ compounds at H = 70kOe field [43].

For Pt free compound, it is found to be as 3.89 μ_B/f.u. For a wider analysis of temperature range between 50-200K (not given in graph here) magnetic moment for x = 0 is found to be as 6 μ_B/f.u. [49]. In our temperature range, inverse magnetic susceptibility in the paramagnetic regime does not have linear temperature dependence. Such non-linear behavior in magnetic susceptibility observed at low temperature can be

Table 5.6 : Magnetic (at low temperature), resistivity and thermoelectric parameters (at room temperature) of $BaFe_{4-x}Pt_xSb_{12}$ compounds.

x	$T_c(K)$	$T_{irr}(K)$	$\mu_B/f.u$	$H_c(Oe)$	$\Theta_p(K)$	$\rho(\mu\Omega\mathrm{m})$	κ(W/mK)	$S(\mu$V/K)
0	48	48	3.89	410	53	3.57	5.53	43
0.1	48	32	3.02	140	10	4.68	5.81	38
0.2	48	30	2.89	125	9.8	5.17	4.56	49

originated by crystal electric field (CEF) effect, valence fluctuations or spin fluctuation origin [52]. Similar results were given to explain the behavior of the skutterudite $LaFe_4Sb_{12}$ presenting non-Fermi liquid (NFL) nature of itinerant d-electrons. We believe that spin fluctuation mechanism is responsible from this non-linearity in our samples [54, 55].Results are published [43].

5.4 Thermoelectric Behavior of Pt doped $BaFe_{4-x}Pt_xSb_{12}$ Samples

Low temperature thermoelectric properties were carried out by longitudinal steady-state measurements in a cryostat [56]. Thermoelectric power (Seebeck coefficient) versus temperature is measured for all compounds and it is shown in Fig. 5.38 (a). Seebeck coefficient sign indicate that major carrier in all compounds are holes. Negative Seebeck coefficient observed in Pt substituted compounds at low temperature is a trace of the presence of two type of carriers in these compounds. The Seebeck coefficient values of Pt doped samples are relatively smaller than in heavily doped skutterudite compounds reported in literature. This might be because Pt substitution induces mixed conduction in structure. In other words, in mixed conducting sample (in which electrons holes are both contribute to transport), Seebeck coefficient can be expressed as $S_{total} = \frac{(S_n\sigma_n + S_p\sigma_p)}{(\sigma_n + \sigma_p)}$ which indicates that Seebeck coefficient value of mixed conductors is smaller than samples have single carriers type [57]. In our samples Pt substitution might induce mixed conduction since Pt have two more valance electron in compare to Fe. Local maximum (or minimum) observed in compounds might be due to paramagnon-drag effect which is attributed by thermally non-equilibrium paramagnons dragging the charge carriers or spin fluctuation effect in materials. [23, 52]. The thermoelectric transport parameters are presented in Table 5.6.

The total thermal conductivity as a function of temperature is shown in Fig. 5.38 (b). The total thermal conductivity was calculated by $\kappa = \frac{P_h}{\Delta T}\frac{L}{A}$ where P_h, ΔT , L and A are

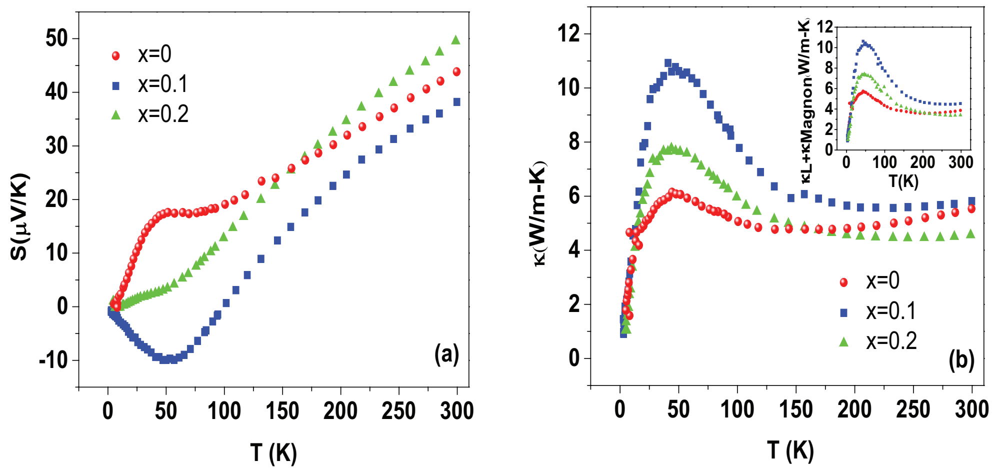

(a) (b)

Figure 5.38 : (a)Temperature dependence of Seebeck coefficient, (b) Total thermal conductivity for $BaFe_{4-x}Pt_xSb_{12}$ compounds (κ_L+κ_{Magnon} vs temperature plot in the inset) [43].

power of heater, temperature difference measured by thermocouple, distance between thermocouple and longitudinal cross section of sample based on steady state technique. The lattice contribution was obtained by subtracting the electronic contribution from the total thermal conductivity. The electronic contribution was calculated via the Wiedemann-Franz law, κ_e = LσT, where L, σ and T are the Lorenz number, electrical conductivity and absolute temperature, respectively. We have used an empirical value of $2 \times 10^{-8} V^2/K^2$ for the Lorenz number. This value of Lorenz number was found previously to be appropriate [58]. The lattice contribution of thermal conductivity depicted in the inset of Fig. 5.38(b). It is seen that the major part of total thermal conductivity is originated from heat carrier phonons.

6. CONCLUSION

Fe-As based $BaFe_2As_2$, $BaFe_{2-x}Pt_xAs_2$ and $Ba_{1-x}La_xFe_{1.9}Pt_{0.1}As_2$ polycrystalline samples are successfully synthesized by a solid-state reaction method. High purity elements are mixed in desired stoichiometry and sealed in quartz tubes to prevent oxidation during melting. In order to avoid gas leaks in the tubes, sintering process are separated into parts gradually for the work safety. Owens placed in the hood controlled by continuous air flow to help air conditioning inside the laboratory. Protective glasses, handgloves and aprons protecting against cuts are weared. Laboratory work is then became appropriate through those precautions.

Structural analyses of samples are made by X-Ray diffraction after the chemical synthesis part. Results are analyzed by FullProf software. Several programs are exist in literature like Maud, Crystal Impact Match, Topaz etc.. The data acquisition on such analyses require detailed information about the scan parameters. It is seen that step sizes bigger than 0.1° make no sense to calculate. The reason for poor spectral line is inadequate data point that diffractometer accumulates to "define" the position of peaks corresponding to the Bragg angles. As a result of skipped peaks, the characteristic behavior for the full with half maximum (FWHM) of a peak will then be damaged or incorrect to take into account. Smaller step size is measured during scans and this problem is solved. Profile matching are done after these simple tricks are achieved for whole samples and structural parameters are determined. Some samples are found single phase in which published in the articles during our study. The work on such compounds was physically remarkable and data obtained from those samples are investigated in detail by Rietveld refinement. Our target to produce "single phase" polycrystalline samples are achieved successfully. Although we do not prefer some strange phases, (generally formed at primitive unit cell) impurities are seen even they have low percentage. Several identification issues are then grouped into two categories. First one is impurities coming from weight part. It is clearly seen that rare earth elements like Lanthanum and Barium are difficult to handle with. Since they have high affinity to construct oxide phase, it is a smart way to work in glovebox. We did not have such opportunity. Alternatively, La, Ba grains are weighted lastly (after the arsenide,iron and platinum elements) as quick as possible and then cut quickly to mix with other reactants. The second one is correct operation temperature for the owens. Since it takes days to make a solid state synthesis, it is impossible to observe electricity cuts. And when it is cut, owen heater stops heating and so temperature decreases rapidly. If it operates again, one can never detect any sign for this irregularity and believe that alloy is formed at the desired stoichiometry. But second phase should survive event at high temperatures. Such situation is the most dangerous problem that we experienced. Technically it should have pressure fluctuations inside the quartz tube. Because a rapid pressure increase inside the owen breaks the tube. So this brings an additional oxide phase as an alternative to your main phase. And economically this is not preferable too. When the cost of elements (high purity) and tubes are take into account, one single sample is about 30-40$ and this situation limits the number of our experiments.

It is seen that unit cell parameters and symmetry group of samples are determined in agreement with the literature. The structural phase transitions from tetragonal $I4/mmm$ to orthorhombic Fmmm lattice in $BaFe_2As_2$ and $BaFe_{1.9}Pt_{0.1}As_2$ samples are observed at 140 K and 138 K respectively. This clearly seen spin density wave transition (SDW) is not seen in La doped $BaFe_{1.9}Pt_{0.1}As_2$ samples. This should be because of number of stackings are increased in La doped unit cell when compared to parent sample.

The idea that we focus on here is to investigate the Fe-As layer rather than the conventional superconductors, Cu-O, like in cuprates. Tetragonal structures having I4/mmm symmetry, are then have an ability to be a "host" material for charge carriers in these types of superconductive alloys. $BaFe_{1.9}Pt_{0.1}As_2$ unit cell should consist Fe-As and Ba layers. Here Fe-As are responsible from charge carriers by platinum doping and Ba layers are said to be reservoirs for conservation of the charge. Superconductivity should be emerged as a result of these interpretations, it is reported in the literature. There are several unit cells adoptable for this purposes. Some examples are LaFeAsO, crystallizes in P4/nmm; SrPtAs, crystallizes in $P6_3/mmc$ etc. In LaFeAsO sample, unit cell consists Fe-As and LaO layers. Fe-As are responsible from charge carriers and LaO layers are said to be reservoirs for the blocking the charge. Both layers are sandwiched together and the integrity of the mechanism is supplied by this way. The doping levels of platinum and lanthanum are investigated in our study and it is seen that samples have the same unit cell to maintain superconductive behavior. As a clear evidence for superconductivity, resistivity measurements are done on samples.

Resistivity measurements are done in liquid nitrogen first and in liquid helium by the help of a hand made glass cryostat. This method facilitates the measurement by providing longer last of the liquid helium. It maintains liquid phase about ten days which makes our measurement economical. Sticking of samples on the sample holder at low temperatures are provided by G-varnish, and it is seen that the temperature dependence of the resistivity for the parent sample, $BaFe_2As_2$ exhibits the same behavior including a very close match to reported values given in the literature. These results include a sharp kink at T = 140 K, where a structural phase transition (from tetragonal to orthorhombic upon cooling) occurs. And this temperature point is compatible with the corresponding XRD measurement (known to be tetragonal at room temperature). Since we don't have opportunity to have XRD measurement at low temperature, symmetry breaking from I4/mmm to Fmmm is not determined but it is shown in resistivity measurement, where it coincides with the onset of antiferromagnetic (AFM) order. This is a first order phase transition. Same SDW anomaly is observed for the platinum doped sample at a slightly reduced temperature (T=138 K) for the $BaFe_{1.9}Pt_{0.1}As_2$ sample, but it is less pronounced. Superconductive phase transition temperature, T_c for the Pt doping is investigated in the literature. It is found that Pt doping is effective on the change of T_c at lower doping rates like $x = 0.2$. x=0 sample is the parent sample ($BaFe_2As_2$) in which it is not superconductive but the $BaFe_{1.9}Pt_{0.1}As_2$ sample has the highest value in Pt doped group for phase transition temperature, T_c. In contrast to the literature, we showed that superconductivity can be observed even in x=0.3 doping rates in such materials.

Lanthanum doped samples are successfully synthesized in addition to the Pt doped ones. And resistivity measurements are showed that superconductivity still can be observed in such tetragonal I4/mmm systems. One of the difference from LaFeAsO materials is the symmetry group and consisting oxide layers. Resistivity of these samples are showed a clear evidence for superconductivity that our results approve.

The magnetic measurements of materials are done by measuring zero field cooling (ZFC) and field cooling (FC) curves and magnetization as a function of applied field. The critical current density, which is a remarkable sign that a superconductor can carry how much charge is estimated by models given in the literature. Ginzburg-Landau parameter also known as coherence length is calculated from the Meissner effects observed in these samples.

Results show that samples based on a tetragonal structure are convenient to be a host material for the superconductive behavior. This means the doping of rare-earth ions to those samples provide materials that have characteristic properties like showing zero resistivity and the exclusion of magnetic field lines. In our study, platinum and lanthanum are doped and new sample sets are prepared. It is seen that ZFC-FC curves are separated in the phase transition temperature, T_c, showing superconductive behavior compatible with the resistivity measurements. Meissner effect is observed in both platinum and lanthanum doped samples. Critical current calculations showed that the highest value, $2.64\times10^4 A/cm^2$ is observed in $Ba_{0.95}La_{0.05}Fe_{1.9}Pt_{0.1}As_2$ sample in which it has the lowest values for the coherence length ζ and the phase transition temperature, T_c obtained from the resistivity measurement. Critical current of all samples have a J_c in 10^4 order and change in $1.10-2.64\times10^4 A/cm^2$ interval. It is noted that samples having a clear XRD result, have perfect Meissner effect without any noise. Phase transition temperature obtained from the magnetic measurements are generally found in 20.2-21.7 K interval for the Pt doped samples. Lanthanum doped samples have a range of T_c in 19.9-23.3 K interval. The lower part of this temperature indicates superconducting regime and this motivated us to have an expectation of exclusion of magnetic field lines and observe Meisnerr effect. M versus H curves are measured in several temperatures below the phase transition temperature. Analysis of the results helped us to calculate coherence length ζ for the samples by obtaining H_c readings at different measurement temperatures. From the M-H curves of samples measured below the T_c, lines are extrapolated to T=0 K and coherence lengths are found in nm range.

By transforming magnetization from emu/g to volume magnetization, susceptibility for the samples are obtained in terms of magnetization data. The termination of ZFC and FC curves in to close values to -1 in y axis, shows that samples are mostly diamagnetic with a high volume fraction. Samples are mostly presented superconductivity in general. Phase transition temperatures found from ZFC-FC curves are compatible with the resistivity data. La doped samples are showed a clear evidence for superconductivity that both resistivity and magnetic results approve.

Resistivity of $BaFe_2As_2$ thin film at liquid He is measured between 4.2-300K. A phase transition at $T_c = 6.7K$ is seen clearly with reproducible experiments which is very similar to a superconductive phase transition. We observe superconductivity for the first time in an amorphous thin film. This result is interesting because current macroscopic theory of superconductivity is based on Cooper pairing mechanism. The drop of resistivity down to zero obeys filamentary superconductivity that is seen in literature in principle.

The difference in our study is that we create a disorder in material and it is amorphous. This process is realized in a simple flash evaporation system under vacuum. This is important because same kind of samples are produced in molecular beam epitaxy (MBE) or similar systems that we are not able to. Some studies are reported that both in bulk and thin film samples, showing that it is possible to apply pressure to the system and create disorder. This method is a way in order to trigger the superconductivity in such systems. For the first time, we observe the superconductivity in an amorphous thin film above the liquid He temperature, $T_c = 6.7K$ at ambient conditions (without applying any pressure). Magnetic characterization of this sample still continues and results will be presented in an appropriate publisher.

In case of any failure in preparing Fe-As layered samples, antimony doped compounds are prepared. $BaFe_4Sb_{12}$ sample is prepared first. This sample is known as skutterudite compound in literature and it is thermoelectrically efficient. Since the synthesis was successful, the thermoelectric and magnetic properties of Pt substituted $BaFe_{4-x}Pt_xSb_{12}$ (x = 0, 0.1, 0.2) compounds were investigated in this part of study. X-Ray diffraction, resistivity, magnetic measurements, Seebeck coefficient and thermal conductivity of samples are measured. Temperature depending resistivity shows that all samples show semi metallic behavior in the temperature range of 4.2 K to 300 K. Increases in resistivity with Pt content is interpreted as existing of different scattering mechanisms such as spin fluctuation and Kondo impurity in these compounds or decreasing hole concentration. Kondo minimum are confirmed by temperature dependence of logarithmic resistivity analysis at 2-50 K which might be due to local deformation in crystal structure as a result of spin fluctuation mechanism. Local minimum and maximum in Seebeck coefficient observed might be due to paramagnon drag or spin fluctuation effect in materials. Magnetic susceptibility for the compounds x = 0.1 and x = 0.2 show that there are two successive transition, paramagnetic to magnetic state at T_c = 48 K and short range magnetic to long range magnetic ordering at lower temperatures, however there is only one transition from paramagnetic to long range ordering transition in Pt free compound.

The lattice part of thermal conductivity versus temperature plot shows that the major part of total thermal conductivity is dominated by lattice contribution.

Local maximum & minimum in Seebeck coefficient versus temperature plot, Kondo minimum observed in logarithmic resistivity show that there is a close relation between magnetic and thermoelectric properties due to spin fluctuation effect in Pt substituted $BaFe_{4-x}Pt_xSb_{12}$ (x = 0, 0.1, 0.2) compounds.

In order to invent original samples, this topic is always open for new synthesis. The quality of results are directly proportional to the sample synthesis method. All types of chemical synthesis including bulk, thin film and single crystal samples of arsenic doped iron pnictide superconductors, thermoelectric samples requiring special technics are hard to produce. These methods require a high level of knowledge and conscious mind. Our group produced these materials successfully and we proved that we could produce these materials by making basic experiments. Our struggle here is to survive by material characterization rather than the competition with famous groups who are already proved their expertise in literature.

REFERENCES

[1] **Onnes, H.K.** (1991). *Through Measurement to Knowledge: The Selected Papers of Heike Kamerlingh Onnes 1853–1926*, Springer Netherlands.

[2] **Berlincourt, T.G. and Hake, R.R.** (1963). Superconductivity at High Magnetic Fields, *Phys. Rev.*, *131*, 140–157.

[3] **Bednorz, J.G. and Müller, K.A.** (1986). Possible high T_c superconductivity in the Ba-La-Cu-O system, *Zeitschrift fur Physik B Condensed Matter*, *64*, 189–193.

[4] **Hor, P.H.**, **Meng, R.L.**, **Wang, Y.Q.**, **Gao, L.**, **Huang, Z.J.**, **Bechtold, J.**, **Forster, K. and Chu, C.W.** (1987). Superconductivity above 90 K in the square-planar compound system *A* $Ba_2Cu_3O_{6+x}$ with A=Y , La, Nd, Sm, Eu, Gd, Ho, Er and Lu, *Phys. Rev. Lett.*, *58*, 1891–1894.

[5] **Dai, P.**, **Chakoumakos, B.**, **Sun, G.**, **Wong, K.**, **Xin, Y. and Lu, D.** (1995). Synthesis and neutron powder diffraction study of the superconductor HgBa2Ca2Cu3O8 + ÎŽ by Tl substitution, *Physica C: Superconductivity*, *243*, 201 – 206.

[6] **Drozdov, A.P.**, **Eremets, M.I.**, **Troyan, I.A.**, **Ksenofontov, V. and Shylin, S.I.** (2015). Conventional superconductivity at 203 kelvin at high pressures in the sulfur hydride system, *Nature*, *525*, 73–76.

[7] **Kamihara, Y.**, **Watanabe, T.**, **Hirano, M. and Hosono, H.** (2008). Iron-Based Layered Superconductor La[$O_{1-x}F_x$]FeAs (x=0.05-0.12) with Tc=26K, *Journal of the American Chemical Society*, *130*, 3296–3297.

[8] **Rotter, M.**, **Tegel, M.**, **Johrendt, D.**, **Schellenberg, I.**, **Hermes, W. and Pöttgen, R.** (2008). Spin-density-wave anomaly at 140 K in the ternary iron arsenide $BaFe_2As_2$, *Phys. Rev. B*, *78*, 020503.

[9] **Rotter, M.**, **Tegel, M. and Johrendt, D.** (2008). Superconductivity at 38 K in the Iron Arsenide $(Ba_{1-x}K_x)Fe_2As_2$, *Phys. Rev. Lett.*, *101*, 107006.

[10] **Saha, S.R.**, **Drye, T.**, **Kirshenbaum, K.**, **Butch, N.P.**, **Zavalij, P.Y. and Paglione, J.** (2010). Superconductivity at 23 K in Pt doped $BaFe_2As_2$ single crystals, *Journal of Physics: Condensed Matter*, *22*, 072204.

[11] **Guo, Y.**, **Wang, X.**, **Li, J.**, **Zhang, S.**, **Yamaura, K. and Takayama-Muromachi, E.** (2012). Superconductivity in Pt Doped $BaFe_2As_2$, *Journal of the Physical Society of Japan*, *81*, 064704.

[12] **Boeri, L.**, **Dolgov, O.V. and Golubov, A.A.** (2008). Is $LaFeAsO_{1-x}F_x$ an Electron-Phonon Superconductor?, *Phys. Rev. Lett.*, *101*, 026403.

[13] **Chu, C. and Lorenz, B.** (2009). High pressure studies on Fe-pnictide superconductors, *Physica C: Superconductivity*, *469*, 385 – 395.

[14] **Paglione, J. and Greene, R.L.** (2010). High-temperature superconductivity in iron-based materials, *Nat Phys*, *6*, 645.

[15] **Mazin, I.I.**, **Singh, D.J.**, **Johannes, M.D. and Du, M.H.** (2008). Unconventional Superconductivity with a Sign Reversal in the Order Parameter of $LaFeAsO_{1-x}F_x$, *Phys. Rev. Lett.*, *101*, 057003.

[16] **Leithe-Jasper, A.**, **Schnelle, W.**, **Geibel, C. and Rosner, H.** (2008). Superconducting State in $SrFe_{2-x}Co_xAs_2$ by Internal Doping of the Iron Arsenide Layers, *Phys. Rev. Lett.*, *101*, 207004.

[17] **Drew, A.J.**, **Pratt, F.L.**, **Lancaster, T.**, **Blundell, S.J.**, **Baker, P.J.**, **Liu, R.H.**, **Wu, G.**, **Chen, X.H.**, **Watanabe, I.**, **Malik, V.K.**, **Dubroka, A.**, **Kim, K.W.**, **Rössle, M. and Bernhard, C.** (2008). Coexistence of Magnetic Fluctuations and Superconductivity in the Pnictide High Temperature Superconductor $SmFeAsO_{1-x}F_x$ Measured by Muon Spin Rotation, *Phys. Rev. Lett.*, *101*, 097010.

[18] **Bell, L.E.** (2008). Cooling, Heating, Generating Power, and Recovering Waste Heat with Thermoelectric Systems, *Science*, *321*, 1457.

[19] **Rowe, D.M.** (2005). *Thermoelectrics Handbook: Macro to Nano*, CRC Press, Boca Raton.

[20] **Slack, G.A.** (1995). *CRC Handbook of Thermoelectricity*, CRC Press, USA.

[21] **Uher, C.** (2001). *Recent Trends in Thermoelectric Materials Research I*, Academic Press, USA.

[22] **Young Cho, J.**, **Ye, Z.**, **Tessema, M.M.**, **Salvador, J.R.**, **Waldo, R.A.**, **Yang, J.**, **Zhang, W.**, **Yang, J.**, **Cai, W. and Wang, H.** (2013). Thermoelectric performance of p-type skutterudites $Yb_xFe_{4-y}Pt_ySb_{12}$ ($0.8 \leq x \leq 1$, y=1 and 0.5), *Journal of Applied Physics*, *113*, 143708.

[23] **Qiu, P.F.**, **Yang, J.**, **Liu, R.H.**, **Shi, X.**, **Huang, X.Y.**, **Snyder, G.J.**, **Zhang, W. and Chen, L.D.** (2011). High-temperature electrical and thermal transport properties of fully filled skutterudites RFe_4Sb_{12} (R = Ca, Sr, Ba, La, Ce, Pr, Nd, Eu, and Yb), *Journal of Applied Physics*, *109*, 063713.

[24] **Sales, B.C.** (2001). *Handbook on the Physics and Chemistry of the Rare Earths*, North Holland, USA.

[25] **Nolas, G.S.**, **Cohn, J.L. and Slack, G.A.** (1998). Effect of partial void filling on the lattice thermal conductivity of skutterudites, *Phys. Rev. B*, *58*, 164.

[26] **Leszczynski, J.**, **Ros, V.D.**, **Lenoir, B.**, **Dauscher, A.**, **Candolfi, C.**, **Masschelein, P.**, **Hejtmanek, J.**, **Kutorasinski, K.**, **Tobola, J.**, **Smith, R.I.**, **Stiewe, C. and Müller, E.** (2013). Electronic band structure, magnetic, transport and thermodynamic properties of In-filled skutterudites $In_xCo_4Sb_{12}$, *Journal of Physics D: Applied Physics*, *46*, 495106.

[27] **Morelli, D.T.**, **Meisner, G.P.**, **Chen, B.**, **Hu, S. and Uher, C.** (1997). Cerium filling and doping of cobalt triantimonide, *Phys. Rev. B*, *56*, 7376.

[28] **Nolas, G.S.**, **Kaeser, M.**, **Littleton, R.T. and Tritt, T.M.** (2000). High figure of merit in partially filled ytterbium skutterudite materials, *Applied Physics Letters*, *77*, 1855.

[29] **Chen, L.D.**, **Kawahara, T.**, **Tang, X.F.**, **Goto, T.**, **Hirai, T.**, **Dyck, J.S.**, **Chen, W. and Uher, C.** (2001). Anomalous barium filling fraction and n-type thermoelectric performance of $Ba_yCo_4Sb_{12}$, *Journal of Applied Physics*, *90*, 1864.

[30] **Zhao, X.Y.**, **Shi, X.**, **Chen, L.D.**, **Zhang, W.Q.**, **Zhang, W.B. and Pei, Y.Z.** (2006). Synthesis and thermoelectric properties of Sr-filled skutterudite $Sr_yCo_4Sb_{12}$, *Journal of Applied Physics*, *99*, 53711.

[31] **Cheng, Z.Z.**, **Cheng, Z. and Wu, M.H.** (2008). Magnetic properties, electronic structure, and optical properties of the filled skutterudite $BaFe_4Sb_{12}$, *Journal of Magnetism and Magnetic Materials*, *320*, 2591.

[32] **Takabatake, T.**, **Matsuoka, E.**, **Narazu, S.**, **Hayashi, K.**, **Morimoto, S.**, **Sasakawa, T.**, **Umeo, K. and Sera, M.** (2006). Roles of spin fluctuations and rattling in magnetic and thermoelectric properties of AT_4Sb_{12} (A=Ca, Sr, Ba, La; T=Fe, Ru, Os), *Physica B: Condensed Matter*, *383*, 93.

[33] **Ashcroft, N.W. and Mermin, N.D.** (1976). *Solid State Physics*, Saunders College.

[34] **Kittel, C.** (2005). *Introduction to Solid State Physics*, John Wiley & Sons, Inc.

[35] **McHenry, M.E. and Sutton, R.A.** (1994). Flux pinning and dissipation in high temperature oxide superconductors, *Progress in Materials Science*, *38*, 159 – 310.

[36] **Chen, D.X. and Goldfarb, R.B.** (1989). Kim model for magnetization of type-II superconductors, *Journal of Applied Physics*, *66*, 2489–2500.

[37] **BEAN, C.P.** (1964). Magnetization of High-Field Superconductors, *Rev. Mod. Phys.*, *36*, 31.

[38] **Gurevich, A.** (2007). Limits of the upper critical field in dirty two-gap superconductors, *Physica C: Superconductivity*, *456*, 160.

[39] **Nishikubo, Y.**, **Kudo, K. and Nohara, M.** (2011). Superconductivity in the Honeycomb-Lattice Pnictide SrPtAs, *Journal of the Physical Society of Japan*, *80*, 055002.

[40] **Ballıkaya, S.** (2010). $CoSb_3$ bazlı katkılı skutteruditelerin transport özellikleri, *Ph.D. thesis*, www.istanbul.edu.tr.

[41] **Url-1**, `http://img.chem.ucl.ac.uk/sgp/large/sgp.htm`, alındığı tarih: 02.02.2016.

[42] **Öveçoğlu, L.**, (2010), MAM503E Structure and Crystallography Lecture Notes, Istanbul Technical University.

[43] **Sertkol, M., Ballıkaya, S., Aydoğdu, F., Güler, A., Özdemir, M. and Öner, Y.** (2016). Thermoelectric and Magnetic Properties of Pt-Substituted $BaFe_{4-x}Pt_xSb_{12}$ Compounds, *Journal of Electronic Materials*, 1–6.

[44] **Yamagishi, T., Ueda, S., Takeda, S., Takano, S., Mitsuda, A. and Naito, M.** (2011). A study of the doping dependence of Tc in $Ba_{1-x}K_xFe_2As_2$ and $Sr_{1-x}K_xFe_2As_2$ films grown by molecular beam epitaxy, *Physica C: Superconductivity*, *471*, 1177.

[45] **Huang, Q., Qiu, Y., Bao, W., Green, M.A., Lynn, J.W., Gasparovic, Y.C., Wu, T., Wu, G. and Chen, X.H.** (2008). Neutron Diffraction Measurements of Magnetic Order and a Structural Transition in the Parent $BaFe_2As_2$ Compound of FeAs-Based High-Temperature Superconductors, *Phys. Rev. Lett.*, *101*, 257003.

[46] **Guler, A., Sertkol, M., Saribaev, L., Ozdemir, M., Oner, Y. and Ross, J.H.** (2015). Superconductivity in Pt- and La-Doped $BaFe_2As_2$ Compounds Prepared by Solid-State Reaction, *IEEE Transactions on Magnetics*, *51*, 1.

[47] **Takeda, N. and Ishikawa, M.** (2004). Competition between Kondo effect and ferromagnetic interaction in skutterudite $La_{1-x}Sm_xFe_4P_{12}$, *Journal of Magnetism and Magnetic Materials*, *272*, 0304.

[48] **Rotundu, C.R., Andraka, B. and Schlottmann, P.** (2007). Exotic Kondo-hole band resistivity and magnetoresistance of $Ce_{1-x}La_xOs_4Sb_{12}$ alloys, *Phys. Rev. B*, *76*, 054416.

[49] **Matsuoka, E., Hayashi, K., Ikeda, A., Tanaka, K., Takabatake, T. and Matsumura, M.** (2005). Nearly Ferromagnetic Metals AFe_4Sb_{12} (A = Ca, Sr, and Ba), *Journal of the Physical Society of Japan*, *74*, 1382.

[50] **Wu, B.M., Li, B., Zhen, W.H., Ausloos, M., Du, Y.L., Fagnard, J.F. and Vanderbemden, P.** (2005). Spin-cluster effect and lattice-deformation-induced Kondo effect, spin-glass freezing, and strong phonon scattering in $La_{0.7}Ca_{0.3}Mn_{1-x}Cr_xO_3$, *Journal of Applied Physics*, *97*, 103908.

[51] **Bergmann, G. and Marquardt, P.** (1978). Temperature dependence of the resistivity in amorphous ferromagnetic alloys: Spin-wave contribution and resistivity minimum, *Phys. Rev. B*, *17*, 1355.

[52] **Oner, Y., Kamer, O., Jr, J.H.R., Lue, C. and Kuo, Y.** (2005). Magnetic phase transitions in intermetallic CeCuGe compound, *Solid State Communications*, *136*, 533.

[53] **Engelmann, J., Grinenko, V., Chekhonin, P., Skrotzki, W., Efremov, D.V., Oswald, S., Iida, K., Hühne, R., Hänisch, J., Hoffmann, M., Kurth, F., Schultz, L. and Holzapfel, B.** (2013). Strain induced superconductivity in the parent compound $BaFe_2As_2$, *Nature Communications*, *4*, 2877.

[54] **Schnelle, W.**, **Leithe-Jasper, A.**, **Rosner, H.**, **Cardoso-Gil, R.**, **Gumeniuk, R.**, **Trots, D.**, **Mydosh, J.A. and Grin, Y.** (2008). Magnetic, thermal, and electronic properties of iron-antimony filled skutterudites $M\mathrm{Fe_4Sb_{12}}$ ($M = \mathrm{Na, K, Ca, Sr, Ba, La, Yb}$), *Phys. Rev. B*, *77*, 094421.

[55] **Viennois, R.**, **Charar, S.**, **Ravot, D.**, **Haen, P.**, **Mauger, A.**, **Bentien, A.**, **Paschen, S. and Steglich, F.** (2005). Spin fluctuations in the skutterudite compound $LaFe_4Sb_{12}$, *The European Physical Journal B - Condensed Matter and Complex Systems*, *46*, 257.

[56] **Uher, C.**, **Li, C.P. and Ballikaya, S.** (2010). Charge-Compensated n-Type Skutterudites, *Journal of Electronic Materials*, *39*, 2122.

[57] **Li, S.S.** (1993). *Semiconductors Physical Electronic*, Plenum Press, New York and London.

[58] **Qiu, P.F.**, **Liu, R.H.**, **Yang, J.**, **Shi, X.**, **Huang, X.Y.**, **Zhang, W.**, **Chen, L.D.**, **Yang, J. and Singh, D.J.** (2012). Thermoelectric properties of Ni-doped $CeFe_4Sb_{12}$ skutterudites, *Journal of Applied Physics*, *111*, 023705.

CURRICULUM VITAE

Name Surname: Murat SERTKOL

Place and Date of Birth: Uzunköprü - 28 August 1981

E-Mail: msertkol@gmail.com

EDUCATION:

- **B.Sc.:** 2005, Marmara University, Atatürk Education Faculty, Department of Physics
- **M.Sc.:** 2009, Fatih University, Science and Art Faculty, Department of Physics

PROFESSIONAL EXPERIENCE AND REWARDS:

- 2005-2009 Research Assistant at Fatih University Department of Physics.
- 2011-2012 Tübitak 1001 Project, 109T687,
- 2012-2014 Tübitak 1001 Project, 111T779,
- 2016-2018 Tübitak 1001 Project, 115F510,
- 2014-2016 Tübitak 2211-C Öncelikli Alanlar Project (PhD Funding Program by TUBITAK).

PUBLICATIONS, PRESENTATIONS AND PATENTS ON THE THESIS:

- **Sertkol, M.** (Corresponding Author), Güler, A., Öner, Y., 2016. Superconductivity In La Doped $BaFe_{1.9}Pt_{0.1}As_2$ Compounds Prepared By Solid State Reaction. *32. Uluslararası Fizik Kongresi*, September 6-9, 2016 Bodrum, Turkey.
- **Sertkol, M.** (Corresponding Author), Ballıkaya, S., Aydoğdu, F., Güler, A., Özdemir, M., Öner, Y., 2016. Thermoelectric and Magnetic Properties of Pt Substituted $BaFe_{4-x}Pt_xSb_{12}$ Compounds, *Journal of Electronic Materials*, DOI: 10.1007/s11664-016-4855-0.
- Güler, A., **Sertkol, M.** (Corresponding Author), Saribaev, L., Özdemir, M., Öner, Y., Ross Jr., J. H., 2015. Superconductivity in Pt And La Doped $BaFe_2As_2$ Compounds Prepared By Solid State Reaction, *IEEE Transactions on Magnetics,* 51, 1-4.

OTHER PUBLICATIONS, PRESENTATIONS AND PATENTS:

- Güner, S., Baykal, A., Amir, Md., Güngüneş, H., Geleri M., Sözeri, H., Shirsath, Sagar E., **Sertkol, M.**, 2016. Synthesis and characterization of oleylamine capped $Mn_xFe_{1-x}Fe_2O_4$ nanocomposite: Magneto-optical properties, cation distribution and hyperfine interactions, Journal of Alloys and Compounds, July 2016, Doi:10.1016/j.jallcom.2016.07.033.

- İ.Ermiş, **M. Sertkol**, V. Çorumlu, Y. Dağdemir, M. Arı, "Synthesis of $(Bi_2O_3)_{0.9-x}(Tb_4O_7)_{0.1}(Sm_2O_3)_x$ electrolyte for IT-SOFCs", Synthesis and Reactivity in Inorganic, Metal-Organic, and Nano-Metal Chemistry, DOI:10.1080/15533174.2016.1157822.

- İ.Ermiş, V. Çorumlu, **M. Sertkol**, M. Öztürk, M.Kaleli, A. Çetin, M.Türemiş, M. Arı, "Microstructure and Electrical Conductivity of ZnO Addition on the Properties of $(Bi_{0.92}Ho_{0.03}Er_{0.05})_2O_3$", Journal of Electronic Materials, DOI:10.1007/s11664-016-4799-4.

- A. Baykal, S . Eryiğit, **M. Sertkol**, S.Ünlü , A. Yıldız, Sagar E.Shirsath, "The Effect of Cr^{3+} Substitution on Magnetic Properties of $CoFe_2O_4$ Nanoparticles Synthesized by Microwave Combustion Route ", Journal of Superconductivity and Novel Magnetism, DOI 10.1007/s10948-016-3533-z.

- I.A. Auwal, A. Baykal, S. Güner, **M. Sertkol**, H. Sözeri, "Magneto-Optical properties $BaBi_xLa_xFe_{2-2x}O_{19}$ $(0.0 \leq x \leq 0.5)$ hexaferrites", Journal of Magnetism and Magnetic Materials, 409 (2016), 92.

- I.A. Auwal, H. Güngüneş, S. Güner, Sagar E. Shirsath, **M. Sertkol**, A. Baykal, Structural, magneto-optical properties and cation distribution of $SrBi_xLa_xY_xFe_{12-3x}O_{19}$ $(0.0 \leq x \leq 0.33)$ hexaferrites, Materials Research Bulletin, 80(2016), 263.

- I.A. Auwal, H. Güngüneş, A. Baykal, S. Güner, Sagar E. Shirsath, **M. Sertkol**, Structural, morphological, optical, cation distribution and Mössbauer analysis of Bi^{3+} substituted strontium hexaferrite, Ceramics International, 42 (2016), 8627.

- A. Baykal, F. Genc, A. Z. Elmal, S. Gökçe, **M. Sertkol**, H. Sözeri, "$MnCr_xFe_2O_4$ Nanoparticles: Magnetic and Microwave Absorption Properties", Journal of Inorganic and Organometallic Polymers and Materials, Oct. 2015, DOI 10.1007 s10904-015-0288-0.

- A. Baykal, A. Z. Elmal, **M. Sertkol**, H. Sozeri, Structural and Magnetic Properties of $NiCr_xFe_{2-x}O_4$ Nanoparticles Synthesized via Microwave Method, Journal of Superconductivity and Novel Magnetism, 28 2015, 3405and3410.

- Md. Amir, B. Ünal, Sagar E. Shirsath, M. Geleri, **M. Sertkol**, A. Baykal, "Polyol synthesis of Mn^{3+} substituted Fe_3O_4 nanoparticles: Cation distribution, structural and electrical properties", Superlattices and Microstructures, 85(2015), 747-760.

- S. Güner, Md. Amir, M. Geleri, **M. Sertkol**, A. Baykal, "Magneto-optical properties of Mn^{3+} substituted Fe_3O_4 nanoparticles", Ceramics International, 41(2015), 10915–10922.

- Md. Amir, **M. Sertkol**, A. Baykal , H. Sözeri, “Magnetic and Catalytic Properties of $Cu_xFe_{1-x}Fe_2O_4$ Nanoparticles”, Journal of Superconductivity and Novel Magnetism, 28 (2015), 2447-2454.

- Md. Amir, A. Baykal, S. Güner, **M. Sertkol**, H. Sözeri, M. Toprak, “Synthesis and Characterization of $Co_xZn_{1-x}AlFeO_4$ Nanoparticles”, Journal of Inorganic and Organometallic Polymers and Materials, 25 (2015), 747-754.

- Md. Amir, A. Baykal, **M. Sertkol**, H. Sözeri, “Microwave Assisted Synthesis and Characterization of $Co_xZn_{1-x}Cr_{0.5}Fe_{0.5}O_4$ Nanoparticles”, Journal of Inorganic and Organometallic Polymers and Materials, 25 (2015), 619-626.

- A. Alemi, S. Khademinia , **M. Sertkol**, “Part III: lithium metasilicate (Li_2SiO_3)-mild condition hydrothermal synthesis, characterization and optical properties”, International Nano Letters, 5(2015), 77-83.

- **M. Sertkol**, Y. Köseoğlu, A. Baykal, H. Kavas, A. C. Başaran, "Synthesis and magnetic characterization of $Zn_{0.6}Ni_{0.4}Fe_2O_4$ nanoparticles via a polyethylene glycol - assisted hydrothermal route", Journal of Magnetism and Magnetic Materials, Vol. 321, Dec. 2008, pp. 157–162.

- H. Kavas , A. Baykal, M. S. Toprak, Y. Köseoğlu, **M. Sertkol**, Bekir Aktaş, "Cation distribution and magnetic properties of Zn doped $NiFe_2O_4$ nanoparticles synthesized by peg assisted hydrothermal route", Journal of Alloys and Compounds, Vol. 479, Jun. 2009, pp. 49-55.

- **M. Sertkol**, Y.Köseoğlu, A.Baykal, H.Kavas, A.Bozkurt, M.S. Toprak, "Microwave Synthesis and Characterization of Zn-doped Nickel Ferrite Nanoparticles", Journal of Alloys and Compounds, Vol. 486, No. 1-2, Nov. 2009, pp. 325-329.

- **M. Sertkol**, Y. Köseoğlu, A. Baykal, H. Kavas, M.S. Toprak, "Synthesis and magnetic characterization of $Zn_{0.7}Ni_{0.3}Fe_2O_4$ nanoparticles via Microwave-assisted combustion route", Journal of Magnetism and Magnetic Materials , Vol. 322, No. 7, Apr. 2010, pp. 866-871.